UNIVERSITÀ
DEGLI STUDI
DI PADOVA

Sede Amministrativa: Università degli Studi di Padova

Dipartimento di Biologia

SCUOLA DI DOTTORATO DI RICERCA IN: BIOSCIENZE E BIOTECNOLOGIE
INDIRIZZO: BIOLOGIA CELLULARE
CICLO: XXVII

NEURONAL HYDROGEN PEROXIDE PROMOTES NERVE TERMINALS REGENERATION AT NEUROMUSCULAR JUNCTION

Direttore della Scuola: Ch.mo Prof. Giuseppe Zanotti
Coordinatore d'indirizzo: Ch.mo Prof. Paolo Bernardi
Supervisore: Dott.ssa Michela Rigoni

Dottorando: Elisa Duregotti

SOMMARIO

La giunzione neuromuscolare (GNM) costituisce il sito di trasmissione di un impulso elettrico dal terminale del motoneurone alla fibra muscolare; l'organizzazione strutturale di questo sistema altamente dinamico è stata ulteriormente complicata dall'aggiunta delle cellule di Schwann perisinaptiche (CSPs), dando origine al concetto di sistema tripartito. Le CSPs sono cellule di Schwann non mielinizzanti strettamente adese alla zona di contatto tra nervo e muscolo; esse partecipano attivamente a molte funzioni fisiologiche della GNM, come il suo sviluppo embrionale ma anche il corretto mantenimento di GNMs adulte. Esse sono inoltre in grado di percepire e modulare l'attività sinaptica, mediante l'attivazione di recettori muscarinici e purinergici presenti sulla loro superficie.

Studi più recenti hanno dimostrato che le CSPs sono coinvolte nei processi di recupero che hanno luogo in risposta ad un danno nervoso; in seguito a denervazione o a ridotta attività sinaptica, le CSPs de-differenziano, diventando CSPs "reattive", ed iniziano a proliferare. Queste CSPs reattive partecipano attivamente ai processi di degenerazione e rigenerazione nervosa: esse subiscono variazioni nella loro espressione genica e acquisiscono attività simil-macrofagiche, contribuendo alla rimozione dei detriti neuronali e reclutando fagociti in seguito al rilascio di citochine e chemochine. Inoltre, in seguito alla degenerazione dei terminali nervosi, le CSPs presenti alle placche motrici denervate estendono lunghi processi citosolici in grado di indurre e guidare la ricrescita neuronale.

Considerando la crescente incidenza di malattie neurodegenerative che inizialmente interessano in maniera selettiva i terminali dei motoneuroni – quali la SLA e le neuropatie autoimmuni -, sarebbe senz'altro utile caratterizzare in maniera più approfondita il *crosstalk* tra terminali nervosi in degenerazione e le adiacenti CSPs. In particolare, l'identificazione di mediatori molecolari coinvolti nell'attivazione delle CSPs e nel processo di rigenerazione nervosa potrebbe rivelarsi cruciale per lo sviluppo di nuovi approcci terapeutici.

A tale scopo, abbiamo adottato un approccio sperimentale innovativo, alternativo al *cut/crush* del nervo sciatico tradizionalmente utilizzato fino ad oggi. Al fine di effettuare un danno localizzato ai soli terminali nervosi, evitando il coinvolgimento di molti tipi cellulari e mediatori dell'infiammazione come accade nel corso della degenerazione Walleriana, abbiamo deciso di sfruttare il meccanismo d'azione di due classi di neurotossine presinaptiche animali: α-Latrotoxin, una tossina formante poro presente nel veleno dei ragni del genere *Latrodectus*, ed alcune neurotossine di serpente dotate di attività fosfolipasica,

denominate SPANs. Entrambi i tipi di neurotossine inducono un'acuta e altamente riproducibile degenerazione dei terminali nervosi dei motoneuroni, seguita entro pochi giorni da una rigenerazione completa: l'azione di tali neurotossine rappresenta quindi un sistema appropriato e controllato per esaminare i meccanismi molecolari alla base della degenerazione e rigenerazione nervosa, come anche il contributo delle CSPs a tali processi.

Abbiamo precedentemente dimostrato che i terminali nervosi esposti ad α-Ltx e SPANs deegenerano a causa di un eccessivo influsso di calcio nel citosol, che a sua volta induce un danno mitocondriale. In questo lavoro, abbiamo dimostrato che neuroni primari intossicati aumentano la produzione di H_2O_2 a livello mitocondriale: il perossido di idrogeno è una molecola stabile e diffusibile attraverso membrane lipidiche, e potrebbe perciò agire come segnale paracrino su cellule adiacenti. Infatti, l'esposizione di cellule di Schwann (CSs) primarie in coltura a basse concentrazioni di H_2O_2 induce la fosforilazione di ERK, con la conseguente attivazione di *pathways* a valle. È stato recentemente dimostrato che la via di ERK gioca un ruolo fondamentale nel controllo della plasticità delle CSs durante la rigenerazione nervosa *in vivo*, ma fino ad oggi i mediatori molecolari responsabili per l'attivazione di tale *pathway* non sono ancora stati identificati: il perossido di idrogeno prodotto dai neuroni in degenerazione costituisce un buon candidato per tale ruolo. In supporto a tale ipotesi, abbiamo osservato che il livello di fosforilazione di ERK è ridotto in co-colture di neuroni e CSs intossicate e pre-incubate con catalasi, che converte rapidamente il perossido di idrogeno in ossigeno ed acqua: ciò conferma che il perossido di idrogeno prodotto dai neuroni diffonde effettivamente nel mezzo extracellulare fino a raggiungere le vicine CSs, nelle quali induce l'attivazione della via di ERK. Tale attivazione è riscontrata anche nelle CSPs alle GNMs intossicate *in vivo*. Per confermare il coinvolgimento del perossido di idrogeno nell'induzione della rigenerazione nervosa, abbiamo effettuato registrazioni elettrofisiologiche ed esperimenti di immunoistochimica, ed entrambi gli approcci sperimentali hanno dimostrato che in la somministrazione di catalasi *in vivo* ritarda il processo di rigenerazione nervosa in muscoli intossicati. Inoltre, il pre-trattamento con un inibitore della via di ERK - PD98059 – rallenta la il recupero dall'intossicazione con una cinetica molto simile a quella osservata in presenza di catalasi, supportando l'idea che in effetti il perossido di idrogeno promuova la rigenerazione nervosa attraverso l'attivazione della via di ERK nelle CSPs.

SUMMARY

The neuromuscular junction (NMJ) is the site of transmission of the electrical impulses from the motor axon terminal to the muscle; the anatomical organization of this highly dynamic system also includes the perisynaptic Schwann cells (PSCs), and therefore the NMJ has to be considered structurally and functionally as a tripartite system. These non-myelinating SCs are intimately associated with the nerve muscle contact and act as dynamic partners at the synapse: they are involved in many physiological functions including the embryonic development and the maintenance of adult NMJs. Moreover, they are able to detect and reciprocally modulate synaptic activity, through the activation of muscarinin and purinergic receptors present on their surface.

In addition, non-traditional roles for PSCs in the recovery after nerve injury are being recognized. Following denervation or reduced synaptic activity, PSCs de-differentiate to an earlier developmental stage, becoming “reactive” PSCs, and start proliferating. These reactive PSCs actively participate in the process of nerve degeneration and regeneration: they undergo changes in their gene expression and acquire macrophagic-like activities, thus contributing to the removal of nerve debris as well as to the recruitment of macrophages, by releasing cytokines and chemokines. Moreover, following nerve terminals degeneration, PSCs at denervated end-plates extend long processes that induce and guide nerve regrowth.

Given the increasing incidence of non cell-autonomous and dying-back axonopathies - such as amyotrophic lateral sclerosis (ALS) and autoimmune neuropathies - which affect predominantly motor axons terminals, it becomes very important to characterize the crosstalk between degenerating nerve terminals and adjacent PSCs at the NMJ; in particular, the identification of molecular mediators involved in PSCs activation and in nerve terminals regeneration would be crucial for the improvement of therapeutic strategies.

This is the general aim of the present thesis and with this purpose in mind, we have adopted an innovative experimental approach, alternative to the traditional cut/crush surgical model employed till now. To confine the nerve damage to the sole motor axon terminal, thus avoiding the involvement of many cell types and inflammatory mediators, we exploited our knowledge on the mechanism of action of two classes of animal presynaptic neurotoxins: α-Ltx, a pore forming toxin of the venom of black widow spiders, and some snake neurotoxins endowed with phospholipase A2 activity called SPANs. Both kinds of neurotoxins induce an acute and highly reproducible motor axon terminal degeneration, which is followed in few

days by complete regeneration: thus, this model represents an appropriate and controlled system to dissect the molecular mechanisms underlying de- and re-generation of peripheral nerve terminals, and to define how PSCs contribute to such processes.

We have previously shown that nerve terminals exposed to spider or snake neurotoxins degenerate owing to calcium overload and mitochondrial failure. Here, we found that toxin-treated cultured neurons increase their mitochondrial production of hydrogen peroxide (H_2O_2), which can easily diffuse across membranes, thus acting as a paracrine signal on neighbouring cellS. Indeed, exposure of cultured SCs to H_2O_2 leads to ERK phosphorylation and to the activation of downstream pathways. The ERK signalling pathway plays a central role in controlling SCs plasticity during nerve repair *in-vivo*, but so far the molecular mediators responsible for its activation were unknown: neurons-derived H_2O_2 represents an ideal candidate for this role.

In support of this hypothesis, we observed that ERK phosphorylation is reduced in intoxicated neurons-SCs co-cultures pre-incubated with catalase - which converts H_2O_2 to oxygen and water -, indicating that H_2O_2 produced inside neurons diffuses to reach nearby SCs, contributing to ERK activation in their cytosol. ERK phosphorylation takes place also in PSCs at intoxicated NMJs *in-vivo*. To confirm the involvement of H_2O_2 in promoting nerve regeneration, we performed electrophysiological recordings and immunohistochemistry on intoxicated muscles, and we found that co-injection of catalase together with neurotoxins delays nerve regeneration, confirming the prominent role of H_2O_2 in promoting NMJ recovery. Injection of the MAP kinase inhibitor PD98059 also impairs nerve repair in a way similar to that observed with catalase, supporting the finding that H_2O_2 enhances nerve terminals regeneration through the activation of ERK pathway in PSCs.

TABLE OF CONTENTS

ABBREVIATIONS

PNS: peripheral nervous system

SCs: Schwann cells

NMJ: neuromuscular junction

Ach: acetylcholine

PSCs: perisynaptic Schwann cells

NRG1: neuregulin 1

ATP: adenosine triphosphate

CNS: central nervous system

ROS: reactive oxygen species

mPTP: mitochondrial permeability transition pore

P0: protein 0

MBP: myelin basic protein

GFAP: glial acidic fibrillary protein

GAP-43: growth associated protein 43

NGF: nerve growth factor

BDNF: brain derived neurotrophic factor

GDNF: glial cell-line derived neurotrophic factor

NT-3: neurotrophin 3

ALS: amyotrophic lateral sclerosis

α-Ltx: α-Latrotoxin

SPANs: snake neurotoxins endowed with phospholipase 2 activity

NRX: neurexin

LPH1: latrophilin 1

PTPσ: protein tyrosin phosphatase σ

PLC: phospholipase C

IP_3: inositol triphosphate

PKC: protein kinase C

PLA2: phospholipase A2

β-Btx: β-Bungarotoxin

Tpx: Taipoxin

APRs: arrays of presynaptic receptors

LysoPC: lysophosphatidylcholine

FAs: fatty acids

MNs: motoneurons

CGNs: cerebellar granular neurons

DAMPs: damage-associated molecular patterns

PAMPs: pathogen-associated molecular patterns

NFPs: N-formyl-peptides

mtDNA: mitochondrial DNA

Cyt c: cytochrome c

SOD: superoxide dismutase

PTPs: protein tyrosine phosphatases

TRXs: thioredoxins

PRXs: peroxiredoxins

MitoPY1: Mitochondria Peroxy Yellow 1

PF6-AM: Peroxyfluor 6 acetoxymethyl ester

PMA: phorbol 12-myristate 13-acetate

ERK: extracellular-signal regulated kinase

MAPK: mitogen activated protein kinase

LAL: *Levator Auris Longus*

EJPs: evoked junction potentials

SNAP25: synaptosomal-associated protein 25

CD68: cluster of differentiation 68

NF: neurofilaments

1. INTRODUCTION

The motor nerve terminal is a highly complex and dynamic compartment responsible for the transduction of electrical impulses to the muscle. The regulation of voluntary and involuntary movements, which relies on this transmission, is crucial for many physiological functions such as breathing, moving and feeding.

Due to its intrinsic functional features and the key role in many survival behaviours, the motor axon terminal represents the main target of several pathogens: during evolution, both animals and bacteria have indeed developed several toxins which selectively interfere with nerve-muscle transmission, causing paralysis and in most severe cases death.

Beside pathogens, many neuromuscular diseases have been shown to compromise the synaptic transmission between motor neurons and muscle cells; most of them are classified as genetic or auto-immuno diseases, and can differ in severity and mortality rate. Although plenty of work has been focused on the etiology of motorneuron disorders, little is known about the pathogenesis of many of them, that still lacks therapeutics.

The peripheral nervous system (PNS) has an intrinsic ability to repair after nerve injury; this capacity depends on patient age, and on type and site of injury (in particular on the distance from the neuronal cell body). The PNS regenerative potential mainly relies on the response to damage of Schwann cells (SCs), the glia of PNS. These cells are known to provide fundamental cues that trigger neuronal regenerative response. Thus, a better understanding of SCs contribution to nerve repair may provide compelling information that could be relevant for many different pathological contexts, and could allow the development of new therapeutic strategies for neurodegenerative diseases.

This work has been focused on the setting up of an innovative experimental system to characterize the crosstalk between degenerating nerve terminals and SCs, with the final purpose of identifying molecular mediators crucially involved in the process of nerve terminals regeneration.

Scientific background, experimental approaches and tools of this study will be elucidated in the following pages.

1.1 THE NEUROMUSCULAR JUNCTION

The neuromuscular junction (NMJ) is a chemical specialized synapse designed to transmit the electrical impulse from the nerve to the skeletal muscle through the release of the neurotransmitter acetylcholine (Ach); in mammals, this finely tuned system relies on at least three components: the motor neuron, the muscle fiber and the perisynaptic/terminal Schwann cells (PSCs) (Fig. 1).

The motor axon terminal, which represents the pre-synaptic element of the NMJ, is the structure where neuroexocytosis occurs; it innervates the muscle at a specialized site called end-plate (post-synaptic element). While approaching the muscle fiber, the motor axon loses its myelin sheath and splits into several fine branches, which form multiple expansions called synaptic boutons.

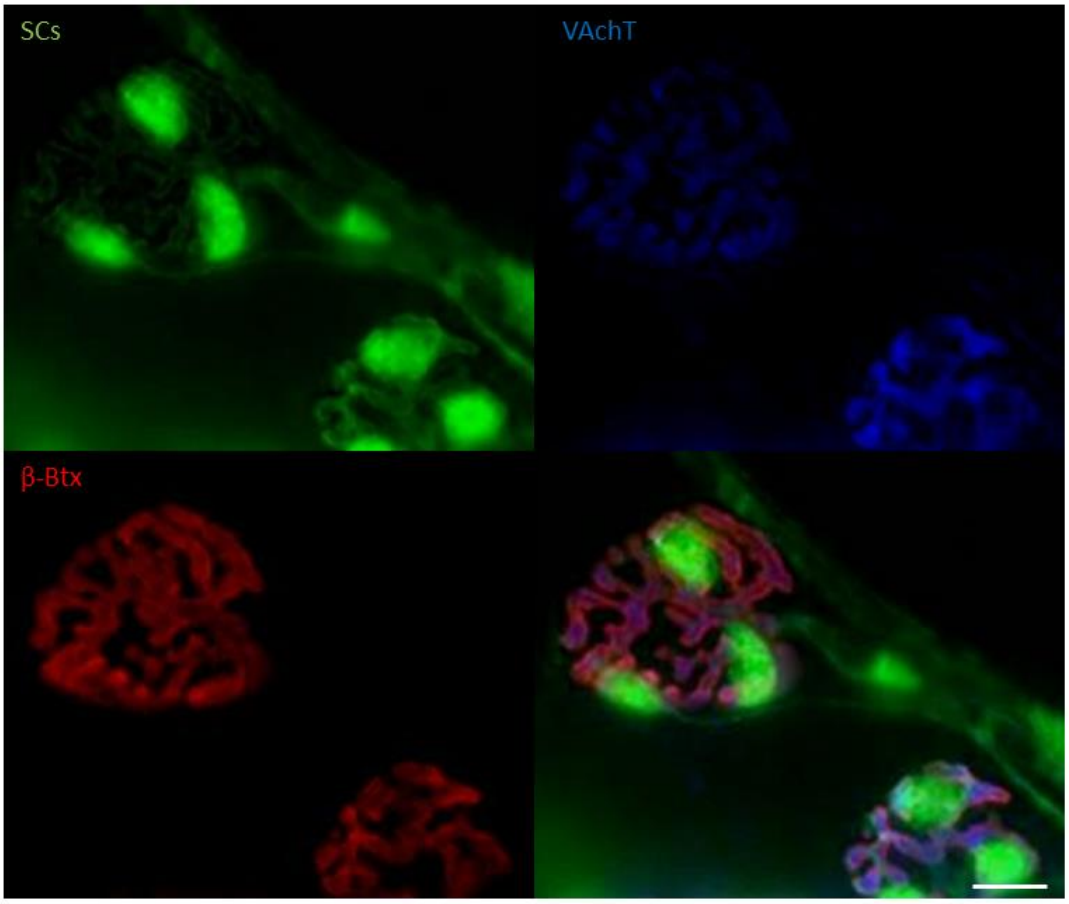

Fig. 1: Anatomical structure of mammalian NMJ. Immunohistochemistry on *Levator Auris Longus (LAL)* muscle of a transgenic mouse expressing GFP in the cytosol of SCs under the *plp* promoter (upper left picture, green). Nerve terminals are labelled with an antibody against the vesicular Ach transporter (VAcht, upper-right picture, blue) and the muscle end-plate is stained with α-Bungarotoxin (α-Btx) Alexa 555-conjugated (bottom left, red). Scale bar: 10 µm.

Each bouton contains all the machinery required for neurotransmission: synaptic vesicles containing Ach and the active zones, regions of the pre-synaptic plasma membrane specialized for vesicular release and enriched in voltage-gated calcium channels.

Active zones are juxtaposed with junctional folds, deep depressions in the surface of the post-synaptic muscle fiber which contain nicotinic receptors for Ach as well as voltage-gated sodium channels.

Upon the arrival of an action potential at the motor axon terminal, voltage-dependent calcium channels open and the resulting calcium influx triggers the fusion of synaptic vesicles with the pre-synaptic plasma membrane: vesicular Ach is therefore poured out into the synaptic cleft, which separates the pre- and post-synaptic membranes, and diffuses to reach nicotinic receptors on the motor end-plate. The opening of these ionotropic receptors induces a depolarization of the end-plate giving rise to an end-plate potential; this in turn opens neighbouring voltage-gated sodium channels, eventually leading to the onset of an action potential, which propagates along the muscle fiber causing muscle contraction [1].

Though it has long been noticed that glial cells named perisynaptic Schwann cells (PSCs) are present at the nerve-muscle contact sites, these non-myelinating SCs have traditionally been considered merely passive supporting players at the synapse. Indeed, PSCs were thought not to actively participate in synaptic transmission at NMJ, partly because they are electrically non-excitable. However, a flurry of recent studies have unravelled the active roles of PSCs in formation, function and maintenance of the NMJ, demonstrating that PSCs are on the contrary integral and essential components of the synapse. Moreover, non-traditional executive roles for PSCs are being recognized in the process of recovery after nerve injury. Taken together, these evidences have led to the concept that NMJ is a tripartite unit, where PSCs must be considered central players in many physiological and pathological processes.

1.2 SCHWANN CELLS

Schwann cells (SCs) are the main glia of the PNS. Named after the German physiologist Theodor Schwann, SCs have long been recognized as crucial components in maintaining a proper environment for neuronal function. Recently, additional and more dynamic roles at synapses have been ascribed to them.

During embryonic development, SCs originate from neural crest cells; in mice, the generation of SCs precursors takes place at E12-E13 (embryonic day 12-13), followed by immature SCs at E13-15, which persist till birth. The postnatal fate of the immature SCs depends on their random association with axons; during the so-called radial sorting, whereby pro-myelinating SCs surround groups of axons by extending processes into axon bundles, those SCs that associate with single large-diameter axons will develop into myelinating SCs. Small diameter axons become instead entrenched in invaginations of non-myelinating SCs, also called Remak bundles [2, 3] (Fig. 2). Non-myelinating SCs also comprise perisynaptic or terminal SCs (PSCs), which cover the NMJ in close proximity to the neuron-muscle contact.

The transition from immature SCs to completely differentiated SCs is reversible: upon loss of axonal contact after nerve section, cells of both types de-differentiate to an earlier developmental stage, re-entering the cell cycle and start proliferating.

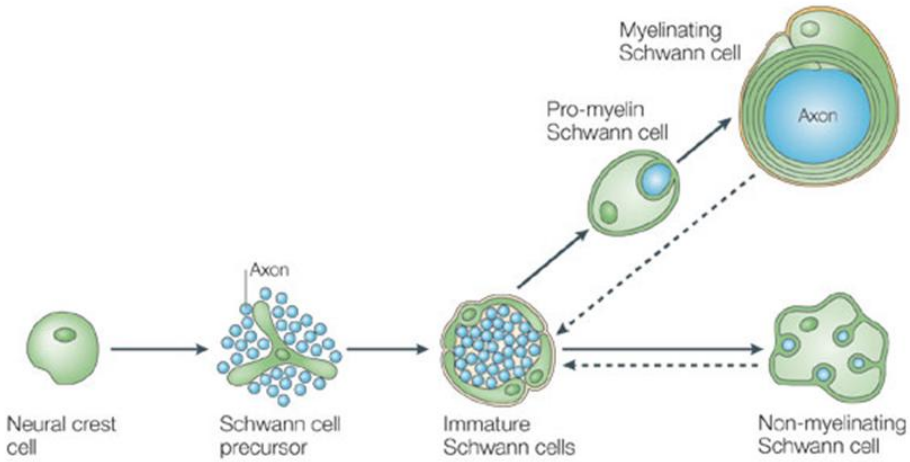

Fig. 2: Schwann cells origin and development. During embryonic development, neural crest cells give rise to SCs precursors, which then develop into different adult phenotypes: myelinating SCs and non-myelinating SCs, which can form Remak bundles along axons or differentiate into PSCs at NMJs. Dashed arrows indicate the reversibility of the final, largely postnatal transition during which mature myelinating and nonmyelinating cells are generated. Figure from Jessen and Mirky, 2005.

1.2.1 SCs in NMJ development

At mammalian and amphibian NMJs there are typically 3 to 5 PSCs: the number of PSCs per NMJ is tightly regulated and related to the end-plate size [4]. Since SCs migrate along the nerve during embryonic development, they are present at the earliest nerve-muscle contact, suggesting their involvement in NMJ formation. Genetic studies of neuregulin-1 (NRG1) and its receptors (erbB2 and erbB3) in mice provided valuable information for the role of SCs in the formation of the NMJ [5, 6]. At developing NMJs, the survival of SCs relies on the axonal supply of NRG-1: indeed, both NRG-1 and erbB mutant mice lack SCs at the periphery. In the absence of SCs, motor axons still project and reach the target muscles, but are markedly defasciculated; this suggests that SCs are dispensable for axon path finding but are essential for nerve fasciculation [5]. Moreover, in NRG-1, erbB2 and erbB3 mutant mice NMJs are initially established but fail to be maintained: thus, SCs are dispensable for the initial nerve-muscle contacts but are necessary for subsequent growth and maintenance of the developing synapse [7]. This observation has been further supported by observations at the developing NMJ in tadpoles, in which the extension of SCs processes always precedes Ach receptors deposition and synaptic growth, thus appearing to guide nerve terminals [8]. When PSCs are selectively killed by complement-mediated cell lysis, synaptic growth is markedly reduced and terminal retractions are widespread. Thus, it is now clear that any consideration of the events underlying NMJ formation and maintenance must take the SCs into account.

1.2.2 SCs in synaptic transmission at adult NMJ

Given the proximity of PSCs processes to the active zones and postsynaptic receptors, it stands out that they are well positioned to detect and modulate synaptic activity. Additionally, PSCs express many more neurotransmitter receptors and ion channels than myelinating SCs: for instance, they have functional L-type voltage-dependent calcium channels, muscarinic, purinergic and substance P receptors [9]. Evidence indicating that PSCs are actually involved in neuromuscular transmission have been reported in many experimental studies. High-frequency nerve stimulation in frogs and mice induces transient elevation in the intracellular calcium level in PSCs, and this increase is greatly reduced when transmitter release is blocked [10, 11]. Local application of ACh and/or ATP, which are

released by nerve terminals during nerve activity, also elicits calcium elevation in PSCs, suggesting the recruitment of their G-coupled muscarinic and purinergic receptors. PSCs responses to Ach or ATP are not impaired in the absence of extracellular calcium, implying that the major source of calcium transients are intracellular stores [10, 12].

Not only do PSCs sense synaptic transmission, they also modulate subsequent synaptic activity [9]; depending on the duration and intensity of nerve stimulation, PSCs react by secreting different neuromodulatory substances. Glutamate release from PSCs has been shown to cause the depression of synaptic activity via the induction of NO synthase in the muscle, whereas it has been proposed that prostaglandins produced by PSCs directly act on the nerve terminal leading to a potentiated neurotransmission [13, 14, 15].

Thus, PSCs act as dynamic partners in the NMJ transmission by providing feedback regulation to the synapse in response to synaptic activity.

1.2.3 SCs in nerve degeneration and regeneration

Beside the important functions exerted by PSCs in the formation, development and maintenance of the NMJ, emerging evidence indicates that they also play, along with myelinating SCs, a key role in nerve terminal degeneration and regeneration.

1.2.3.1 Nerve degeneration

Axon degeneration is a prominent early feature of most neurodegenerative disorders and can also be induced directly by nerve injury in a process known as Wallerian degeneration. The latter was first described by Augustus Waller in 1850 [16], when he found that following the cut or crush of a nerve fiber, the axon segment detached from the neuronal cell body undergoes an acute axonal degeneration (also called acute axonal degeneration [17]).

Wallerian degeneration occurs in both PNS and central nervous system (CNS) and usually begins within 24-36 hours from the lesion (Fig.3). Early pathological changes in the distal stump include failure of synaptic transmission, target denervation and granular disintegration of the axonal cytoskeleton. Increased intra-axonal calcium and calpains activation are well established events in the execution phase of Wallerian degeneration: this leads to fragmentation of axonal cytoskeleton and inner organelles, together with axolemma swelling and bead-like formation. Early alterations also include endoplasmic reticulum

degradation and accumulation of swelled mitochondria at the paranodal regions at the site of injury [18, 19]. Mitochondria have been proposed to have one or more key roles in Wallerian degeneration: in the earliest phase they swell, accumulate at paranodal sites and lose their membrane potential. Mitochondrial disfunction lowers ATP levels, generates reactive oxygen species (ROS) and impairs calcium buffering, leading to cellular homeostasis imbalance, mitochondrial permeability transition pore (mPTP) opening, release of pro-apoptotic signals and activation of other cell death mechanisms. However, whether these changes are a cause or simply a consequence of degeneration remains unclear [20].

At the end of the process, the axon undergoes complete fragmentation; the rate of degradation depends on the type of injury and is slower in the CNS than in the PNS. Another factor that affects degradation rate is the axon diameter: in longer axons the cytoskeleton degrades more slowly and thus longer axons take longer to degenerate.

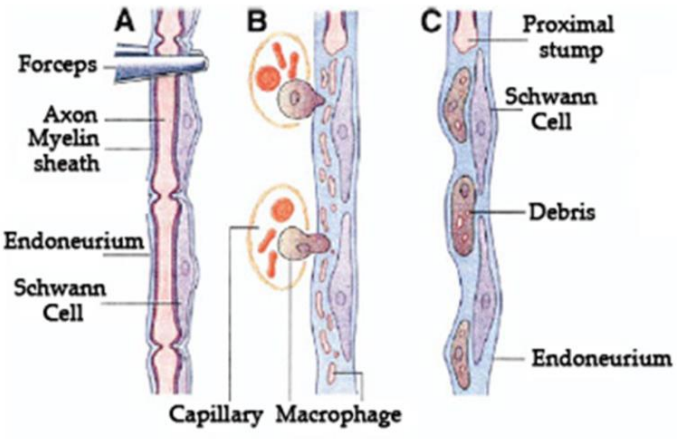

Fig. 3. Main steps of Wallerian degeneration. Following axon damage (A), the distal stump degenerates undergoing fragmentation (B). Activated SCs de-differentiate and start proliferating, secreting chemokines and cytokines which recruit macrophages at the site of injury (B). Both activated SCs and macrophages contribute to nerve debris clearing (C). From Fitzgerald MJT, Folan-Curran J. Clinical Neuroanatomy and Related Neuroscience. 4th ed. Philadelphia, Pa: WB Saunders; 2002.

The SCs response to axonal injury is rapid; within few hours, myelinating SCs associated with damaged axons de-differentiate to a progenitor-like state, becoming “reactive”, and start proliferating [21]. They undergo changes in gene expression, down-regulate structural proteins - such as protein zero (P0), myelin basic protein (MBP) and myelin associated glycoprotein -, whilst up-regulate cell-adhesion molecules and glial fibrillary acidic protein (GFAP), along with growth factors [22]. The myelin sheaths separate from the axons, rapidly deteriorate and shorten to form bead-like structures. Moreover, reactive SCs acquire macrophagic-like activities and start clearing up the axonal and myelin debris; they also

recruit macrophages by releasing cytokines and chemokines, thus improving the clearing rate of cell debris favouring regeneration [23, 24].

PSCs at NMJs undergo similar alterations upon degeneration of the motor axon terminal: they de-differentiate and re-enter cell cycle. It has been shown that a reduced synaptic activity (which follows denervation) leads to an increased expression of the cytoskeletal protein GFAP and of the p75 neurotrophin receptor, whereas the loss of nerve contact up-regulates GAP-43 (growth associated protein 43) and down-regulates the cytosolic protein S-100. In addition, PSCs at degenerating NMJs contribute to the removal of debris originating from degenerating nerve terminals; once completed the clearing, they move to occupy the denervated synaptic cleft and start releasing ACh, giving rise to miniature endplate potentials in the muscle fiber [9, 25].

1.2.3.2 Nerve regeneration

In the PNS injured axons can spontaneously regrow. This is in contrast to the CNS, where severed axons rarely show significant levels of regeneration, probably due to lack of glial support: several studies revealed that the failure of CNS neurons to regenerate is not an intrinsic deficit of neurons, but rather a characteristic feature of the damaged environment that either do not support or prevented regeneration [26]. In particular, the clearing up process of myelin debris seems to be delayed in the CNS with respect to the PNS, and this could possibly hinder the process of nerve regrowth [27].

In the PNS, soon after nerve injury the proximal stump of damaged axon – which is still connected to the neuronal cell body – undergoes deep reorganization which leads to the formation of a fundamental structure for nerve regeneration: the growth cone [28]. Growth cones are highly motile structures that explore the extracellular environment, determine the direction of growth, and then guide the extension of the axon in that direction (Fig. 4). The main morphological characteristic of a growth cone is a sheet-like expansion of the growing axon at its tip, called lamellipodium. The highly dynamic nature of growth cones allows them to respond to the surrounding environment by rapidly changing direction and branching in response to various stimuli. Overall, axon elongation is the product of a process known as tip growth.

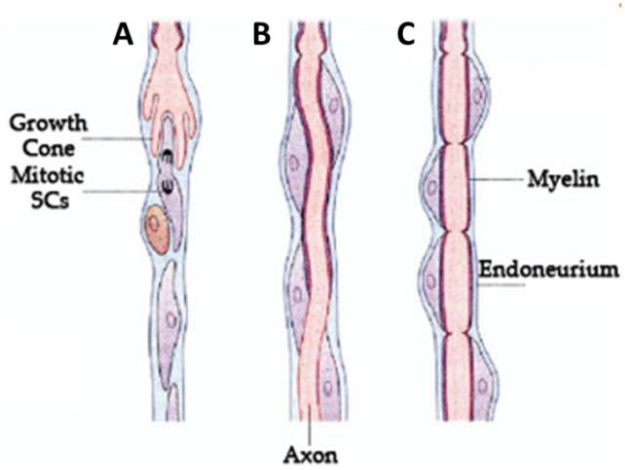

Fig. 4. Principal steps of nerve regeneration. Soon after nerve injury, growth cone forms at the proximal stump of damaged axon (A), and proliferating SCs organize to form bands of Bungner (B) along which the regenerating axon grows to re-innervate its target site (C). From Fitzgerald MJT, Folan-Curran J. Clinical Neuroanatomy and Related Neuroscience. 4th ed. Philadelphia, Pa: WB Saunders; 2002.

In this process, new material is added at the growth cone while the remainder of the axonal cytoskeleton remains stationary. This occurs via two processes: cytoskeletal-based dynamics and mechanical tension. With cytoskeletal dynamics, microtubules polymerize into the growth cone and deliver vital components. Mechanical tension occurs when the membrane is stretched due to force generation by molecular motors in the growth cone and strong adhesions to the substrate along the axon. Laminins of the basal membrane interact with the integrins of the growth cone to promote the forward movement of the axon tip [29]. Additionally, axon outgrowth is also supported by the stabilization of the proximal ends of microtubules, which provide the structural support for the axon.

SCs play a crucial role in repair of peripheral axons [30, 31]. Beside the release of growth factors such as NGF, BDNF, GDNF and NT-3, they also provide structural guidance to further enhance regeneration [32]. During their proliferation phase, SCs begin to form a line of cells called Bands of Bungner within the basal laminar tube: axons have been observed to regenerate in close association to these cells [33]. Also, SCs up-regulate the production of cell surface adhesion molecules further promoting growth. These Bands of Bungner guide the axon elongation in the proper direction.

Also PSCs at NMJs greatly contribute to axonal regeneration after nerve injury: their crucial roles in such process were initially demonstrated by Son and Thompson in 1995 using elegant immunohistochemistry experiments [34, 35]. They found that shortly after a full resection of the nerve PSCs extend processes – called “sprouts” – that grow through the muscle, reaching lengths of several hundred micrometers, and forming a network of processes interconnecting the denervated endplates (Fig. 5). Regenerating axons grow back to the muscle following the endoneurial tubes provided by de-differentiated myelinating

SCs, and are led to denervated endplates. Motor axons approaching muscle fibers proceed to re-occupy the endplate sites, but do not stop their growth there. Rather, they grow out along PSCs processes extended from the endplate, forming the so-called “excaped fibers”. In this manner, PSCs processes act as bridges between endplates for reinnervating axons.

A similar phenomenon is observed also following partial denervation: here, PSCs processes from denervated endplates find the still-innervated ones, where they induce a nerve terminal sprout that is then guided back to the denervated site [9, 25].

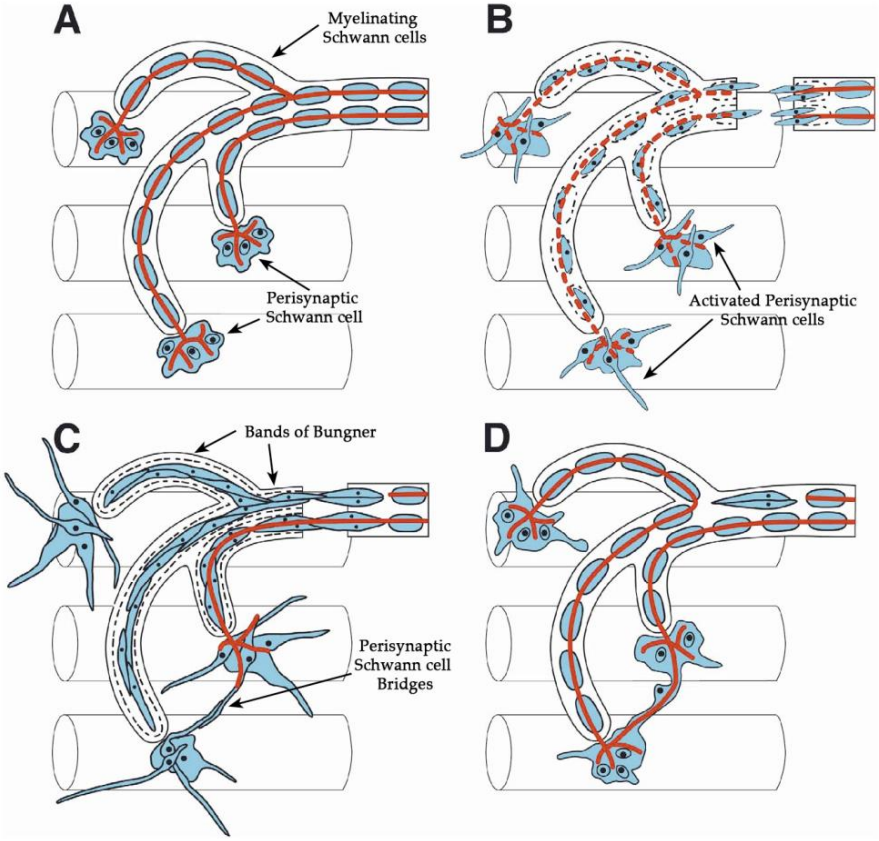

Fig. 5. The proposed role of SCs in regeneration of peripheral nerves and muscle re-innervation. (A) The normal innervation of 3 muscle fibers by an intramuscular nerve containing two myelinated motor axons (in red), one of which forms branches that innervate two different muscle fibers. PSCs (in blue) cover the NMJs. In (B) the nerve is resected and the axons are degenerating distal to the lesion site (dashed red lines). The myelin coating of the former axons disintegrates, and activated SCs begin to extend processes within the endoneurial tubes of the nerve. Activated PSCs at denervated NMJs start extending processes over the muscle fibers. (C) The SCs of the nerve form a bridge across the lesion site (Band of Bungner) through which one axon regenerates. Processes of PSCs have extended from each endplate forming in some cases fascicles which interconnect denerveted endplates. A regenerating axon arriving at one endplate re-innervates this muscle fiber and extends beyond this endplate (that is, “excaped fiber”) by growing onto PSCs processes. (D) The axon in C has grown along PSCs sprouts to innervate also the lower endplate, and keeps growing in a retrograde direction up the endoneurial tube. At the end, all three muscle fibers become innervated by the same axon, thus leading to a clustered distribution of the motor units fibers. Polineurally innervation of a single muscle cell is also often observed following nerve regeneration (modified from Son and Thompson 1995).

As a consequence of the reinnervation process, muscle fibers often become polineurally innervated; moreover, adjacent muscle fibers are frequently innervated by the same axon, leading to a clustered distribution of a motor unit fibers [25].

Thus, SCs function as leaders rather than followers during regeneration: indeed they lead and guide reinnervating nerve-sprouts in order to re-establish a functional reinnervation of muscle fibers.

1.3 EXPERIMENTAL MODELS TO STUDY NERVE TERMINALS REGENERATION

Although clearly documented, the regeneration of damaged motor axons is still ill-known in some of its cellular and molecular aspects. The traditional experimental approach used to investigate such process is the *in-vivo* cut or crush of sciatic nerves in rodents, and much of our knowledge about how nerve regeneration occurs comes from this kind of studies.

As mentioned above, Wallerian degeneration, which is set in motion following such mechanical injury, is a very complex process: it triggers a pronounced inflammatory response, all along the nerve, involving many cell types and inflammatory mediators. This surgically-induced nerve degeneration closely mimics the cascade of events which occurs in traumatized patients – i. e. calcium overload, mitochondrial impairment and cytoskeletal fragmentation of injured nerves -, thus representing a well-established model to characterize these pathological conditions. However, many other motor neuron diseases do not share some of the pathogenic features of Wallerian degeneration: indeed, in non cell-autonomous and dying-back axonopathies such as ALS and autoimmune neuropathies, including the Guillain-Barré and Miller-Fisher syndromes, many molecular changes influencing motor neuron degeneration are thought to occur at the NMJ at very early stages of the disease prior to symptom onset [36, 37, 38, 39]. Therefore, experimental models which allow a more focused examination of pathogenic events ongoing during motor axon terminals degeneration are needed in order to get useful information about this distally-localized process.

Beside this, a better understanding of PSCs roles in nerve terminals degeneration and regeneration may also be provided by experimental models in which the nerve injury only affects axon terminals, thus confining the major effects of such damage at NMJ.

To this purpose, the ideal condition would be to provide a very specific and localized damage of the nerve terminal in order to avoid the activation and involvement of many cell types – including myelinating SCs – and the massive production of inflammatory mediators. Moreover, this localized injury should reproduce the chain reaction of molecular events that leads to nerve terminal degeneration in sick or injured patients.

To fully meet these requirements, we decided to exploit our knowledge on the mechanism of action of two classes of animal neurotoxins that induce a selective and reversible degeneration of motor axon terminals (Fig. 6). In particular, we focused our attention on α-Latrotoxin (α-Ltx), a pore-forming toxin of the venom of black widow spiders [40], and on

some snake neurotoxins endowed with phospholipase A2 activity, called SPANs [41, 42]. A recent side-by-side comparative study of α-Ltx and SPANs action showed that, despite their different biochemical activities, both kind of neurotoxins exert their degenerative activities mainly by inducing a large calcium influx inside nerve terminals, due to toxins-induced plasma membrane permeability alterations [43]. This uncontrolled calcium overload triggers a massive neuroexocytosis followed by muscle paralysis and progressive degeneration of the motor axon terminal. Interestingly, α-Ltx- and SPANs-induced peripheral paralysis is followed by a complete and rapid recovery: regeneration and re-innervation are almost fully restored in rodents by 5 to 10 days [44, 45].

The regeneration steps that take place upon animal neurotoxins poisoning are likely to be similar to those that follow the cut or crush of nerves, since a closely similar cascade of toxic events occurs in both conditions (i.e. calcium overload, cytoskeleton degradation and mitochondria impairment); moreover, this alternative and innovative approach provides the advantage of being much more controlled and more reproducible. In addition, it does not involve the death of many cell types, it is strictly limited to the end-plate and the biochemical mechanism of action of the toxins is well characterized – see next sections-.

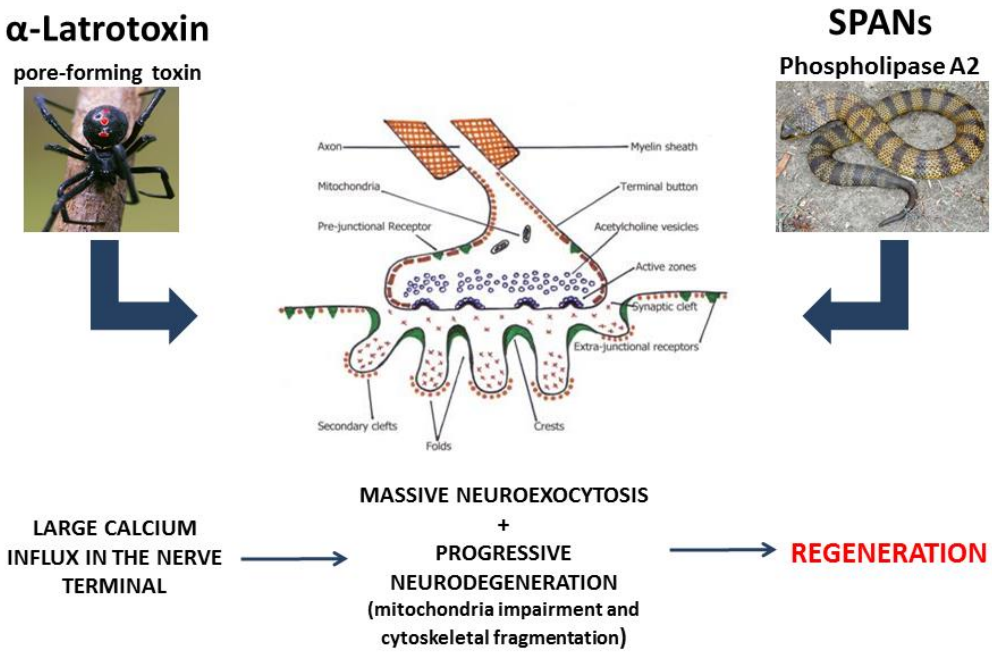

Fig. 6. Animal presynaptic neurotoxins induce a localized and reversible motor axon terminal degeneration. α-Ltx from black widow spiders and snake neurotoxins (SPANs) target specifically the presynaptic element of the NMJ, causing a toxic calcium influx. This cytosolic calcium overload triggers massive neuroexocytosis, followed by vesicles depletion and muscular paralysis; in a later stage of intoxication it sets in motion the progressive degeneration of motor axon terminals. In mice a complete and functional regeneration is achieved in few days after intoxication.

Therefore, the mouse NMJ treated with α-Ltx or SPANs represents a relevant model of acute motor axon terminal degeneration and regeneration, which is likely to provide information useful not only to the understanding of the pathogenesis of envenomation but, more in general, of other human pathological syndromes.

1.3.1 Animal presynaptic neurotoxins

The understanding of the molecular mechanism of action of these animal neurotoxins is fundamental to better understand their role in this study; thus, a detailed decription of their structure, mechanism of action and toxic effects will be illustrated in the next sections.

1.3.1.1 α-Latrotoxin

The black widow spiders (genus *Latrodectus*) are largely diffused in many parts of the world. The venom of *Latrodectus spp.* contains at least 86 unique proteins [46], some of which play a role in its toxicity toward insects and crustaceans, with only one component, α-Ltx, targeting vertebrates specifically [47]. This 130-kDa protein induces exhaustive release of neurotransmitters from nerve terminals and endocrine cells, and has been employed for many years as a molecular tool to study exocytosis [48, 49].

α-Ltx is synthetized as a 157 kDa polypeptide in the cytosol of secretory epithelial cells of spiders venom glands (Fig. 7) [50, 51]. These cells disintegrate and expel toxin into the gland lumen together with various proteases [46]. Here, the toxin is cleaved at both termini by a furin-like protease, producing an active α-Ltx of 131 kDa [52]. The most striking feature of α-Ltx primary structure is a series of 22 ankyrin repeats; the N-terminal of the toxin shows no significant homology with other proteins and contains three conserved cysteines important for the structural stability and activity of all Ltxs [50].

Although some monomers - consisting of a wing, a body and a head domain - have been observed by cryo-electron microscopy in EDTA-treated α-Ltx, the toxin almost always exists as a stable dimer in which the monomers are associated “head to tail” [50]. Association of dimers, strongly catalysed by divalent cations, produces a cyclical structure that can contain four monomers only. The bottom region of this bowl-like structure is important for penetration into lipid bilayers, and it is likely that structural rearrangements required for tetramerisation expose the surface regions favourable to interaction with lipid membranes.

Above this, in the centre of the "bowl", the four heads form a cylindrical assembly surrounding the channel, which is restricted at one point to 10 Å; this constriction probably corresponds to the cations binding site of the α-Ltx channel. The wings extend sideways from the body domains perpendicular to the central symmetry axis of the tetramer, and could participate in the binding to some receptors (Fig. 7, 8) [40].

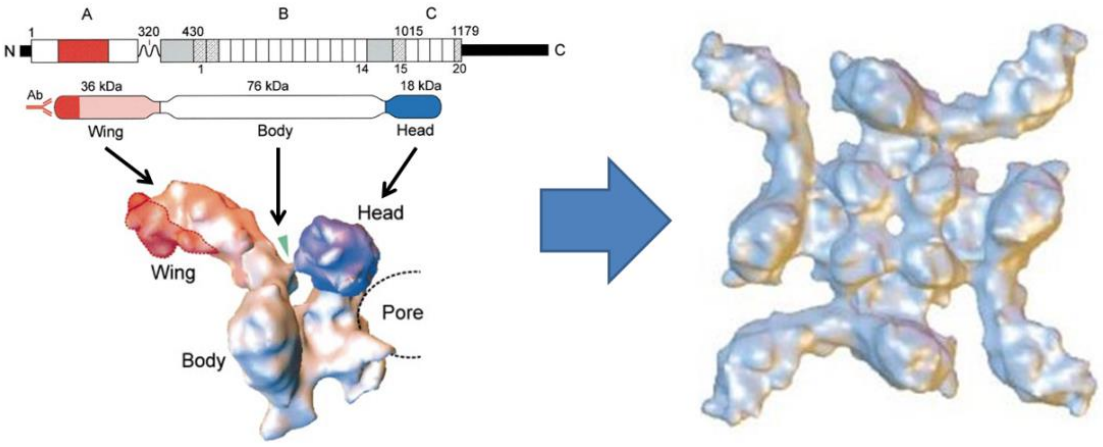

Fig. 7. Protein structure of α-Ltx. Top left: diagram of α-Ltx sequence and a linear representation of its domain structure; narrow boxes numbered 1-20 correspond to ankirin repeats, thick black lines are fragments proteolitically removed during α-Ltx maturation. Bottom left: view of the monomer illustrating the three structural domains of the molecule: wing (pink), body(silver), and head (blue); the arrowhead points at a connection between the head and the body. Right: top view of the tetramer. From Orlova et al., 2000.

Although α-Ltx is able to insert into pure lipidic membranes, reconstituted receptors greatly enhance the rate of insertion. It is not clear whether some receptors are directly involved in membrane insertion, if they simply concentrate toxin near membrane or if they organise membrane lipid domains to make them accessible to α-Ltx. At present, three surface-proteins have been identified to be selectively bound by α-Ltx: neurexin (NRX) (calcium-dependent interaction), latrophilin 1 (LPH1) and protein tyrosin phosphatase σ (PTPσ) (calcium-independent interaction). Such receptors are present mostly in the brain, but they have also been found, though in small amounts, in other secretory tissues such as pancreas, lung and kidney. Thus, receptors confer specificity to the pore-mediated effects of α-Ltx [40]. Once bound to its target membrane, α-Ltx can cause both calcium-dependent and -independent release of neurotransmitters. Part of its calcium-dependent action is due to the pore formation and resulting calcium influx (Fig. 8) [53]; this mechanism triggers the release

of both the readily releasable and the reserve pools of vesicles [54]. Another action is based on receptor-mediated signalling, which involves stimulation of PLC, production of IP_3 and dyacil glycerol, with release of stored calcium and activation of PKC respectively. This mechanism, most likely mediated by LPH1, affects the readily releasable vesicles only. Both the pore- and receptor-mediated signals can be amplified by the release of intracellular calcium and the extracellular calcium influx. In the absence of extracellular calcium, vesicle secretion may be caused by sodium and potassium currents through the channel, associated with the efflux of small molecules and the influx-efflux of water. In addition, transmitter release can be due to membrane perturbations or direct interaction with the secretory machinery. However, the toxin effect in the absence of calcium remains so far mostly unclear [40, 55].

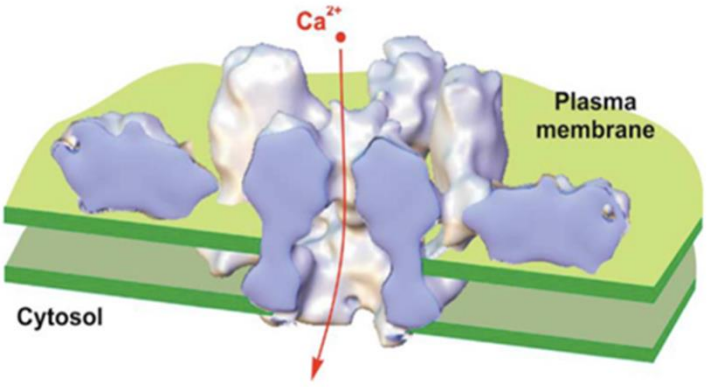

Fig. 8. A model of the α-Ltx pore in membrane bilayer. The base of the tetramer fully penetrates the membrane, whilst the wings are attached to the outer membrane surface. Cations can enter the cytosol through the channel, as shown by the arrow. From Ushkaryov et al. 2004.

The effects of α-Ltx at NMJ can be observed starting from 10 minutes from toxin administration. Electrophysiologically it causes an increase in the frequency of spontaneous miniature postsynaptic potentials (mepps), and it also affects evoked action potentials (epps) and synchronous release in a time-dependent manner, eventually inhibiting them, thus leading to skeletal muscles paralysis [49, 56, 57].

Electron microscopy studies show that in the earliest stages of intoxication motor nerve terminals become markedly swollen - as a consequence of the toxin-mediated entry of cations – and depleted of synaptic vesicles - due to the massive vesicle fusion; mitochondria appear also swollen and rounded (Fig. 9) [44, 58]. The massive calcium influx also cause the activation of calcium-dependent proteases – such as calpains -, triggering cytoskeletal

fragmentation [59]: thus, in a later stage of intoxication, nerve terminals completely degenerate, losing both their structure and their functionality.

Noteworthy, the nerve terminal regenerates in a short time, leading to a fully recovery of the NMJ [44].

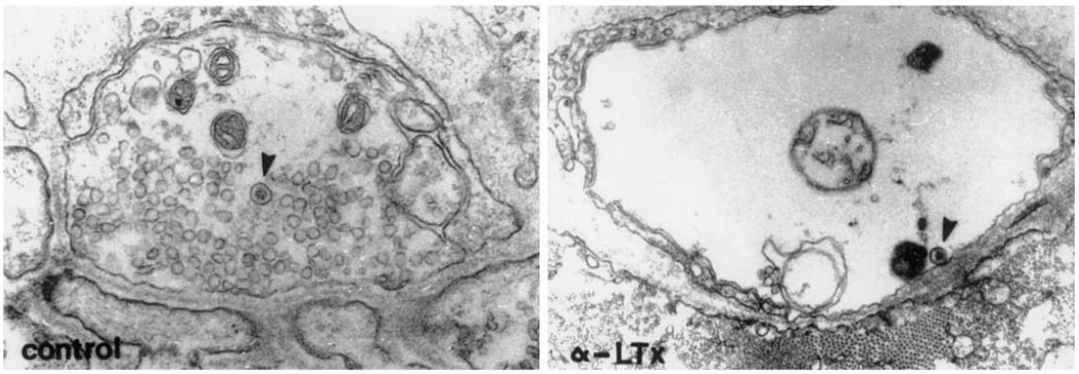

Fig. 9. Electron microscopy of a frog NMJ treated with α-Ltx. α-Ltx causes a massive release of small synaptic vesicles. This leads to an enlargement of the plasmalemma and a total depletion of the neurotransmitter containing vesicles, but not of the large dense-core vesicles containing neuropeptides (arrow). Nerve terminal is swollen as a consequence of a toxin-mediated entry of cations. From Matteoli et al. 1988.

1.3.1.2 Presynaptic snake neurotoxins endowed with PLA2 activity (SPANs)

Presynaptic snake neurotoxins endowed with PLA2 activity are major components of the venom of four families of venomous snakes (*Crotalidae, Elapidae, Hydrophiidae* and *Viperidae*) (Fig. 10) [60, 61, 45, 62]. These neurotoxins play a major role in the envenomation of the prey by causing a persistent blockade of neurotransmitter release from nerve terminals [63, 64]. Several venom components are biologically active but most of the neurological signs and symptoms are due to SPANs action.

Fig. 10. Major families of venomous snakes containing SPANs in their venoms. *Notechis scutatus* (top left), *Bungarus multicinctus*(top right), *Oxyuranu sscutellatus* (bottom left), and *Pseudonaja textilis* (bottom right) are elapid snakes originary from Australia and South East of Asia. Their venom contains the highly neurotoxic phospholipases A2 responsible for the neuromuscular paralysis of their prey.

Phospholipases are enzymes that hydrolyze phospholipids into fatty acids and other lipophilic substances; there are four major classes, termed A1, A2, C and D, distinguished by the type of reaction they catalyze. Phospholipases A2 hydrolyze the sn-2 acyl bond of phospholipids generating fatty acids and lysophospholipids.

More than 800 different PLA2s have been classified, depending on their structure and mechanism of action; the two most notable families comprise cytosolic and secreted PLA2s. SPANs belong to the latter group, which also includes mammalian isoforms implicated in the digestion of phospholipids compounds in dietary fat, as well as in the production of inflammatory mediators.

Secreted PLA2s were the first type of PLA2 enzymes discovered: they are characterized by a low molecular weight (m.w. 13-15 kDa), one histidine in the catalytic site, calcium bound in the active site, and six conserved disulfide bonds - with one or two variable disulfide bonds.

Depending on their quaternary structure, SPANs are further divided in four classes [63]:

- Class I: includes monomeric toxins with a m.w. ranging from 13 to 15 kDa and 7 disulfide bonds. Notexin, isolated from the venom of *Notechis scutatus*, belongs to this class.
- Class II: includes neurotoxic PLA2s composed of two non-covalently linked homologous subunits, at least one of which endowed with PLA2 activity.
- Class III: includes heterodimers of non-homologues subunits kept together by disulfide bonds. β-Bungarotoxin (β-Btx) from *Bulgarus multicinctus* venom belongs to this group; it is composed by a 120 residues-long subunit, with 6 disulfide bonds and endowed with PLA2 activity, bound by a disulfide bridge to a 7 kDa (60 aa) non PLA2-subunit, homologous to Kunitz protease inhibitors.
- Class IV: includes oligomers composed by homologues non-covalently associated subunits. Taipoxin (Tpx), from the venom of *Oxyranus scutellatus scutellatus* belongs to this class; it is a 40 kDa toxin composed by three subunits: one extremely basic PLA2-endowed subunit, one non-toxic subunit and one glycoprotein with 8 disulfide bonds, non-toxic but endowed with PLA2 activity.

The secondary structure of PLA2 SPANs subunits is highly conserved: it includes 3 α-helix and 2 β-sheets linked by 6 or 7 disulfide bonds, which make the enzyme resistant to proteolysis and denaturation (Fig. 11) [63].

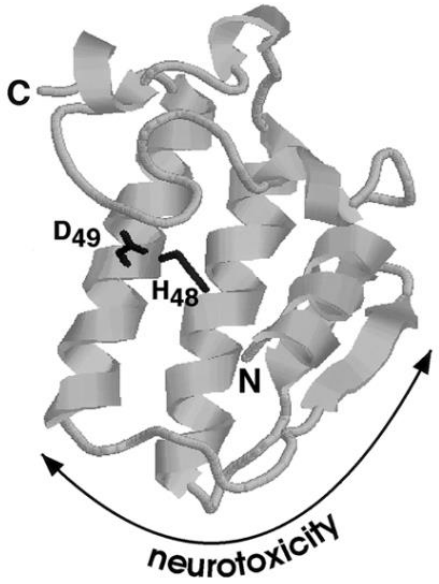

Fig. 11. Ribbon drawing of the 3-dimensional structure of notexin. His-48 and Asp-49 residues essential for PLA2 activity are shown. Chemical modification experiments indicate that neurotoxicity is associated with the bottom part and the right-hand side of the molecule. From Schiavo et al. 2000.

High resolution structural studies revealed that they include a PLA2 domain with a calcium atom that stabilizes and activates the enzyme, which on the other hand can be inactivated by other divalent ions, such as Sr^{2+}, Ba^{2+} and Zn^{2+}. A remarkable feature of PLA2 subunits is a hydrophobic channel that accommodates the fatty acid chain of the phospholipid molecule and places the ester bond to be cleaved into the active site. The key residues directly involved in catalysis are the conserved histidine (His48), which hydrogen-binds the water molecule used for hydrolysis, and an aspartate (Asp49), which positions the Ca^{2+} ion coordinating both the phosphate and the sn-2 carbonyl groups of the phospholipid molecule. In addition, chemical modification studies have identified two segments of the PLA2 subunit involved in neurotoxicity (Fig. 11) [63].

SPANs are widely heterogeneous in structure, enzymatic activity and neurotoxicity; apparently no direct correlation exists between the relative enzymatic activities of snake PLA2 neurotoxins *in vitro* and their lethal potencies *in vivo*. However, a recent study demonstrated that at variance from their enzymatic activities *in vitro*, these neurotoxins display comparable kinetics of lysophospholipids release in cultured neurons, reconciling the large discrepancy between their *in vivo* toxicities and *in vitro* enzymatic activities (table 1) [65]. Anyway, beside the PLA2 activity, toxicity depends also on many pharmacokinetics parameters, including site of injection, toxin redistribution within the body, presynaptic binding, sequestration, degradation, neutralization and excretion.

	In vivo PLA_2 activity (nmols of PL hydrolysed/ min/nmol of toxin)	*In vitro* PLA_2 activity (nmols of PL hydrolysed/ min/nmol of toxin)	*In vitro* PLA_2 activity[a] (nmols of PL hydrolysed/ min/nmol of toxin)	Toxicity[a] (mouse LD50, μg/kg)
Ntx	49 ± 14	5009 ± 29	19 460	45
β-Btx	41 ± 12	4578 ± 149	1281	30
Tpx	19 ± 5	4500 ± 668	18	2
Tetx	15 ± 4	700 ± 248	224	1

SPANs, snake pre-synaptic PLA_2 neurotoxins; Ntx, notexin; Tpx, taipoxin; Tetx, textilotoxin; β-Btx, β-bungarotoxin; PL, phospholipids.
The data obtained here (first and second column) are the means of at least three independent experiments ± SD.
[a]Data from Rosenberg (1997).

Table 1. Comparison between PLA2 activity of four SPANs on cultured neurons and on synthetic substrates and relative toxicity. From Paoli et al., 2000.

Neurotoxicity results from the coexistence of several factors: the ability to recognize the nerve terminal, to bind efficiently and to concentrate there the enzymatic activity, and the capability of efficiently hydrolyzing phospholipids of the presynaptic membrane. Despite the high specificity of SPANs for motor axon terminals, at present no receptors for SPANs have been identified at the level of presynaptic membrane, with the exception of β-Btx, which has been shown to bind to a class of voltage-dependent K^+ channels, blocking them [66]. However, the kinetics of paralysis of the pray after snake bite and after SPANs injection suggest that they rapidly find their way to peripheral nerve terminals, to which they bind quickly and specifically [45, 64, 67] .

A very interesting proposal for the binding of SPANs comes from Montecucco at al., 2004, where the concept of "Array of Presynaptic Receptors" (APR) developed for botulinum neurotoxins (BoNTs) is proposed to be extended also to SPANs [68]. In this paper, APRs are hypothesized to be dynamic microdomains of the presynaptic membrane where several molecules endowed with neurotoxins-binding properties are localized. The oligosaccharide portions of polysialogangliosides are suggested to act as initial neurotoxins-binding factors because of their high local concentration on the presynaptic membrane, their high lateral mobility and the ability of the oligosaccharide moiety to act as "antennas" that can engage multiple bonds and thus effectively capture neurotoxins molecules present in the intersynaptic fluid. This first "capture step", which is expected to be reversible and fast on-rate, brings about a very large membrane concentration effect, and is followed by additional interactions with arrays of receptors molecules, arranged in membrane microdomains, which render the neurotoxin binding practically irreversible. In the light of the blockade of

neurotransmission by the toxins, it is tempting to speculate that APRs coincide with the active zones of the presynaptic membrane, where synaptic vesicle fusion takes place.

Once bound to the presynaptic plasma membrane, SPANs start hydrolyzing phospholipids, generating mainly lysophosphatidylcholine (LysoPC) and fatty acids (FAs) (Fig. 12), with low amounts of lysophosphatidyl-ethanolamine and -serine [69, 65]. This indicate that SPANs act mainly on the outside leaflet of the plasma membrane, as phosphatidylcholine is the major phospholipid of this layer.

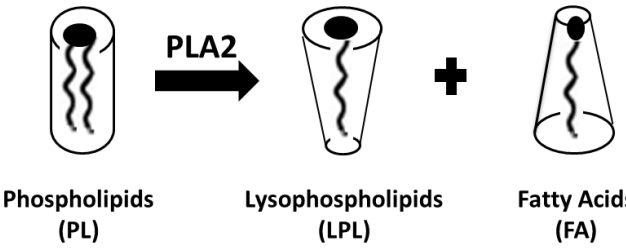

Fig. 12. Major lipid products of PLA2 activity. SPANs enzymatic activity on presynaptic membrane generates lysophospholipids and fatty acids; the molecular shape of these lipid products – inverted-cone and conic, respectively – is not compatible with the bilayer membrane structure, whose curvature is altered following their accumulation.

Under physiological conditions, such lyso-lipids are present only in minute amounts, as their molecular shape is not compatible with the bilayer membrane structure [70]. Indeed, LysoPC is an inverted cone-shaped lipid which forms spheroidal micelles, and FAs are cone-shaped (Fig. 12); moreover, LysoPC cannot flip-flop across the lipid bilayer of the membrane, whereas FAs are capable of a very rapid *trans*-bilayer movement. Consequently, as FAs are produced by SPANs on the external leaflet of the plasma membrane, they redistribute among the two membrane layers, whereas LysoPC remains outside (Fig. 13). In such way LysoPC, which induces a positive curvature of the membrane, is present in *trans*, and FAs, which induce a negative curvature, are present in *cis* with respect to the fusion site of synaptic vesicles [71, 72].

It has been experimentally documented that this membrane conformation promotes ready-to-release synaptic vesicle fusion via pore formation from an hemifusion intermediate, with release of their neurotransmitter content in the extracellular compartment (Fig. 13) [72, 73, 74]. At the same time, for the same membrane topological reasons, the opposite process of endocytosis is inhibited, thus leading to a strong imbalance in the exo- endocytosis cycle.

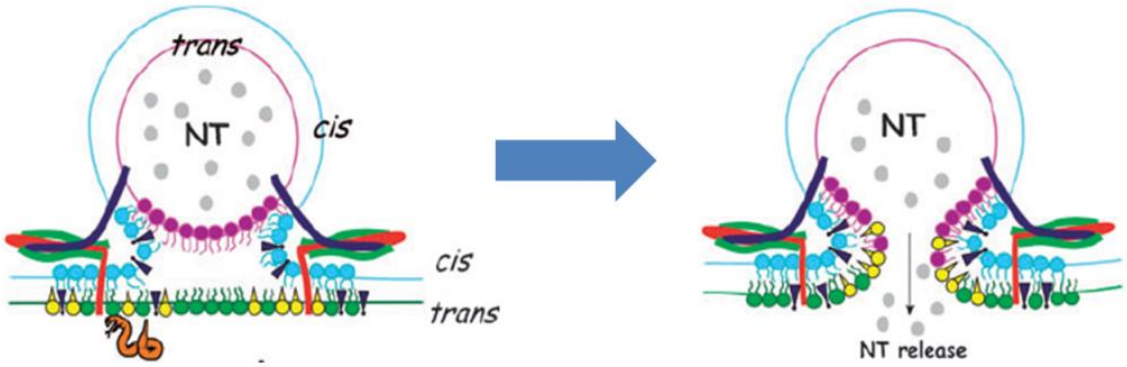

Fig. 13. SPANs action promotes the exocytosis of already-docked synaptic vesicles. Left: SPANs PLA2 activity on the external layer of presynaptic plasma membrane generates LysoPC (yellow) and FA (black). Accumulation of lysolipids alters the plasma membrane curvature, promoting the fusion of already-docked synaptic vesicles via pore formation from an hemifusion intermediate (right). From Rossetto et al., 2006.

Moreover, accumulation of LysoPC and FAs alters plasma membrane permeability, allowing the formation of transition pores which mediate transient calcium currents to the cytosol [75].

The key-role of the PLA2 lipidic products in the process of nerve degeneration upon SPANs intoxication has been further confirmed by the evidence that equimolar mixtures of FA and LysoPLs closely mimic the effect of the toxins on nerve terminals [69].

Similarly to α-Ltx intoxication, calcium overload in the presynaptic nerve terminal enhances the fusion of both ready-to-release and reserve synaptic vesicle pools, also leading to mitochondria impairment and calcium-dependent enzymes activation [76, 59, 60, 77]. In addition, SPANs can enter neurons *in-vitro* and selectively bind to mitochondria, inducing the opening of the mitochondrial permeability transition pore (mPTP): as a result of this interaction, mitochondria depolarize and undergo a profound shape change, from elongated to rounded and swollen, together with impairment in functionality [78].

When SPANs are added to *ex-vivo* nerve-muscle preparations, neurotransmission fails with a triphasic trend: an initial phase of weak inhibition of Ach release is followed by a second prolonged phase of facilitated release, and then by a third one of progressive decline of neurotransmission [79].

Electron microscopy pictures taken at the third stage show swollen and enlarged nerve terminals, with depletion of synaptic vesicles; several clathrin-coated Ω-shaped plasma membrane invaginations are observed at the plasma membrane level, as a consequence of abortive attempts of endocytosis; at a later stage, mitochondria appear damaged, with

altered cristae and large vacuoles (Fig. 14) [60, 45, 77]. As it happens with α-Ltx, also SPANs intoxication eventually leads to a complete degeneration of nerve terminals, which is followed in few days by regeneration and rescue from muscle paralysis [45].

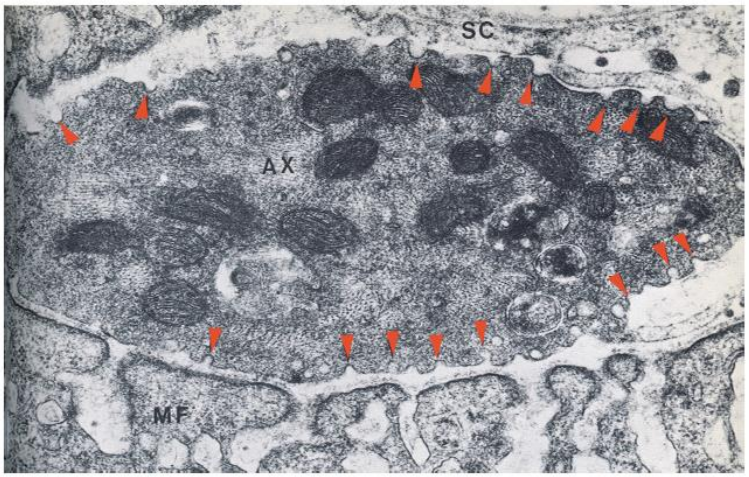

Fig. 14. Electron microscopy of a mouse neuromuscular junction intoxicated with taipoxin. The axon terminal is almost devoid of synaptic vesicles and shows numerous axolemma indentations, signs of unsuccessful endocytosis events (red arrowheads). Mitochondria look rounded-shaped and swollen. From Cull-Candy et al., 1976.

1.3.2 Experimental models to study animal presynaptic neurotoxins mechanism of action

Ex-vivo nerve-muscle preparations have been for a long time the election experimental model for the characterization of the effects of animal presynaptic neurotoxins; indeed, *ex-vivo* NMJ is an ideal tool, since it represents the target site of these neurotoxins *in-vivo*.
Electrophysiological recordings as well as electron microscopy studies on intoxicated NMJs have shed light on many aspects of the intoxication processes, both from a functional and a morphological point of view, and much of our knowledge about the effects of SPANs and α-Ltx arises from these kinds of experimental approaches.
Despite many studies, the molecular mechanism of action of these neurotoxins have remained elusive for a long time. Owing to the complexity of the anatomically fine structure of NMJ and to the inherent limited possibility of experimental manipulation of this tissue preparation, further progress has required the validation of *in-vitro* neuronal models amenable to biochemical and imaging investigations. Several studies have been performed in order to characterize the neurotoxic effects of SPANs and α-Ltx on different kinds of primary cultured neurons from rats; in addition to cultured spinal motorneurons (MNs), also

cerebellar granular neurons (CGNs), cortical neurons and hippocampal neurons were found to be extremely sensitive to animal neurotoxins action, despite they belong to the CNS, thus not representing the real *in-vivo* target site of intoxication [75, 76, 78].

A recent side by side comparative study of SPANs and α-Ltx action on primary cultured neurons showed that, despite the different molecular mechanism of intoxication, both kind of toxins exert their degenerative activity via inducing a large calcium influx [43]. The earliest morphological sign of intoxication by both SPANs and α-Ltx is the formation of swellings along neurites, called *bulges*, hallmarks of neurotoxicity (Fig. 15). Bulges are sites of unbalanced endo-exocytosis, since they expose on their surface the luminal domain of proteins of the synaptic vesicles membrane. With both toxins bulges accumulate calcium right inside (Fig. 15), although with different kinetics, which are accounted for by the different biochemical activities of the two types of toxins. Calcium overload triggers a series of degenerative events, such as the activation of calpains [59] - which are responsible for cytoskeleton degradation -, and the impairment of mitochondria, which become depolarized and swollen [75, 78].

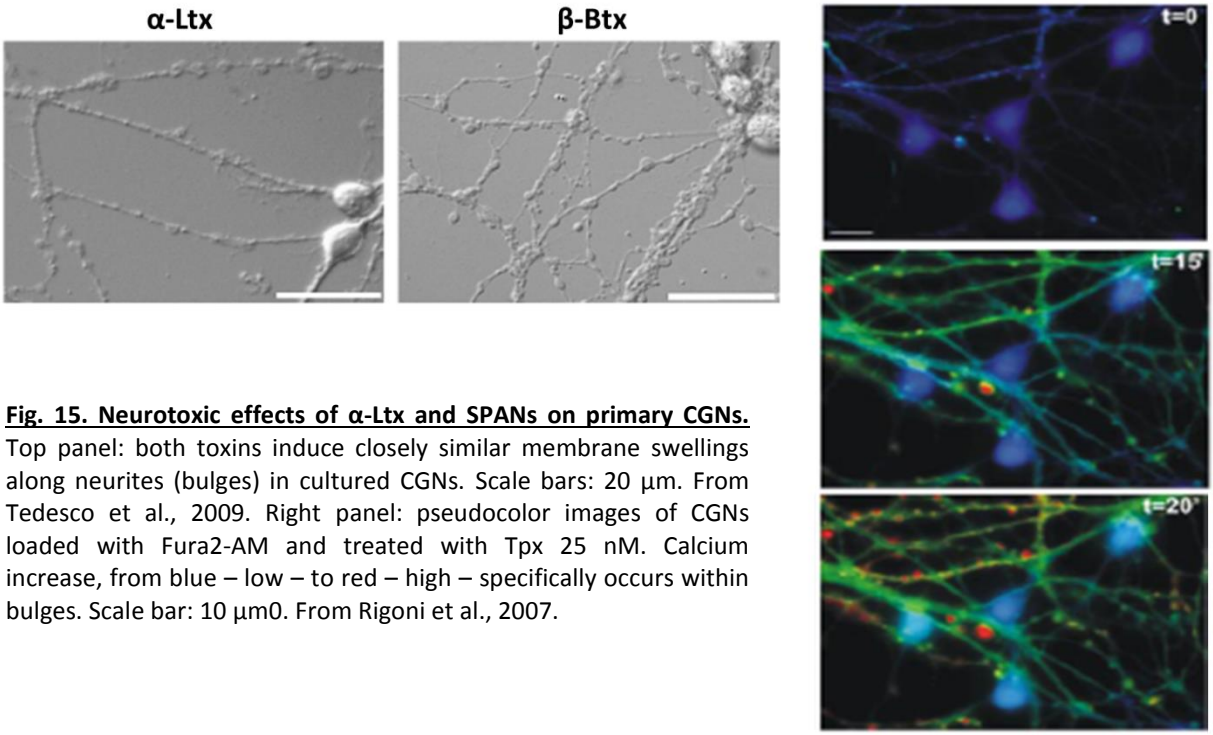

Fig. 15. Neurotoxic effects of α-Ltx and SPANs on primary CGNs. Top panel: both toxins induce closely similar membrane swellings along neurites (bulges) in cultured CGNs. Scale bars: 20 µm. From Tedesco et al., 2009. Right panel: pseudocolor images of CGNs loaded with Fura2-AM and treated with Tpx 25 nM. Calcium increase, from blue – low – to red – high – specifically occurs within bulges. Scale bar: 10 µm0. From Rigoni et al., 2007.

These *in-vitro* experimental models well reproduce the neurotoxic effects observed at the NMJ – i.e. membrane swelling, imbalanced endo-exocytosis, cytoskeleton fragmentation, mitochondria impairment – thus representing a reliable and simpler alternative approach to advance our understanding of the mechanism of action and toxicity of SPANs and α-Ltx.

1.4 MITOCHONDRIAL-DERIVED ALARMINS

Cell death and injury often lead to the release intracellular molecules called damage-associated molecular patterns (DAMPs) [80, 81]; they can result from tissue injury, secretion, release and/or exposure on the outer leaflet of the plasma membrane of normally intracellularly-sequestered molecules or their derivatives. Once released or exposed extracellularly, DAMPs activate the innate immune-response through their interaction with pattern recognition receptors – the same receptors that detect pathogen associated molecular patterns (PAMPs) [82] -, thus revealing similarities between pathogen-induced and non-infectious inflammatory responses.

Many DAMPs derive from plasma membrane, nucleus, endoplasmic reticulum and cytosol. Recently, mitochondria have emerged as major sources of DAMPs [83]. Mitochondria host several essential metabolic processes of apoptotic and necrotic cell death; according to the endosymbiontic hypothesis, mitochondria still possess many morphological and biochemical features of their bacterial ancestors – such as the circular genome containing CpG DNA and the presence of N-formyl peptides (NFPs) – which make them ideal candidates as a source of PAMP-like DAMPs.

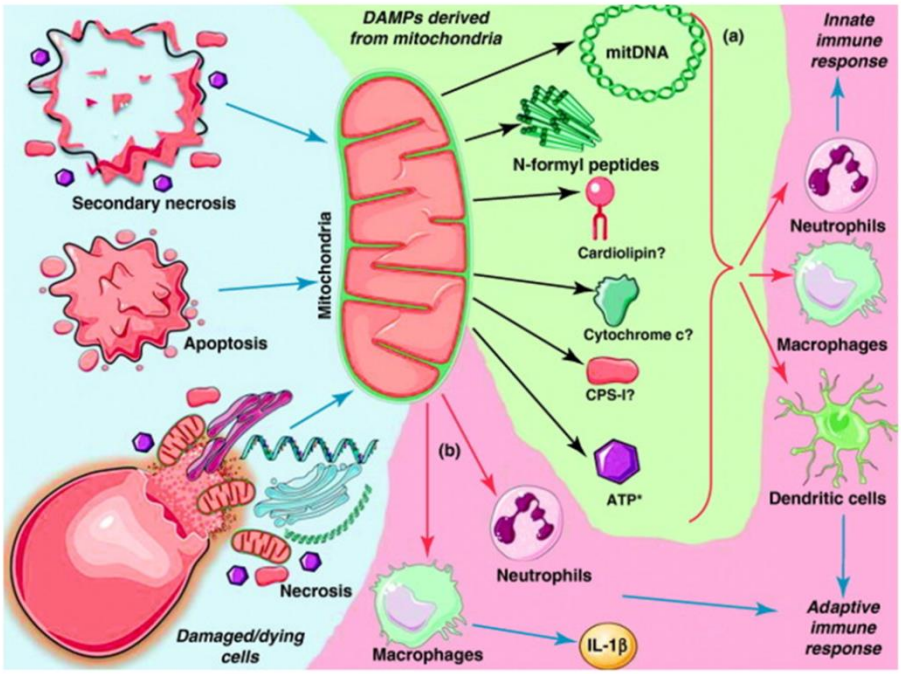

Fig. 16. DAMPs derived from mitochondria. (a) Mitochondrial DNA, N-formyl peptides and cytochrome c are examples of mito-DAMPs that once released into the extracellular space – following cell death or tissue injury - can stimulate the innate and adaptive immune responses. (b) Intact mitochondria derived from cells dying by accidental necrosis after mechanical disruption can induce IL-1b production by macrophages, and attract neutrophils upon i.p. injection. Question marks indicate links that are not yet proven. From Krysko et al., 2011.

Emblematic examples of mitochondrial derived DAMPs are mitochondrial DNA (mtDNA), which activates phagocytes through its binding to Toll-like receptor 9 [83, 84], NFPs, which act as chemoattractants by interacting with formyl-peptide receptors (FPRs) [85, 86], and cytochrome c (Cyt c), which is also endowed with pro-inflammatory activities, although still not well documented [87] (Fig. 16).

Involvement of mitochondrial DAMPs has already been demonstrated in many pathological conditions, including trauma, SIRS [88, 89, 83, 90], rheumathoid arthritis [84], liver injuries [91] and myocardial infarction [92], as well as following snake myotoxins-induced muscle damage [93], where they contribute to the local or systemic inflammatory responses associated with such conditions. Moreover, we found that mtDNA and cytochrome c are also released by cultured neurons upon intoxication with snake and spider neurotoxins [42].

Recently, reactive oxygen species (ROS), which are efficiently produced by mitochondria under stressing and oxidizing conditions, are also emerging as important mitochondria-derived alarmins, being involved in many intra- and inter-cellular signalling.

1.4.1 Hydrogen peroxide as signalling molecule

ROS have long been regarded as harmful molecules generated as by-products of respiration, causing oxidative damages to various cellular components. The accumulation of such damages is thought to be responsible for ageing and multiple disorders, such as cancers, neurodegenerative diseases and diabetes mellitus [94]. However, accumulating evidences from recent studies have uncovered a role for oxidants as essential second messengers in many intra- and inter-cellular signalling pathways [95, 96, 97].

ROS are generated by multiple processes and enzymes, such as NADPH oxidases (Nox and Dual oxidases) in the plasma membrane, lipid metabolism in peroxisomes, and cytosolic enzymes such as cyclo-oxygenases. However, the major source of ROS in aerobic cells is cellular respiration and oxidative phosphorylation within the mitochondria, and this production is extremely enhanced under many stressing conditions.

Mitochondrial-ROS (mtROS) such as superoxide ($O_2^{\bullet -}$) are thought to be short lived *in-vivo*, being converted to more stable species such as hydrogen peroxide (H_2O_2): this process can occur spontaneously, but is enhanced at least 1000-fold by superoxide dismutases (SOD). H_2O_2 is the most abundant ROS, with the highest half-life; the relative stability and uncharged nature of H_2O_2 permits its enhanced diffusion across long distances and

membranes. Owing to these peculiar features, H_2O_2 represents an ideal candidate to act as both an intracellular messenger and a paracrine signal [95, 98].

Contrary to the great advances in understanding the ROS-generation mechanism, the molecular signalling events downstream of ROS are poorly understood. An important cellular target or "sensor" of ROS is the thiol (RSH) functional group of the amino acid cysteine, which can exist in a number of oxidation states and form disulfide bonds with another thiol moiety [99]. Several proteins have been shown to function as ROS effectors, modifying their function following cysteines oxidation, thus enabling signal transmission to downstream targets. The number of redox-responsive proteins is increasingly accumulating: among them protein tyrosine phosphatases (PTPs), thioredoxins (TRXs) and peroxiredoxins (PRXs) family proteins share special protein structures that contain redox-active cysteines, which sensitively respond to ROS. Progress in the identification of ROS-effector proteins is revealing the pleiotropic functions of mtROS in many physiological and pathological processes, which can range from cell proliferation [100], regulation of mitophagy and autophagy [101], adaptation to hypoxia [102, 103] and regulation of immunity [104].

Unexpected roles for extracellular ROS are also emerging in a wide range of contexts; extracellular ROS have long been known to play antimicrobial roles after tissue injury or infection, in a process known as respiratory burst. Recent experimental evidence in different animal models demonstrates that a rapid concentration gradient of H_2O_2 functions as a long-range chemoattractant that recruits leukocytes at wound sites [105, 106]. Furthermore, recent studies highlight the crucial roles of injury-induced ROS, and in particular of H_2O_2, in several cellular processes involved in tissue regeneration [107]: Love et al. (2013) showed that amputation-induced ROS are required for successful *Xenopus* tadpole tail regeneration, since lowering ROS levels by pharmacological or genetic approaches reduces the level of cell proliferation through the inhibition of the Wnt/β-catenin signalling [108]. mtROS inhibition also delays actin-based wound closure in *Caenorhabditis elegans* [109].

In the light of these findings, the understanding of ROS signaling and redox regulation of protein function are of crucial importance and may lead to the development of new therapeutic strategies.

2. AIM

The PNS can spontaneously regrowth injured axons; this ability can be attributed to both intrinsic regenerative capacity of neurons, and to the favourable environment which surrounds them. Indeed, the glia of PNS, SCs, has been shown to actively participate in the process of nerve regrowth, providing essential supports to stimulate neuronal regenerative response [30, 31].

PSCs play crucial roles in the regeneration of nerve terminals at NMJs, thus promoting the re-innervation of muscle end-plates: in response to denervation, they de-differentiate, contribute to the clearing-up of nerve debris and extend cytosolic processes which induce and guide nerve terminals re-growth [25].

Although clearly documented, the regeneration of motor axon terminals is still ill-known in many cellular and molecular aspects; therefore, the aim of this work is to shed light on the crosstalk between degenerating nerve terminals and adjacent PSCs at NMJs. More in detail, we would like to identify molecular mediator/s involved in PSCs activation and in nerve regeneration: such findings could also provide information useful to the understanding and treatment of some pathological syndromes.

We adopted an innovative experimental approach based on the use of some animal presynaptic neurotoxins – α-Ltx and SPANs – to induce a localized and reversible nerve degeneration [42]. This model provides the advantage of being much more controlled and reproducible than the traditional cut/crush surgical approaches: indeed, these presynaptic neurotoxins target specifically the motor axon terminals inducing a localized entry of calcium, which cause a degeneration limited and self-contained to the end-plate, thus confining the damage at the NMJ; importantly, a complete and functional regeneration is achieved in few days following intoxication [44, 45].

Thus, this work is also aimed at validating this neurotoxins-based approach as a relevant model to study motor axon terminal degeneration and regeneration, which allows a better characterization of PSCs contribution to these processes.

3. MATERIALS AND METHODS

3.1 MATERIALS

Toxins. α-Ltx and Tpx were purchased from Alomone, β-Btx from SIGMA. The purity of the toxins was checked by SDS-PAGE and their neurotoxicity by *ex-vivo* mouse nerve-hemidiaphragm preparation as previously described [69].

Chemicals. Unless otherwise stated all reagents were purchased from SIGMA.

Animal strains. C57BL/6 mice expressing cytosolic GFP under the *plp* promoter [110, 111] were kindly provided by Dr. W.B. Macklin (Aurora, Colorado) via the collaboration of Dr. T. Misgeld (Munchen, Germany). All experiments were performed in accordance with Italian animal care guidelines, law no. 116/1992.

3.2 METHODS

3.2.1 Primary cells cultures

3.2.1.1 Cerebellar granular neurons

Rat cerebellar granular neurons (CGNs) were prepared from 6-days-old Wistar rats as described elsewhere [112]. Briefly, neurons were isolated from freshly dissected cerebella by mechanical disruption in the presence of trypsin (0,08% m/w) and DNase I (0,08 mg/ml) and then seeded onto 24-wells culture plates coated with poly-L-lysine (10 μg/ml). Cells were seeded at a density of 3 x 10^5/well in BME (Life Technologies) supplemented with 10% FBS (Euroclone), 25 mM KCl, 2 mM glutamine and 50 μg/ml gentamycin. Cultures were maintained at 37 °C in a humidified atmosphere of 95% air, 5% CO_2. Cytosine arabinoside (10 μM) was added to the culture medium 18-24 hours after plating to arrest the growth of non-neuronal cells. Experiments were performed at 6 days *in-vitro*.

3.2.1.2 Spinal motoneurons

Primary rat spinal motoneurons (MNs) were isolated from Sprague-Dawley rat embryos (embryonic day 14) and cultured following previously described protocols [113]. Briefly,

spinal cords were dissected from E14 rat embryos, treated with trypsin (0,025% m/w) and DNase (0,1 mg/ml) and collected under a bovine serum albumin (BSA) cushion. Cells were then resuspended in Neurobasal medium (Life Technologies) supplemented with 2% B27 supplement (Life Technologies), 2% horse serum (Euroclone), 0,5 mM glutamine, 25 μM 2-mercaptoethanol, 10 ng/ml CNTF (R&D Systems), 100 pg/ml GDNF (R&D Systems), 5 μg/ml Pen/Strep and 25 μM L-glutamic acid, and seeded on poly-ornithine and laminin coated plates. Cultures were maintained at 37 °C in a humidified atmosphere of 95% air, 5% CO_2, and experiments were performed at 6 days *in-vitro*.

3.2.1.3 Schwann cells

Primary SCs were purified from sciatic nerves of six P3 Wistar rats. Briefly, sciatic nerves were dissected and tissues digested in 0.1% w/v collagenase, 0.25% w/v trypsin in L15 medium (Life Technologies) plus 0.3% BSA for 1 h. Dissociated cells were seeded onto uncoated Petri dishes in DMEM (Life Technologies) 10% FBS and 50 μg/ml gentamycin; 24 h after seeding 10 μM arabinoside C was added to the medium and kept for 2 days to prevent fibroblasts mitosis. Five days after seeding an immunopanning with an anti-Thy1.1 antibody (1:500, 30 min at 37 °C) followed by rat complement addition (1:10, 2 hours) were performed to eliminate contaminating fibroblasts. Purified SCs were subsequently plated on poly-L-lysine-coated dishes and allowed to grow in Expansion Medium consisting of DMEM, supplemented with 10% FBS, 2 μM forskolin and 10 nM heregulin β-1. SCs were then seeded on laminin-coated 24 wells-dishes (2 x 10^4 cells/well) and kept in Expansium Medium.

3.2.1.4 Neurons-SCs co-cultures

CGNs and spinal MNs were used to set up co-cultures with primary SCs. Briefly, 4 days after primary neurons seeding, primary SCs were added to neuronal cultures at an average density of 1 x 10^4 cells/cm^2. Co-cultures were kept for 2-3 days in CGNs or MNs medium respectively.

3.2.2 Cell treatments

CGNs, spinal MNs or neurons-SCs co-cultures (6 d.i.v.) plated onto 24 wells-plates were exposed for different incubation time to SPANs (6 nM) or to α-Ltx (0.1 nM) at 37°C in Krebs Ringer Buffer (KRH: Hepes 25 mM, pH 7.4, NaCl 124 mM, KCl 5 mM, MgSO4 1.25 mM, CaCl2 1.25 mM, KH2PO4 1.25 mM, glucose 8 mM, pH 7,4). In a set of experiments, CGNs were treated with PMA (phorbol 12-myristate 13-acetate) 500 µg/ml for 20 min in KRH at 37°C.
Primary SCs were exposed to different amounts of H_2O_2 (10 µM or 100 µM) for different incubation times or with SPANs (6 nM) or α-Ltx (0.1 nM) for 60 min in KRH at 37°C.
In some experiments, primary neurons, SCs or co-cultures were pre-incubated for 5 min with 1000 U/well catalase or for 1 hour with the MEK1 inhibitor PD98059 (80 µM) (Cell Signaling) before toxin addition; catalase and PD98059 were kept throughout the experiments.
Samples were then processed for Western blotting or immunofluorescence.

3.2.3 Western Blot

Primary cell cultures were treated as described above, and then lysed in Lysis Buffer (Hepes 10 mM, NaCl 150 mM, SDS 1%, EDTA 4 mM, protease inhibitors cocktail (Roche), and phosphatase inhibitor cocktail). Samples were then denaturated at 95°C for 5 min, loaded on precast 4-12% SDS-polyacrylamide gels (Life Technologies) and transferred to a nitrocellulose membrane in a refrigerated chamber. Following saturation, membranes were incubated o.n. with primary antibodies (polyclonal anti-Phospho-p44/42 MAPK, Cell Signaling, 1:1000, monoclonal anti-Hsc70, Synaptic Systems, 1:10000, monoclonal anti-Hsp90, BD transduction Laboratories, 1:1000), followed by a secondary antibody HRP-coniugated (Life Technologies, 1:10000). Chemiluminescence was developed with Luminata TM Crescendo (Millipore) or ECL Advance western blotting detection system (GE Healthcare), and emission measured with ChemiDoc XRS (Bio-Rad). For densitometric quantification the software Quantity One (Bio-Rad) was used, and the bands of interest were normalized to the housekeeping protein Hsc70 or Hsp90. None of the bands reached signal saturation.

3.2.4 Immunofluorescence

Following treatments, isolated SCs or co-cultures were fixed for 15 min in 4% PFA in PBS, quenched (0.38% glycine, 0.24% NH_4Cl in PBS) and permeabilized with 0.3% Triton X-100 in PBS for 5 min at RT. After saturation with 3% goat serum in PBS for 1 h, samples were incubated with primary antibodies (polyclonal anti-Phospho-p44/42 MAPK, Cell Signaling, 1:1000; monoclonal anti- anti-NF200, SIGMA, 1:200; monoclonal anti-S100, SIGMA, 1:1000; polyclonal anti p47Phox, Santa Cruz, 1:200) diluted in 3% goat serum in PBS o.n. at 4°C, washed, and then incubated with the correspondent secondary antibodies (Alexa-conjugated, 1:200, Life Technologies) for 1 h at RT. Nuclei were stained with Hoechst. Coverslips were mounted in Mowiol and examined by confocal (Leica SP5) or epifluorescence (Leica CTR6000) microscopy.

3.2.5 Hydrogen peroxide detection

Hydrogen peroxide generation in primary neurons was measured using Mitochondria Peroxy Yellow 1 (MitoPY1) [114] or Peroxyfluor 6 acetoxymethyl ester (PF6-AM) [115], synthesized in the lab of Prof. Chang (Berkeley, California), specific probes that allow to detect H_2O_2 production in mitochondria and cytoplasm respectively. Both probes were loaded at 5 μM for 30 min at 37°C in KRH. Images were acquired at different time points following toxins exposure with a DMI6000 inverted epifluorescence microscope (Leica, Germany) equipped with a 63x HCX PL APO oil immersion objective NA 1.4. Filter cubes (Chroma Technology, USA) have an excitation range of 470/40 nm, a dichroic mirror 495LPXR and an emission of 525/50 nm. Images were acquired with an Orca-Flash4 digital camera (Hamamatsu, Japan). Illumination was kept at a minimum to avoid ROS generation due to phototoxicity. To detect neuronal *bulges* we took advantage of DIC microscopy. Fluorescence intensity quantification was carried on with ImageJ and the statistical analysis with Prism (GraphPad, USA).

3.2.6 NMJ immunohistochemistry

α-Ltx (5 μg/kg) or β-Btx (10 μg/kg) were diluted in 15 μl of physiological saline (0.9% w/v NaCl in distilled water) and injected subcutaneously in proximity of *Levatoris auris longus* (LAL) muscle of anesthetized transgenic C57BL/6 male mice (expressing a cytosolic GFP

under the *plp* promoter [111, 112]) of around 20-25 gr. Control animals were injected with saline. LAL muscles were dissected at different time points after injections and fixed in 4% PFA in PBS for 30 min at RT. Samples were quenched, permeabilized and saturated for 2 h in 15% goat serum, 2% BSA, 0.25% gelatin, 0.20% glycine and 0.5% Triton X-100 in PBS. Incubation with the following primary antibodies was carried out for at least 48 h in blocking solution: anti-neurofilaments (mouse monoclonal, anti-NF200 SIGMA, 1:200), anti-SNAP-25 (SMI81 mouse monoclonal, Covance, 1:200), anti-CD68 (mouse monoclonal, Santa Cruz, 1:200). Muscles were then washed and incubated with secondary antibodies (Alexa-conjugated, 1:200 in PBS, Life Technologies). Nuclei were stained with Hoechst. For p-ERK detection incubation with the primary antibody (anti-Phospho-p44/42 MAPK, Cell Signaling, 1:1000) was carried out for 72 h and the tyramide signal amplification kit (Perkin Elmer) was used [116].

To stain acidic compartments, LAL muscles collected after 4 h of intoxication were loaded *ex-vivo* with LysoTracker Red DND-99 (1:5000, Life Technologies) for 2-3 min [117], while being continuously perfused with oxygenated Neurobasal A medium (Life Technologies). Samples were then fixed and processed for indirect immunohistochemistry as described above. Images were collected with a Leica SP5 Confocal microscope equipped with a 63x HCX PL APO NA 1.4. Laser excitation line, power intensity and emission range were chosen accordingly to each fluorophore in different samples in order to minimize bleed-through.

3.2.7 Electrophysiological recordings

Electrophysiological recordings were performed in oxygenated Krebs-Ringer solution on sham or α-Ltx-injected soleus muscles (α-Ltx 5 μg/kg, with or without 750 U catalase) using intracellular glass microelectrodes (WPI, Germany) filled with one part of 3 M KCl and two parts of 3 M CH_3COOK. In another set of experiments muscles were locally injected with PD98059 (50 μg in DMSO) 1 hour before α-Ltx injection.

Evoked neurotransmitter release was recorded in current-clamp mode and resting membrane potential was adjusted with current injection to −70 mV. Evoked junction potentials (EJPs) were elicited by supramaximal nerve stimulation at 0.5 Hz using a suction microelectrode connected to a S88 stimulator (Grass, USA). To prevent muscle contraction after dissection samples were incubated for 10 min with 1 μM μ-Conotoxin GIIIB (Alomone, Israel). Signals were amplified with intracellular bridge mode amplifier (BA-01X, NPI,

Germany), sampled using a digital interface (NI PCI-6221, National Instruments, USA) and recorded by means of electrophysiological software (WinEDR, Strathclyde University). EJPs measurements were carried out with Clampfit software (Molecular Devices, USA), statistical analysis with Prism (GraphPad Software, USA).

3.2.8 Statistical analysis

The sample size (N) of each experimental group is described in each corresponding figure legend, and at least with three biological replicates were performed. GraphPad Prism software was used for all statistical analyses. Quantitative data displayed as histograms are expressed as means ± SEM (represented as error bars). Results from each group were averaged and used to calculate descriptive statistics. Significance was calculated by Student's t-test (unpaired, two-side). P- values less than 0.05 were considered significant.

4. RESULTS

4.1 HYDROGEN PEROXIDE IS PRODUCED BY NEURONS EXPOSED TO α-Ltx AND SPANs

Mitochondria are abundant subcellular components of the motor axon terminals: upon intoxication with both α-Ltx and SPANs they become severely damaged, as shown in EM pictures of intoxicated NMJs, where they appear swollen and rounded-shaped [58,77]. This is due mainly to the runaway calcium overload in the cytosol, which in turns leads to an excessive calcium accumulation inside the mitochondrial matrix, eventually resulting in mitochondria impairment [43, 75]. In addition to that, SPANs can enter primary cultured neurons and selectively bind to mitochondria, facilitating the opening of their permeability transition pores, thus enhancing the progressive neuronal degeneration [78].

Mitochondria represent the major source of ROS inside cells, since superoxide anion is formed as a side-product during the process of oxidative phosphorylation; however, ROS production is increased under many different stressing conditions, resulting in significant damage of cell structures, in a process known as oxidative stress [94]. Beyond their traditional harmful roles, ROS are recently being recognized also as essential second messengers in many intra- and inter-cellular signalling pathways: in particular H_2O_2, which is much more stable than superoxide and highly diffusible across membranes, is an ideal mediator of signal transduction processes and paracrine communication [95, 107].

Based on these premises, we wondered whether (i) mtROS – and in particular H_2O_2 – are produced by degenerating neurons upon intoxication, and (ii) whether they might play a role in the crosstalk between degenerating nerve terminals and adjacent PSCs at NMJs.

To address the first question, we performed experiments on primary cultured CGNs and spinal MNs, which represent well-established models to study the processes of intoxication with α-Ltx and SPANs *in-vitro.* In order to detect and quantify intracellular H_2O_2, we took advantage of two specific H_2O_2 probes with different cellular localization, kindly given by Prof. Chang. MitoPY1 is a bi-functional molecule that combines a chemoselective boronate-based switch and a mitochondrial-targeting phopshonium moiety for the detection of H_2O_2 localized to mitochondria [114]. PF6-AM on the other hand takes advantage of multiple masked carboxylates to increase cellular retention, and hence sensitivity to low levels of peroxide. In its ester-protected form, PF6-AM can readily enter cells: once in the cytosol, the

protecting group are rapidly cleaved by intracellular esterases to produce their anionic carboxylate forms, which are effectively trapped within cells [115].

We loaded CGNs with H_2O_2-specific probes and then we intoxicated them with spider and snake neurotoxins, monitoring them for up to an hour. After exposure to α-Ltx or Tpx, H_2O_2 levels increased with time, markedly at the level of bulges, as shown in Fig. 17. Bulges are site of calcium overload and impaired mitochondria accumulation, so the localized Mito-PY1-fluorescence increase strongly supports the idea that H_2O_2 is produced by damaged mitochondria upon neurons intoxication.

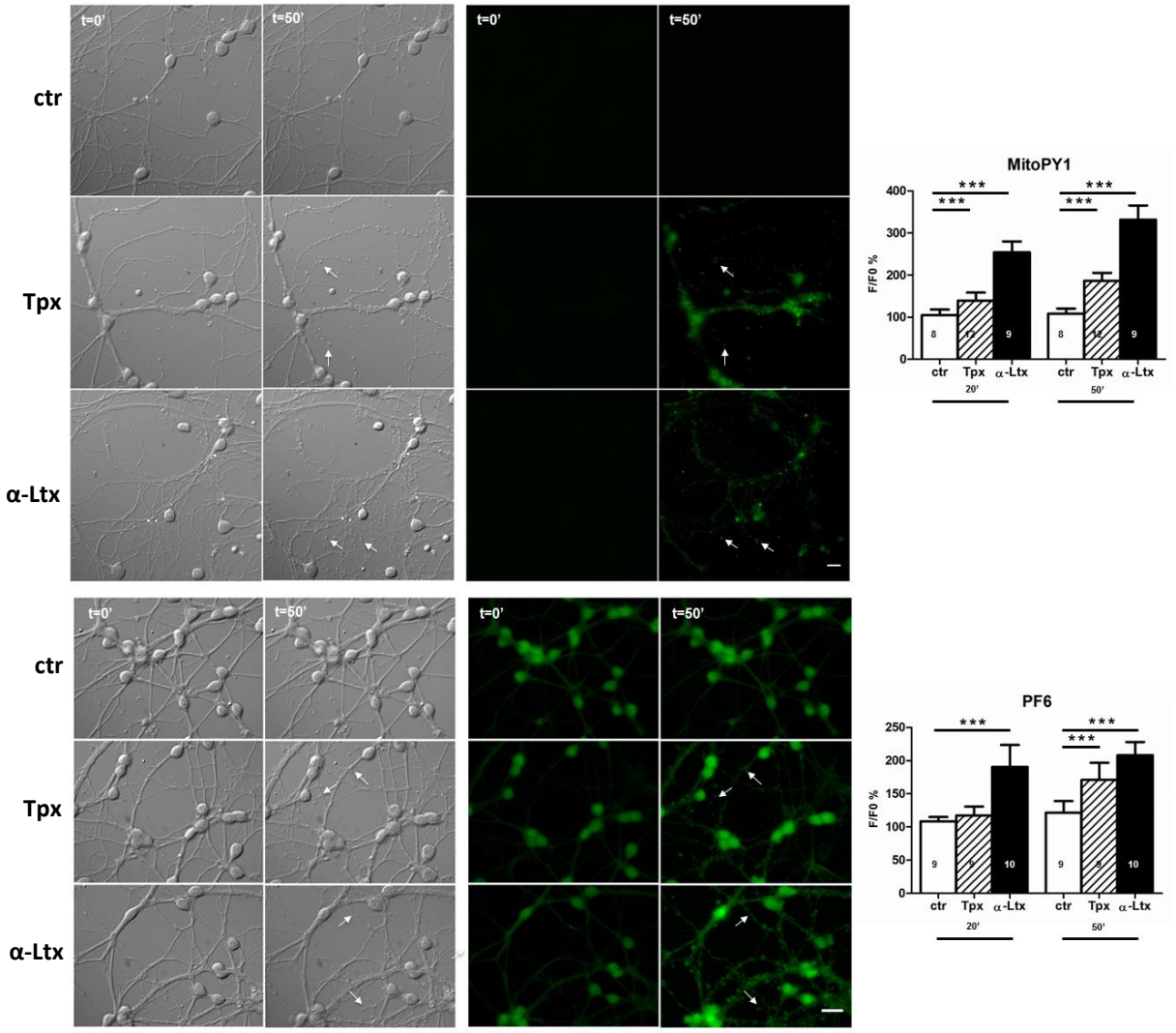

Fig. 17. ***Live-imaging*** **of neuronal hydrogen peroxide production.** Rat CGNs were loaded with the H_2O_2 specific probes MitoPY1 (upper panel) or PF6 (lower panel), washed and then exposed to Tpx 6 nM or to α-Ltx 0.1 nM for 50 min. Changes in fluorescence due to H_2O_2 production were monitored with time and expressed as percentage of the fluorescence value at t=0 (right panels). Arrows in brightfield images and in the green channel point to neuronal *bulges*. Scale bars: 10 μm

H_2O_2 then diffuses to the cytosol, as suggested by the changes in fluorescence of PF6 signal (Fig. 17), and it is reasonable to speculate that it also permeates across the plasma membrane, exiting neurons along its concentration gradient.

Quantification of the fluorescent signal during the time-course of intoxication indicates a more pronounced effect of α-Ltx with respect to Tpx, in agreement with the fact that the pore formed by the former neurotoxin mediates a larger and faster calcium entry than Tpx [43]. Similar kinetics of H_2O_2 production were also observed in rat spinal MNs (Fig. 18).

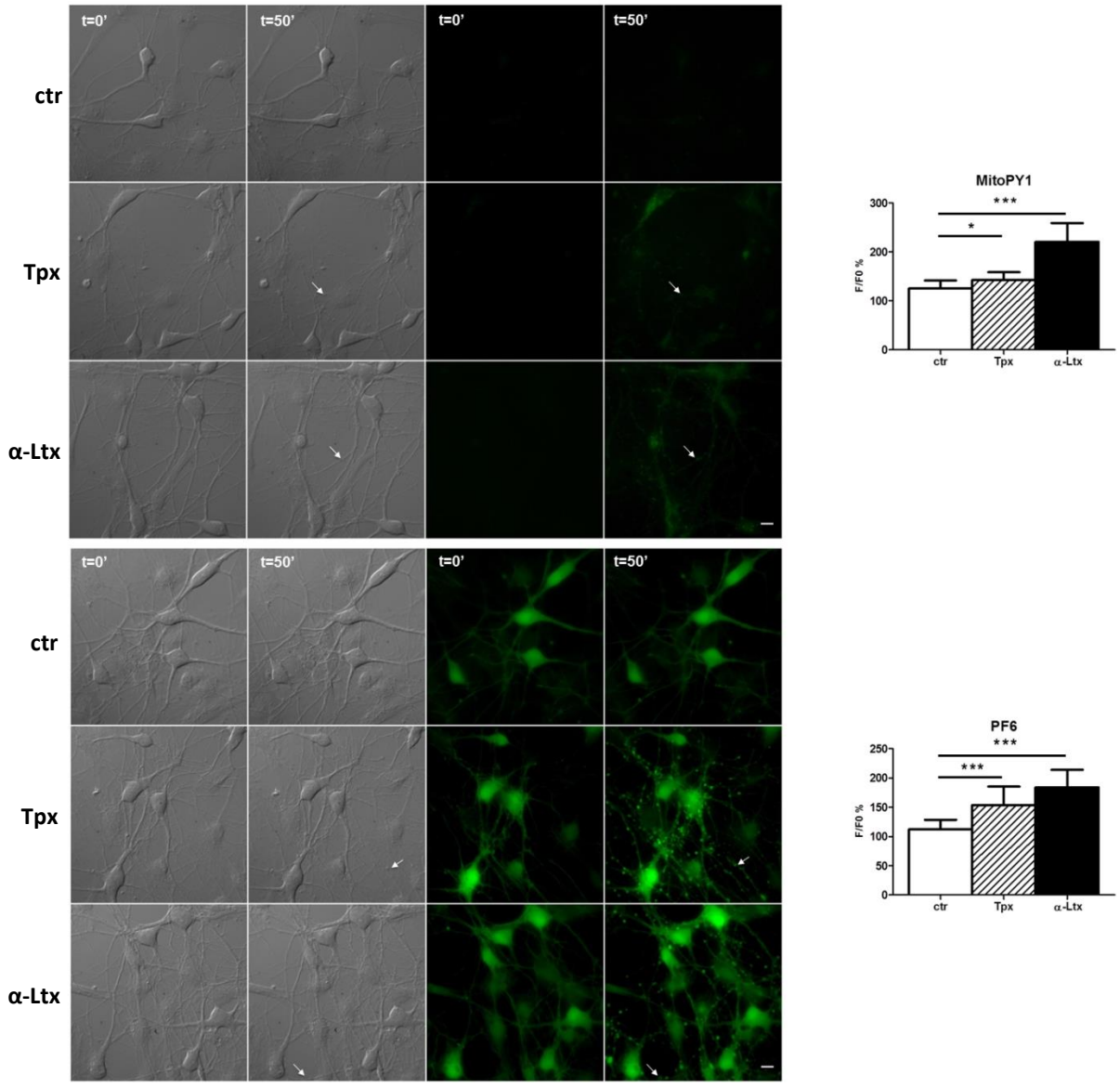

Fig. 18. *Live-imaging* of neuronal hydrogen peroxide production in spinal cord MNs. Rat MNs were loaded with the H_2O_2 specific probes MitoPY1 (upper panel) or PF6 (lower panel), washed and then exposed to Tpx 6 nM or to α-Ltx 0.1 nM for 50 min. Changes in fluorescence due to H_2O_2 production were monitored with time. Arrows in brightfield images and in the green channel point to neuronal *bulges*. Scale bars: 10 μm.

To further confirm the mitochondrial origin of H_2O_2, we checked the activation state of the NADPH oxidase complex in cultured neurons upon intoxication. NADPH oxidases are a family of plasma membrane-associated enzymes which generate superoxide – and thus, indirectly, H_2O_2 – by transferring electrons from NADPH to molecular oxygen. The most thoroughly studied of these isoforms is the leukocyte NADPH oxidase, which is found in professional phagocytes and B lymphocytes; however, other family members are present in a variety of different tissues, including neurons [118]. Activation of NADPH oxidase complex occurs in response to many different stimuli and requires the correct assembly of all the complex subunits; in particular, the cytosolic regulatory component p47phox must be phosphorylated in order to move to the plasma membrane.

To investigate the involvement of NADPH oxidase in our experimental system, we performed immunofluorescence (IF) on treated CGNs, labelling p47phox in order to check its cellular localization. Intoxication of CGNs with α-Ltx did not induce any translocation of p47phox to the plasma membrane, since its staining remained homogeneously distributed in the cytosol (Fig. 19); a similar distribution was also observed in untreated neurons but not in samples treated with PMA - a known trigger of NADPH oxidase activation -, where p47phox signal accumulated at the level of the plasma membrane (Fig. 19). This evidence allowed us to exclude any contribution of the NADPH oxidase system in the production of H_2O_2 observed in cultured neurons upon intoxication.

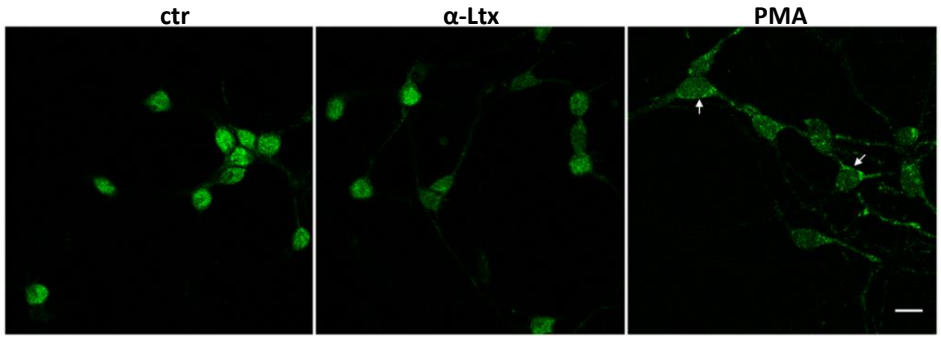

Fig. 19. NADPH oxidase is not involved in hydrogen peroxide production. p47phox staining was performed in CGNs exposed to α-Ltx (0.1 nM for 50 min) or to PMA (500 μg/ml, 20 min) as positive control for p47phox translocation. Arrows point to membrane accumulation of p47phox signal in PMA-treated cells. Scale bar: 10 μm.

4.2 NEURONAL HYDROGEN PEROXIDE ACTIVATES ERK PATHWAY IN SCs *IN VITRO*

First candidate targets of neurons-derived H_2O_2 at intoxicated NMJs are non-myelinating PSCs, which are in close apposition to the motor axon terminal. Thus, we tried to identify the potential target pathway/s of neuronal H_2O_2 in PSCs.

Growing evidence indicates that H_2O_2 is a largely used inter- and intra-cellular signalling molecule regulating kinase driven pathways, mainly through chemoselective oxidation of cysteine residues in signalling proteins [99, 107]. H_2O_2 has indeed been shown to trigger ERK phosphorylation in different cell types [119, 120, 121], with consequent activation of downstream gene transcription.

ERK (extracellular-signal regulated kinase) is a widely expressed MAP-kinase, activated downstream of the Ras-Raf-MEK cascade in the cytosol of cells in response to many different stimuli; this pathway is normally involved in many physiological processes, such as cell differentiation and proliferation. Interestingly, ERK activation has also been shown to drive SCs dedifferentiation *in vitro* and following nerve wounding *in vivo* [122]; it has also been demonstrated that activation of an inducible Raf-kinase transgene in myelinating SCs leads to a severe demyelination – even in the absence of axonal damage – and induces much of the inflammatory response important for nerve repair *in vivo*, identifying ERK pathway as a central player in the process of nerve regeneration [116].

To date nothing is known about the mediator/s responsible for ERK activation in myelinating SCs; it is likely that this rapid, currently unknown signal, derives from damaged axons warning SCs of their intention to degenerate: H_2O_2, produced by neurons mitochondria upon intoxication, is an ideal candidate for this function.

To address the potential role of neuronal H_2O_2 as a paracrine signal for SCs, we checked whether primary cultured SCs isolated from rat sciatic nerves were responsive to H_2O_2 in terms of ERK activation. For this purpose, we analyse ERK phosphorylation levels in SCs by Western blotting (WB) and IF. As shown in Fig. 20, exposure of primary SCs to H_2O_2 led to ERK phosphorylation in a dose- and time-dependent manner, with a peak of p-ERK signal after 20 minutes of incubation. IF results showed that in many cells H_2O_2 treatment induces p-ERK translocation to the nuclei, where it is known to initiate transcriptional programmes controlling cellular responses (Fig. 20) [123].

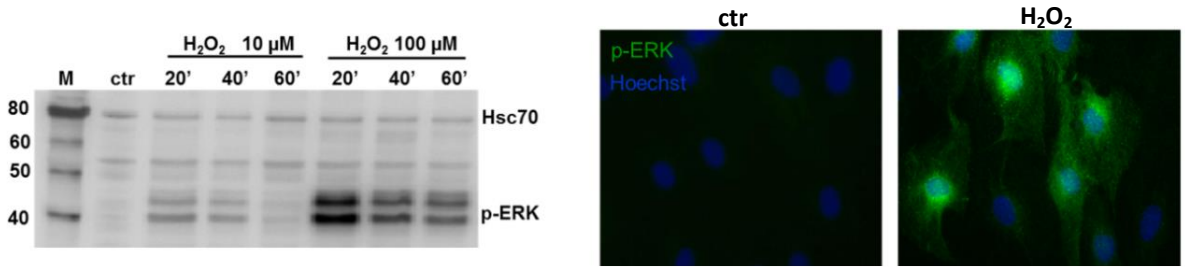

Fig.20. Primary SCs respond to hydrogen peroxide by phosphorylating ERK. Left: kinetics and dose-dependence of ERK phosphorylation induced in primary SCs by H_2O_2. Right: immunofluorescence of p-ERK (green) in SCs following exposure to H_2O_2 (100 µM for 60 min). Nuclei are stained in blue. Scale bar: 10 µm.

We next wondered whether ERK phosphorylation in SCs also occurs in our experimental system, i.e. in response to neurotoxin-induced neurodegeneration. For this aim, we set up neurons-SCs co-cultures, we intoxicated them with α-Ltx and Tpx and we performed IF, labelling p-ERK and neurofilaments. As it is shown in Fig 21, upon treatment with neurotoxins bulges appeared along neuronal processes, proving the successful intoxication; p-ERK labelling was detectable in the cytosol and nuclei of SCs of intoxicated co-cultures, but not in untreated ones (Fig. 21). The co-staining of p-ERK and the specific SCs marker S-100 confirmed that p-ERK positive cells were actually SCs (fig. 22). The score of S-100 positive cells that also became p-ERK positive cells upon co-cultures intoxication was 59% with β-Btx (n=81 from two different experiments) and 78% in the case of α-Ltx (n=69 from two different experiments); these percentages were obtained by counting many S-100 positive cells randomly distributed in different fields, but the value was actually higher if one considered only clustered SCs in close proximity of intoxicated neurites. This observation further supports the conclusion that molecules released by injured neurons reach nearby SCs, thus activating them; however, these data do not provide any information about the identity of such molecular mediator/s.

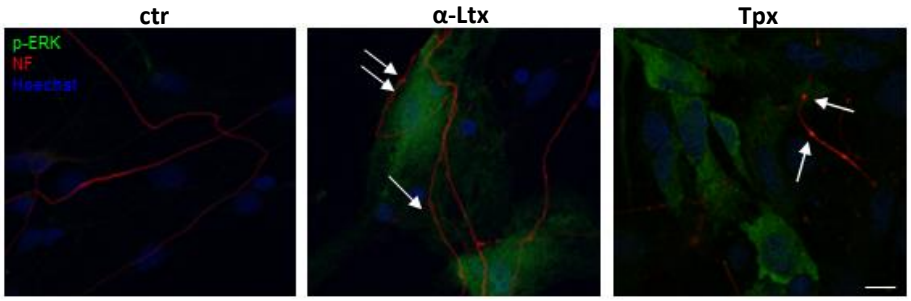

Fig. 21. ERK becomes phosphorylated in SCs co-cultured with neurons upon intoxication. p-ERK (green) was detected in primary SCs co-cultured with spinal cord MNs upon exposure to α-Ltx (0.1 nM) or SPANs (6 nM) for 50 min by IF. Arrows point to neuronal *bulges* stained with an antibody against neurofilaments (NF, red). Nuclei are stained with Hoechst (blue). Scale bars: 10 µm.

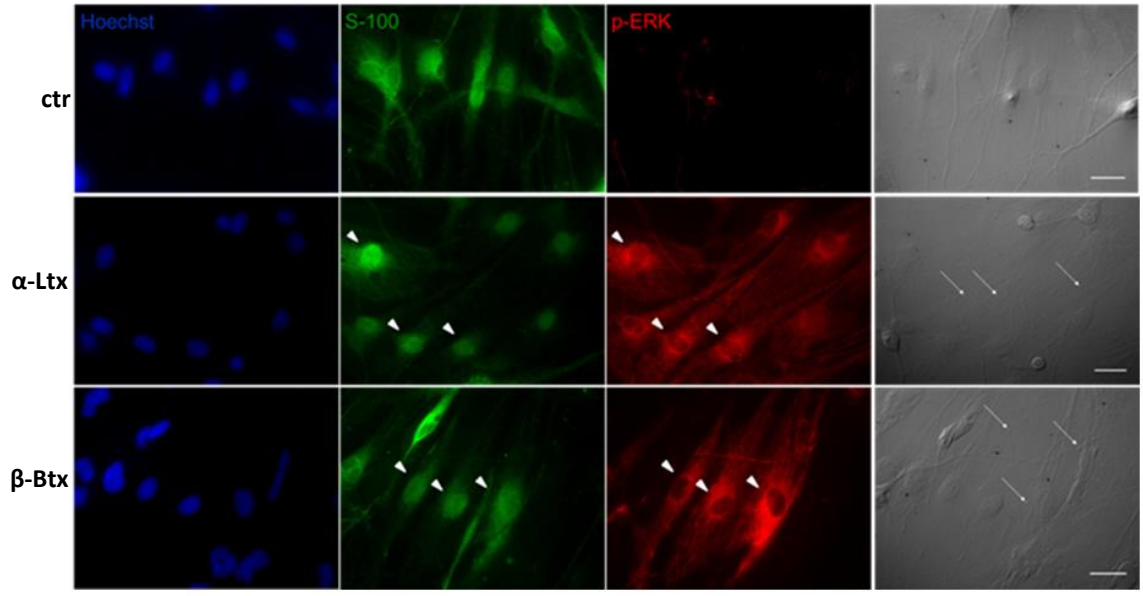

Fig. 22. p-ERK positive cells in intoxicated co-cultures are SCs. p-ERK positive cells (red) in SCs-MNs co-cultures exposed to the neurotoxins are positive for the SCs marker S-100 (green, arrowheads). Arrows in brighfield panels point to *bulges*. Scale bar: 20 μm

To address the involvement of neuronal H_2O_2 in the activation of ERK pathway in SCs, we intoxicated neurons-SCs co-cultures in absence or presence of catalase; this large enzyme can not enter cells, thus remaining in the extracellular medium where it converts H_2O_2 to oxygen and water, neutralizing its potential effect on target molecules (fig. 24). As it is shown in Fig. 23, pre-incubation with catalase reduced ERK phosphorylation levels of intoxicated co-cultures, indicating that H_2O_2 produced inside neurons actually diffuses outside to reach nearby SCs, contributing to ERK phosphorylation in their cytosol. We also determined that ERK phosphorylation was not altered in neurons upon intoxication, confirming that changes in p-ERK levels observed in co-cultures can be attributed mainly to SCs; also, we excluded a direct effect of neurotoxins on SCs, since incubation of isolated SCs with α-Ltx and Tpx did not induce any p-ERK increase (Fig. 24).

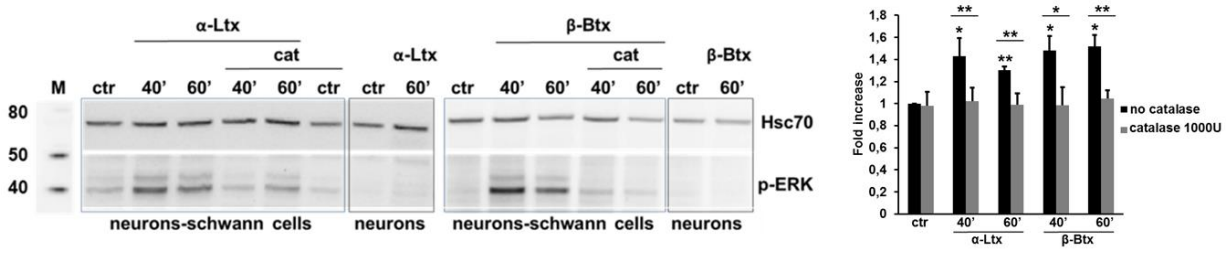

Fig. 23. Catalase prevents ERK phosphorylation in SCs co-cultured with neurons upon intoxication. Catalase pre-treatment of co-cultures (1000 U) significantly reduced ERK phosphorylation induced by the toxins (WB and quantification). No ERK phosphorylation is induced in neurons by the toxins.* p<0.05, ** p<0.01; N=4.

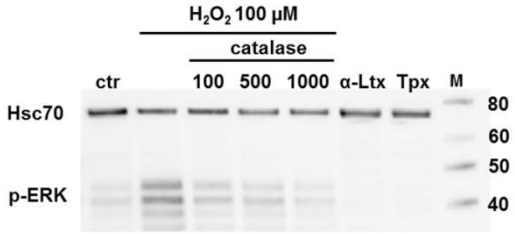

Fig. 24. H_2O_2 - but not neurotoxins - is responsible for ERK phosphorylation in cultured SCs. Pre-incubation of SCs with increasing amounts of catalase prevents ERK-phosphorylation by H_2O_2 to a different extent. Both α-Ltx and SPANs are ineffective in phosphorylating ERK in SCs.

Taken together, these observations indicate that H_2O_2, produced by neuronal mitochondria upon intoxication, is responsible for ERK activation in co-cultured SCs *in vitro.*

4.3 HYDROGEN PEROXIDE ACTIVATES ERK PATHWAY IN PSCs AT NMJ STIMULATING NERVE REGENERATION

We next wondered whether neurons-derived H_2O_2 also plays a crucial role in the crosstalk between degenerating nerve terminals and adjacent PSCs at NMJ *in vivo*. Our *in vivo* experiments were performed on transgenic mice, expressing a cytoplasmic GFP specifically in SCs under the *plp* promoter [110, 111]. Fluorescence levels in *plp*-GFP SCs are not changed upon denervation, differently from what observed in S100-GFP transgenic mice, where the activation of SCs in response to nerve injury is associated with a decreased GFP signal, due to S100 down-regulation. Therefore, *plp*-GFP transgenic mice represent ideal tools to image SCs morphological behaviours during nerve degeneration and regeneration.

To test whether ERK becomes phosphorylated also in PSCs upon nerve terminals intoxication, sub-lethal doses of α-Ltx (5 μg/kg) and β-Btx (10 μg/kg) were injected subcutaneously (s.c) at the level of *Levator Auris Longus* (LAL), a very thin muscle of mice ears, ideal for imaging [124] (Fig. 25). 24 hours later, muscle were dissected and processed for indirect immunohistochemistry (IHC); a clear p-ERK staining was detected at the level of PSCs of intoxicated NMJs, but not in untreated ones, thus extending *in vivo* the results obtained in co-cultures (Fig. 25).

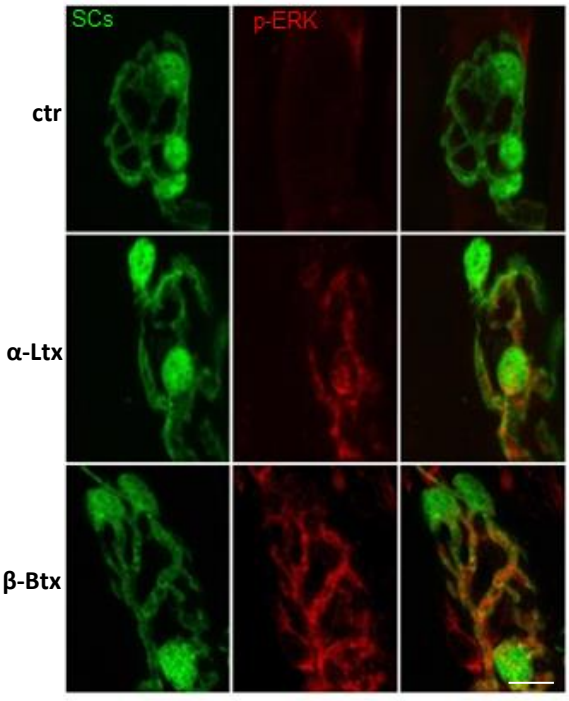

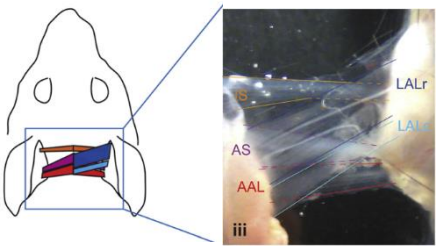

Fig. 25. Neurotoxins injection triggers ERK phosphorylation in PSCs at NMJs *in vivo*. α-Ltx or β-Btx subcutaneously injections in LAL muscle (top, from Murray et al., 2010) from transgenic mice trigger ERK phosphorylation (p-ERK, red) in PSCs (green) (left panel). Muscles were collected 24 hours after injection. Scale bars: 10 μm.

The importance of ERK pathway for SCs activation and nerve regeneration in our experimental system was addressed by a pharmacological approach, using the MEK1 inhibitor PD98059 [126]. We tested the efficacy of PD98059 in inhibiting ERK phosphorylation *in vitro*: as shown in Fig. 26, neurons-SCs co-cultures exposed to α-Ltx showed a decreased p-ERK level when pre-incubated with PD98059, which is therefore working correctly. To evaluate the contribution of ERK activation to nerve repair, we compared the kinetics of functional regeneration in muscles injected with α-Ltx alone and in those pre-treated with PD98059: we injected PD98059 intramuscularly in *soleus* muscles of mice prior to α-Ltx injection, and then performed electrophysiological recordings at different time points. As reported in Fig. 26, 3 days after treatment muscles pre-treated with MEK1 inhibitor and then locally injected with α-Ltx showed evoked junction potentials (EJPs) with significantly smaller amplitudes with respect to those injected with toxin only, meaning that inhibition of ERK pathway actually delays the process of nerve regeneration.

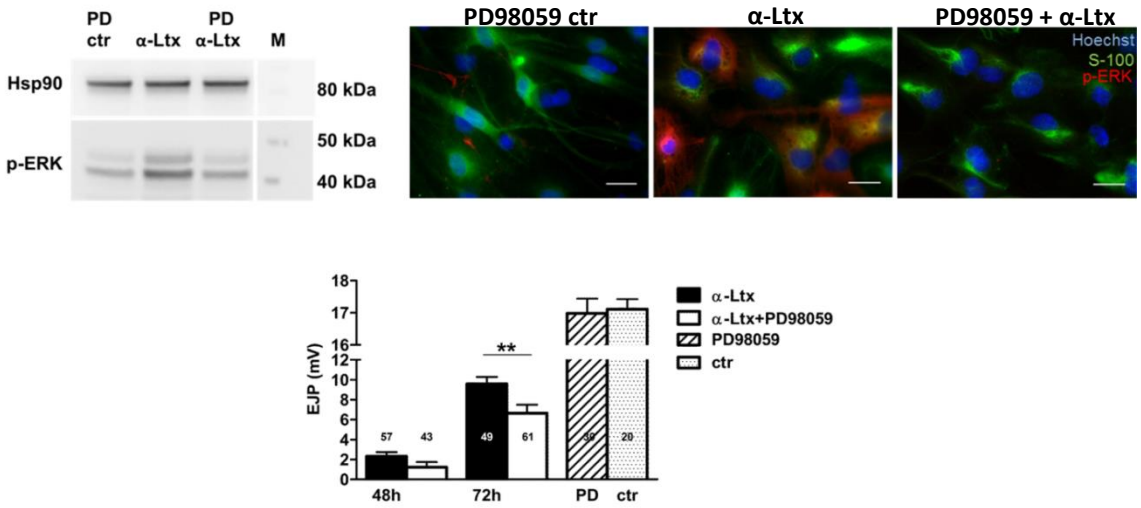

Fig. 26. ERK pathway is involved in SCs activation and in nerve regeneration. Top: SCs-MNs co-cultures were pretreated with the MEK1 inhibitor PD98059 prior to α-Ltx exposure and then probed for p-ERK both in WB (left) and in IF (right). The red channel represents p-ERK, the green one the S-100 marker. Scale bar 20 μm. Lower histogram: electrophysiological recordings of EJPs at *soleus* NMJs treated with α-Ltx alone (5 μg/ml, black bars) or pre-treated with PD98059 (50 μg) prior to α-Ltx injection (white bars). At 72 hours EJP amplitudes of fibers pre-treated with the inhibitor are significantly smaller than those exposed to the sole toxin (** $p<0.01$).

According to our model H_2O_2, produced by degenerating nerve terminals upon intoxication, is responsible for ERK phosphorylation in PSCs; activation of ERK pathway is in turn necessary to activate PSCs and thus to promote nerve regeneration [116]. If this hypothesis is correct, neutralizing H_2O_2 produced during nerve terminals degeneration should reduce ERK activation in PSCs, thus leading to an impaired or delayed nerve regeneration.

To address this point, we compared the kinetics of nerve degeneration and regeneration in mice treated with catalase and in untreated ones. Electrophysiological recordings were performed at different time points on *soleus* muscles injected with α-Ltx alone or with α-Ltx plus catalase. 24 hours after treatments no EJPs were detected, meaning that the process of nerve degeneration took place successfully in both conditions (Fig. 27); moreover, muscles treated with catalase alone showed EJPs indistinguishable from control ones. Similarly to what observed in experiments with PD98059, 72 hours after treatments muscle fibers injected with toxin plus catalase showed significantly smaller EJPs with respect to those of muscles exposed to toxin only, indicating also in this case a slowdown of the regeneration process.

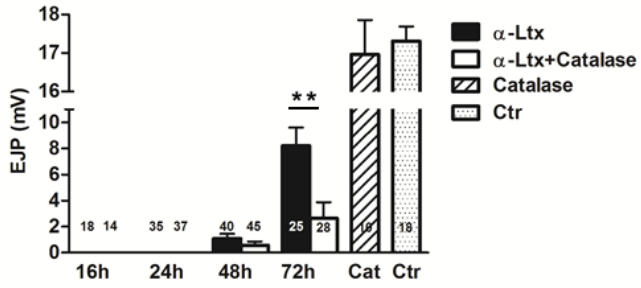

Fig. 27. Catalase delays functional regeneration following intoxication *in vivo*. Electrophysiological recordings of EJPs at *soleus* NMJs treated with α-Ltx alone (5 μg/ml, black bars) or with α-Ltx plus catalase (750 U, white bars). At 72 hours EJP amplitudes of fibers exposed to toxin plus catalase are significantly smaller than those exposed to the sole toxin (** $p<0.01$).

The effect of catalase on the rescue from intoxication was investigated also by performing IHC on LAL muscles.

Again, we injected LAL muscles s.c. with α-Ltx or with α-Ltx plus catalase, we dissected them at different time points and labelled the presynaptic protein SNAP25 (Synaptosomal-associated protein 25), which is very abundant at the presynaptic site, in order to monitor the structural degeneration of nerve terminals. As shown in Fig. 28, 4 hours after treatments the staining of SNAP25 accumulated inside vacuole-like structures in PSCs, which we demonstrated to be phagosomes – see next section; at 16 hours, SNAP25 completely

disappeared at the level of NMJs, meaning that nerve terminals degeneration and debris clearing were occurring successfully in both conditions. However, at 24 hours the regeneration of motor axon terminals appeared to be delayed in muscle injected with toxin plus catalase, with SNAP25 signal still missing in the vast majority of the analysed NMJs (17% positive for SNAP25 staining against 80% in LAL injected with α-Ltx alone at the same time point, N=40). A similar trend was observed also at 48 hours, when only 30% of NMJs treated with α-Ltx plus catalase showed SNAP25 labelling against 90% SNAP25-positive NMJs in muscles injected with only toxin. Catalase did not interfere with the process of nerve degeneration, since the disappearance of SNAP25 occurred with a closely similar kinetics under the two conditions.

In conclusion, these data strongly support the evidence that H_2O_2 plays a crucial role in activating PSCs during intoxication *in vivo*, thus promoting the regeneration of motor axon terminals.

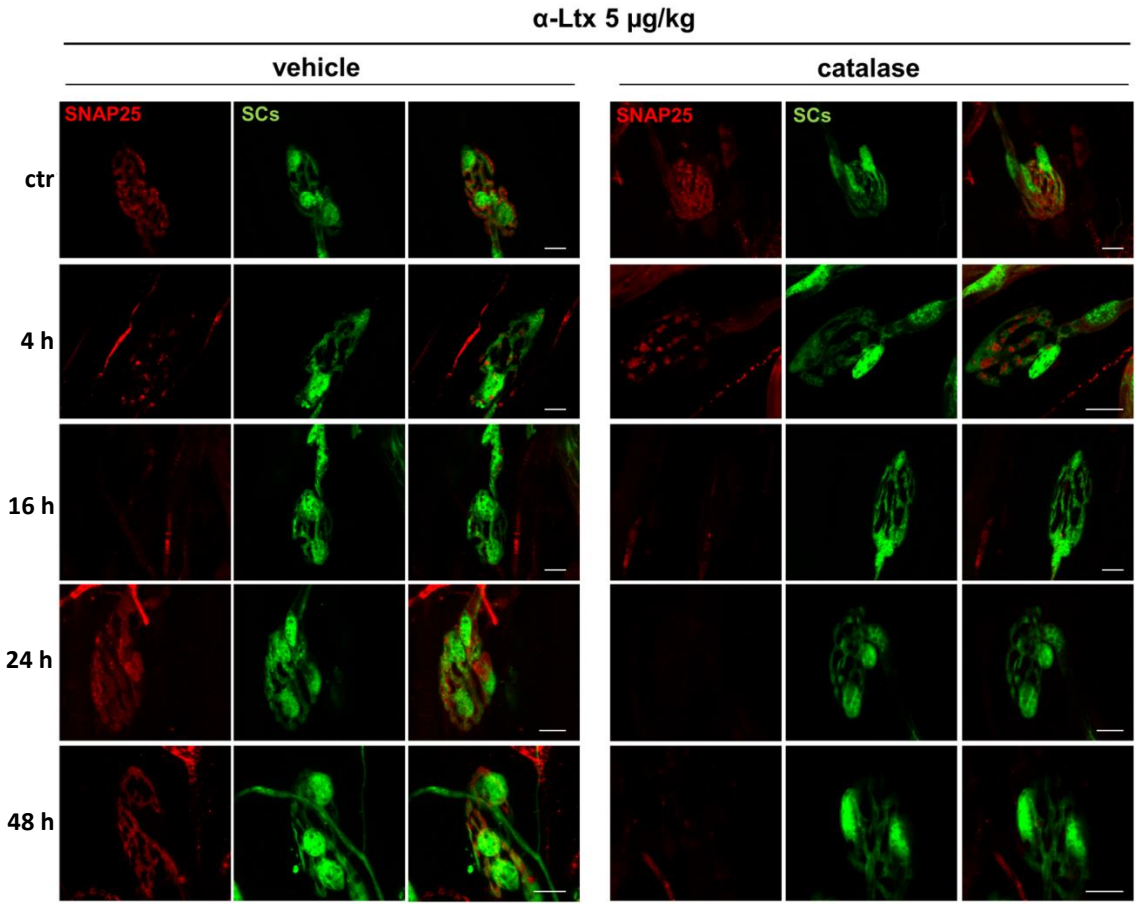

Fig. 28. Regeneration of poisoned presynaptic nerve terminals is delayed by catalase. SNAP-25 labeling (red) was used to monitor the degeneration and regeneration of nerve terminals at the NMJs of LAL muscles subcutaneously injected with α-Ltx or α-Ltx plus catalase (750 U). Muscles were collected after 4, 16, 24 and 48 hours and representative images are shown. Scale bars: 10 μm.

4.4 PHAGOCYTOSIS IS INDUCED IN PSCs DURING NERVE TERMINAL DEGENERATION

Upon nerve damage, SCs undergo changes in their gene expression, becoming reactive and acquiring peculiar features. Following the cut or crush of sciatic nerves, PSCs at denervated end-plates extend long cytosolic processes, called sprouts, which support the process of reinnervation and which are an hallmark of SCs activation. Reactive SCs contribute to the removal of nerve debris by phagocytosing them and by recruiting macrophages through the release of chemokines and cytokines [9, 25, 24].

To further validate our experimental system as a model to study degeneration and regeneration processes, we decided to better characterize the behaviour of PSCs in response to neurotoxins-induced neurodegeneration.

As shown in Fig. 29, by the first day of α-Ltx injection PSCs responded to intoxication by forming sprouts which in some cases grew to form bridges between junctions of different fibers; as expected, these processes disappeared soon after reinnervation.

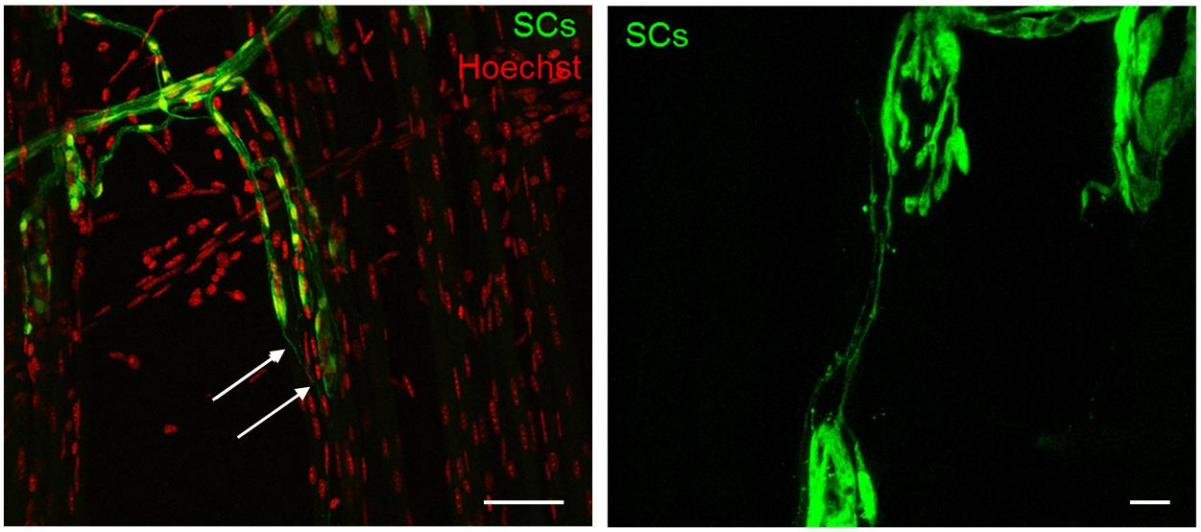

Fig. 29. PSCs activation following toxins-induced nerve terminal degeneration. Left: PSCs sproutings (green), typical hallmarks of activation, are observed at poisoned LAL NMJs by 24 hours from α-Ltx injection. Nuclei are stained with Hoechst (red); scale bar: 50 μm. Right: PSCs sproutings form sometimes bridges between adjacent NMJs. Scale bar: 10 μm.

Moreover, during nerve terminals degeneration PSCs at poisoned NMJs showed a number of intracellular structures which appeared dense of material by light microscopy observations (Fig. 30). These structures were particularly evident 4 hours after α-Ltx injection, with a reduction in number and size with time.

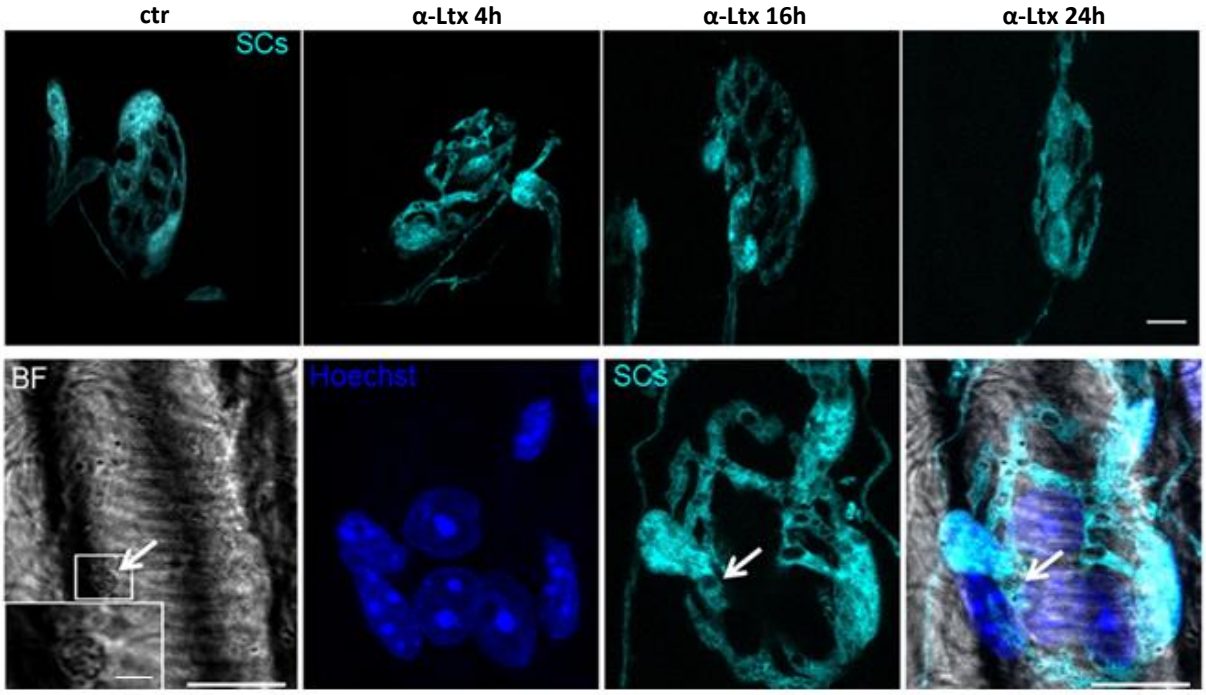

Fig. 30. PSCs show intracellular dense-of-material organelles following α-Ltx injection *in vivo*. Upper panels: LAL muscles from transgenic mice were injected with α-Ltx (5 μg/Kg), collected after different time points (4, 16 and 24 hours) and processed for indirect immunohistochemistry. PSCs (cyan) show intracellular structures of different size that are particularly evident after 4 hours of intoxication. These structures appear dense of material by light microscopy (brightfield, lower panels, arrows). Nuclei are stained with Hoechst (blue). Scale bars: 10 μm.

The appearance and life span of these organelles paralleled nerve terminal degeneration, suggesting that they might be phagosomes involved in the clearance of nerve debris. Accordingly, immunostaininig of sham or poisoned LAL muscles for the scavenger macrophage receptor CD68 was performed [127].

After α-Ltx injection, perineural SCs of LAL NMJs did express CD68 on these intracellular structures, supporting their phagocytic role (Fig. 31). CD68-positive organelles also appeared after β-Btx treatment, although at a later time point (16 hours), in agreement with the different time course of pathogenesis of the two kind of neurotoxins. Lysotracker-positive staining confirmed the acidic nature of such compartments, reinforcing the idea that they are actually phagosomes (Fig. 31).

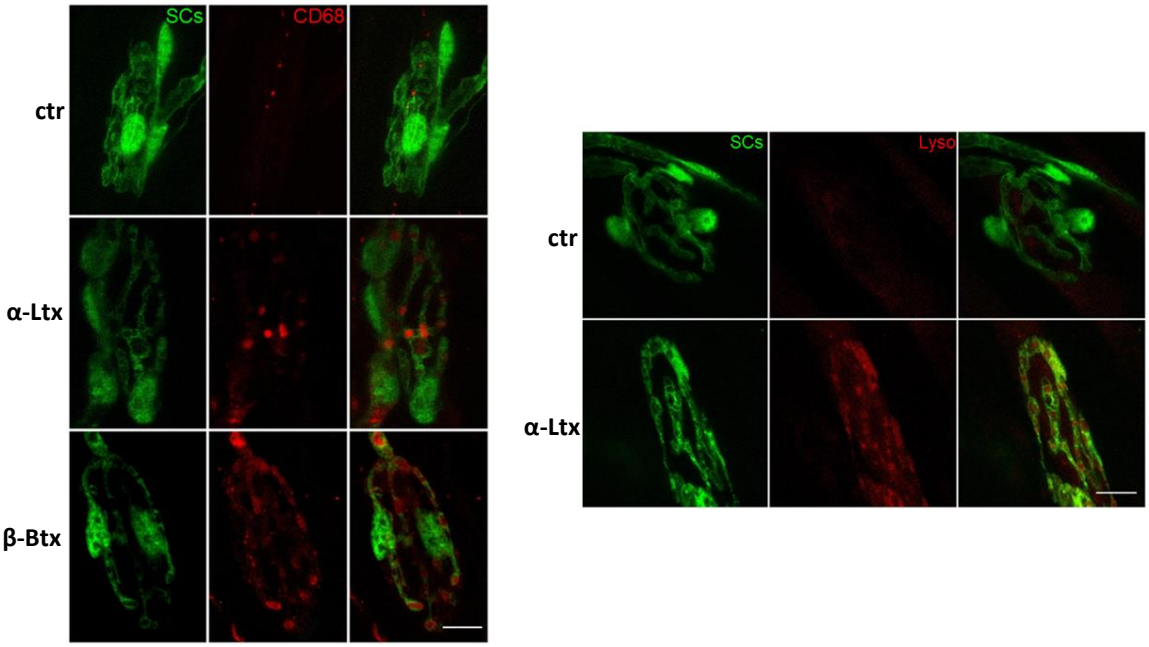

Fig. 31. Intracellular structures in activated PSCs at intoxicated NMJs are phagosomes. Left panel: PSCs (green) at α-Ltx and β-Btx-treated NMJs (4 and 16 hours respectively) are positive for the phagocytic marker CD68 (red), that stains intracellular vesicular structures. Scale bars: 10 μm. Right panel: *ex-vivo* Lysotracker staining (red) of α-Ltx–treated LAL (4 hours) confirms the acidic nature of intracellular vacuoles. Scale bar: 10 μm.

We also investigated the content of such phagosomes, by labelling presynaptic elements on LAL intoxicated muscles. As shown in Fig. 32, 4 hours after α-Ltx injection the distribution of the presynaptic markers neurofilaments (NF) and SNAP25 was altered, with a clear fragmentation in most of the NMJs, as a result of the specific and localized nerve terminal degeneration induced by the neurotoxins. SNAP25- and NF-positive spots localized within PSCs phagosomes (Fig. 32), as further demonstrated by orthogonal projections, thus confirming that PSCs are actually phagocytosing nerve terminal debris.

At a later stage of degeneration (16 hours) CD68-positive macrophages were also found in the proximity of intoxicated NMJs (Fig. 33), where they participate in the clearing of debris; this is consistent with the well-known chemoattractant role of H_2O_2 [105, 106]. Recruitment of macrophages is likely to be induced also by PSCs-secreted cytokines and chemokines [24].

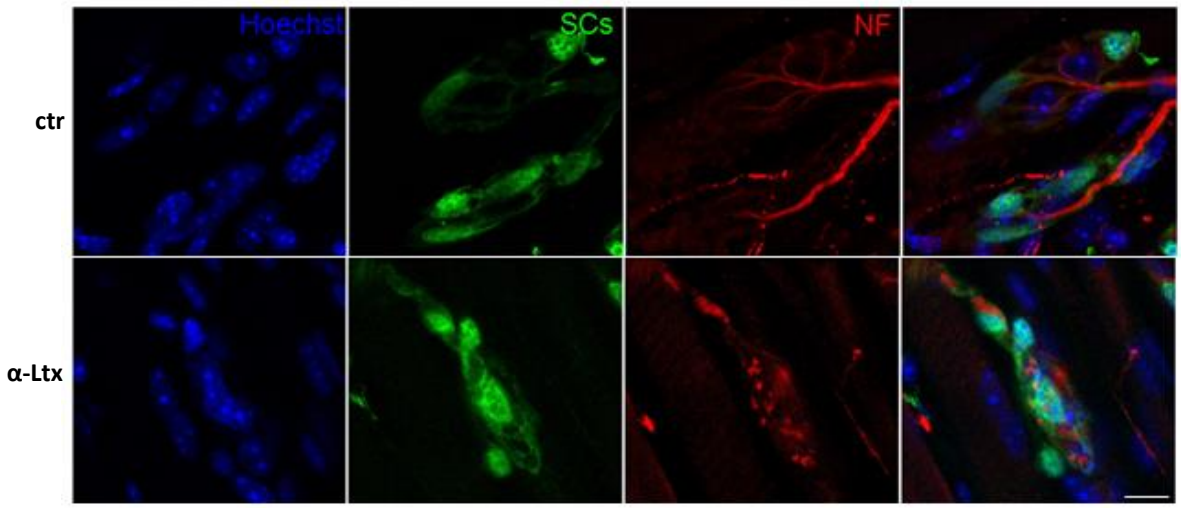

Fig. 32. Degenerating terminals are engulfed by perisynaptic SCs. Upper panels: PSCs engulf presynaptic components as shown by neurofilament (NF)-positive staining of PSCs phagosomes at NMJs treated for 4 hours with α-Ltx (red). Nuclei are stained with Hoechst (blue). Similar results were obtained with β-Btx (not shown). Scale bars: 10 μm. Lower panels, left: control NMJs with typical SNAP-25 presynaptic localization (red). In α-Ltx-treated NMJs (4 hours) SNAP-25 aggregates localize within PSCs phagosomes. The same results were obtained with β-Btx (not shown). Scale bars: 10 μm. Lower panel, right: orthogonal projections of α-Ltx-treated NMJs show that SNAP-25 positive aggregates are inside PSCs phagosomes.

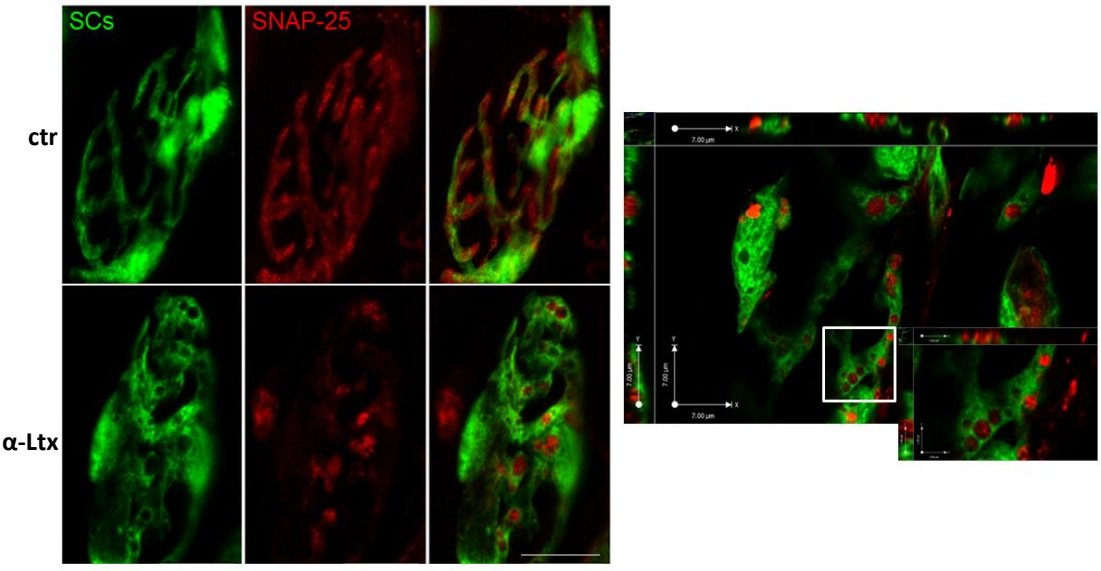

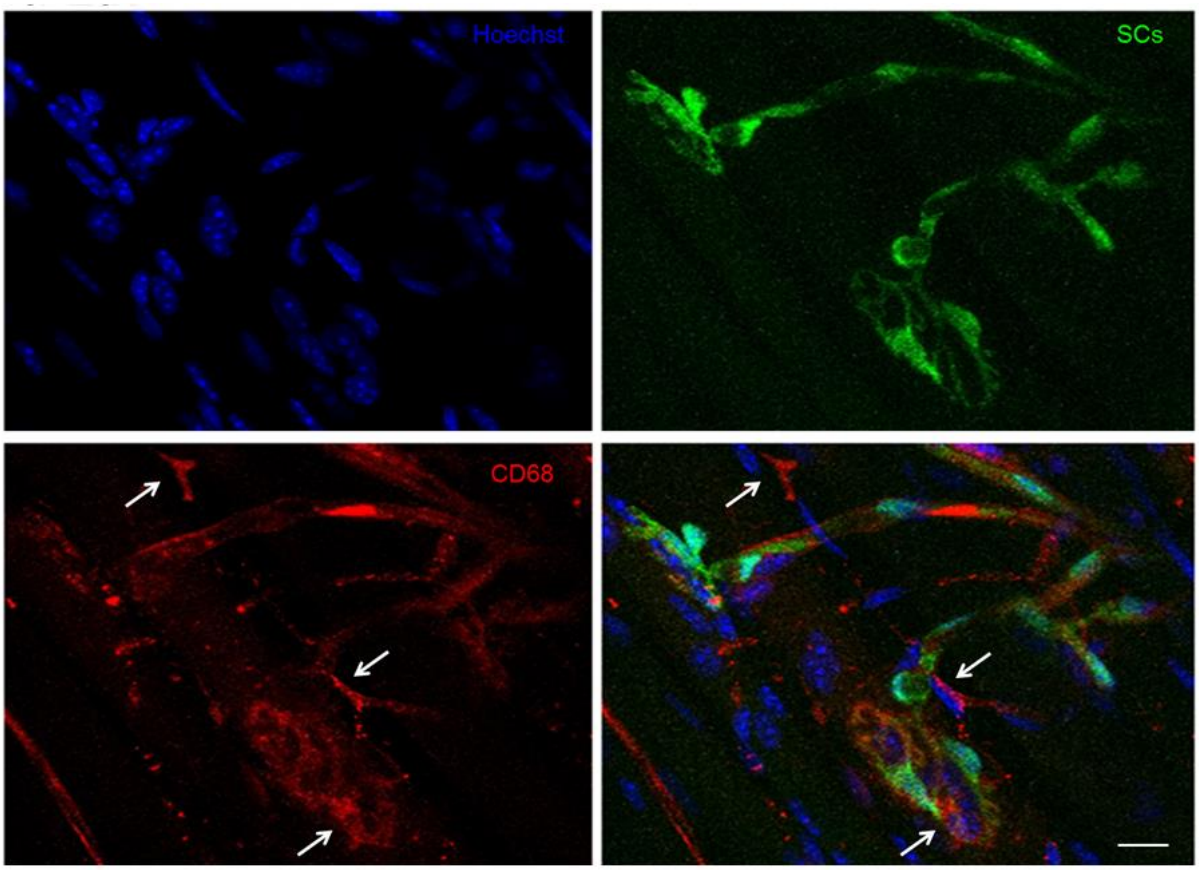

Fig. 33. Macrophages are recruited at the poisoned NMJ. CD68-positive macrophages (red, white arrows) are observed at the NMJs of LAL muscles injected with α-Ltx during nerve terminal degeneration (16 hours intoxication). Scale bar: 10 μm.

Thus, PSCs respond to nerve terminal intoxication by extending long sprouts, by removing nerve debris and by recruiting macrophages; these aspects well resemble the ones observed in canonical experimental models of nerve injury and regeneration, such as the cut or crush of sciatic nerves. On the whole, these observations strongly support the idea that this neurotoxins-based system represents a relevant and reliable model of acute motor axon terminal degeneration and regeneration, since it reproduces already-established crucial aspects occurring during these processes.

5. DISCUSSION

The repair of injured peripheral nerves involves the coordinated action of different cell types, among which SCs were shown to provide fundamental assistance for axon regeneration to occur. In response to nerve injury, both myelinating and perisynaptic SCs de-differentiate to a progenitor-like state and start proliferating; they also contribute to the removal of nerve debris, and recruit macrophages to the damage site by releasing cytokines and chemokines. Moreover, upon an extensive cytoskeletal reorganization, PSCs at denervated end-plates extend long processes or sprouts, which induce and guide nerve regrowth, facilitating the re-innervation of muscle fibers [9, 25].

While the remarkable plasticity of the SCs in response to nerve damage has been extensively documented, the intracellular signalling events that control the transition to this peculiar cell state are still poorly understood. Interestingly, it was recently shown that the MAPK signalling pathway has a central role in controlling SCs plasticity and peripheral nerve regeneration via the activation of ERK1/2 and JNK [122, 116]. Activation of an inducible Raf/MEK/ERK pathway in SCs of transgenic mice is sufficient to induce severe demyelination in the absence of axonal damage; it also promotes much of the inflammatory response important for nerve repair, with breakdown of the blood-nerve barrier and influx of inflammatory cells [116]. c-Jun, once activated downstream of JNK pathway, strongly promotes axonal regeneration via paracrine signalling by increasing the expression of several neurotrophic factors in SCs [128].

The initiator of this injury response is likely to be a signal coming from damaged axons that alerts adiacent SCs of their intention to degenerate: this signal is detected by SCs that are induced to de-differentiate. However, to date the identity of such mediator/s remains unknown, along with other cellular and molecular aspects regarding the regeneration of peripheral nerves.

In this study, we have adopted an original approach to study motor axon terminals degeneration and repair [42]. This model system is based on the use of animal presynaptic neurotoxins – α-Ltx and SPANs –, which are highly specific for nerve terminals and have a well-defined biochemical mechanism of action, part of which has been characterized in our laboratory [40, 74, 69, 39]. Here these neurotoxins are used as tools to induce a localized and completely reversible nerve terminals degeneration: this system avoids the activation of

a complex inflammatory response, and provokes a damage which remains strictly confined to the endplate. Moreover, it prevents some adverse effects of injury techniques such as laser ablation (high temperatures, photo-oxidation, etc.).

The experimental approach proposed here is therefore better suited to study the inter- and intra-cellular signalling events underlying the regeneration process. The localized injury provided by neurotoxins allows a more defined and reliable examination of PSCs specific roles in motor axon terminals repair.

Spider and snake presynaptic neurotoxins induce, by different biochemical mechanisms, a large entry of calcium in axon terminals, which in turn leads to mitochondria failure and, at a later stage, to degeneration of nerve terminals [43, 75]. Mitochondria are abundant and fundamental components of motor axon terminals, and have recently emerged as major sources of DAMPs: following different kinds of tissue injury, mtDAMPs – such as mtDNA and Cyt c – are released, and contribute to the activation of inflammatory responses even in the absence of infection [80, 83]. In addition, mitochondria-derived ROS are also acquiring very important roles as activators of injury-induced responses, acting as alarmins and promoting regeneration following different kinds of tissue damage [107, 108, 109]. Among ROS H_2O_2 has been shown to act as second messenger and paracrine signal in different physiological and pathological contexts, thanks to its high stability and membrane permeability [95].

ROS mitochondrial production increase under many stress conditions. In our experimental system, the rapid cytosolic calcium overload which takes place upon intoxication of nerve terminals was found to severely impair mitochondria, which undergo evident structural alterations and depolarization [75, 77, 58]. Based on these premises, we decided to image H_2O_2 in primary cultured neurons, taking advantage of novel specific fluorescent probes [114, 115]; live-imaging experiments showed that intoxicated neurons strongly increase mitochondrial production of H_2O_2, which then diffuses to the cytosol where it can easily permeate the plasma membrane to reach the extracellular medium. Since PSCs and axon terminals are in close contact within the NMJ, significant amounts of H_2O_2 released by intoxicated axon terminals can reach PSCs before being inactivated by cellular antioxidant defense systems. Once inside the target cell, H_2O_2 can act as second messenger via chemo-selective oxidation of cysteine residues in signalling proteins and via ERK activation [99, 119, 120, 121]. Indeed, H_2O_2 induces ERK phosphorylation in isolated cultured SCs, in a dose- and

time-dependent manner; p-ERK levels are also significantly increased in SCs co-cultured with neurons upon intoxication with α-Ltx and SPANs, meaning that ERK activation in SCs also occurs in our neurotoxins-based experimental system. Pre-incubation with catalase strongly prevents ERK phosphorylation in intoxicated co-cultures, suggesting that H_2O_2 produced inside neurons diffuses to reach nearby SCs, where it is responsible for ERK activation.

The results obtained in *in vitro* systems are also well reproduced *in-vivo*: indeed, a strong p-ERK signal is detectable in PSCs of intoxicated NMJs. Co-injection of α-Ltx and catalase significantly delays nerve terminal repair, both from a functional and a structural point of view, supporting the crucial involvement of H_2O_2 in promoting motor axon terminals regeneration.

The importance of ERK pathway for SCs activation and nerve regeneration was confirmed by a pharmacological approach: pre-treatment with the MEK1 inhibitor PD98059 decreases ERK phosphorylation levels in SCs of poisoned co-cultures and slows down the process of nerve repair following neurotoxins injections *in-vivo* in a way similar to that observed upon treatment with catalase.

Thus, H_2O_2 released by intoxicated nerve terminals activates PSCs *in-vitro* and *in-vivo*, playing a prominent role in nerve regeneration.

PSCs at intoxicated NMJs undergo deep morphological and functional alterations aimed at promoting NMJ repair, confirming their endowed high plasticity. Indeed, during nerve terminals degeneration PSCs extend long sprouts, which are an hallmark of their activated state [9, 25]. They become CD-68 positive, indicating an acquired phagocytic activity, and start engulfing nerve debris: the macrophagic-like features of PSCs described here represent an additional early read-out of PSCs activation at injured NMJ. Macrophages are also recruited in the proximity of neurotoxins-treated NMJs: it is therefore possible that they are attracted by H_2O_2, although we do not know how far H_2O_2 can migrate from the site of production as the circulating extracellular fluids contain many H_2O_2 quenching molecules. It is likely that other more stable mediators, released by the neurons or by the activated PSCs, are involved in macrophages recruitment [24, 105, 106].

These observations support the idea that the neurotoxins-based experimental system described here represents a reliable model to study nerve terminal degeneration and regeneration processes: indeed, PSCs reaction in response to intoxication well resembles the

main features observed in traditional experimental models, such as *in-vivo* cut/crush of sciatic nerve.

For the future, we plan to investigate more in detail the intracellular signalling and transcriptomic events taking place in activated PSCs, in order to identify additional pathways and molecular mediators involved in nerve terminal regeneration. It is also planned to investigate whether H_2O_2 is produced in response to other kinds of injury, such as the cut/crush of nerves, in order to replicate what happens during traumatic accidents.

More in general, there are reasons to support the possibility that the present experimental approach will provide information that are relevant to the investigation of other motor neurons diseases with similar pathogenetic features, as dying-back axonopathies and autoimmune neuropathies.

6. REFERENCES

1. Kandel Erik R., Schwartz James H., Jessel Thomas M.(2000) Principles of Neural Sciences. Fourth edition, McGraw-Hill.
2. Jessen KR & Mirsky R (1998) Origin and early development of Schwann cells. *Microsc Res Tech* 41(5):393-402.
3. Jessen KR & Mirsky R (2005) The origin and development of glial cells in peripheral nerves. *Nat Rev Neurosci* 6(9):671-682.
4. Love FM & Thompson WJ (1998) Schwann cells proliferate at rat neuromuscular junctions during development and regeneration. *J Neurosci* 18(22):9376-9385.
5. Morris JK*, et al.* (1999) Rescue of the cardiac defect in ErbB2 mutant mice reveals essential roles of ErbB2 in peripheral nervous system development. *Neuron* 23(2):273-283.
6. Lin W*, et al.* (2000) Aberrant development of motor axons and neuromuscular synapses in erbB2-deficient mice. *Proc Natl Acad Sci U S A* 97(3):1299-1304.
7. Wolpowitz D*, et al.* (2000) Cysteine-rich domain isoforms of the neuregulin-1 gene are required for maintenance of peripheral synapses. *Neuron* 25(1):79-91.
8. Reddy LV, Koirala S, Sugiura Y, Herrera AA, & Ko CP (2003) Glial cells maintain synaptic structure and function and promote development of the neuromuscular junction in vivo. *Neuron* 40(3):563-580.
9. Auld DS & Robitaille R (2003) Perisynaptic Schwann cells at the neuromuscular junction: nerve- and activity-dependent contributions to synaptic efficacy, plasticity, and reinnervation. *Neuroscientist* 9(2):144-157.
10. Jahromi BS, Robitaille R, & Charlton MP (1992) Transmitter release increases intracellular calcium in perisynaptic Schwann cells in situ. *Neuron* 8(6):1069-1077.
11. Reist NE & Smith SJ (1992) Neurally evoked calcium transients in terminal Schwann cells at the neuromuscular junction. *Proc Natl Acad Sci U S A* 89(16):7625-7629.
12. Rochon D, Rousse I, & Robitaille R (2001) Synapse-glia interactions at the mammalian neuromuscular junction. *J Neurosci* 21(11):3819-3829.
13. Pinard A, Lévesque S, Vallée J, & Robitaille R (2003) Glutamatergic modulation of synaptic plasticity at a PNS vertebrate cholinergic synapse. *Eur J Neurosci* 18(12):3241-3250.
14. Thomas S & Robitaille R (2001) Differential frequency-dependent regulation of transmitter release by endogenous nitric oxide at the amphibian neuromuscular synapse. *J Neurosci* 21(4):1087-1095.
15. Rousse I & Robitaille R (2006) Calcium signaling in Schwann cells at synaptic and extra-synaptic sites: active glial modulation of neuronal activity. *Glia* 54(7):691-699.
16. Waller A (1850) Experiments on the section of the glossopharyngeal and hypoglossal nerves of the frog, and observations of the alterations produced thereby in the structure of their primitive fibres. *Philosophical Transactions Royal Society London* 140, 423-429.
17. Kerschensteiner M, Schwab ME, Lichtman JW, & Misgeld T (2005) In vivo imaging of axonal degeneration and regeneration in the injured spinal cord. *Nat Med* 11(5):572-577.
18. Ma M, *et al.* (2013) Calpains mediate axonal cytoskeleton disintegration during Wallerian degeneration. *Neurobiol Dis* 56:34-46.

19. Conforti L, Gilley J, & Coleman MP (2014) Wallerian degeneration: an emerging axon death pathway linking injury and disease. *Nat Rev Neurosci* 15(6):394-409.
20. Sievers C, Platt N, Perry VH, Coleman MP, & Conforti L (2003) Neurites undergoing Wallerian degeneration show an apoptotic-like process with Annexin V positive staining and loss of mitochondrial membrane potential. *Neurosci Res* 46(2):161-169.
21. Clemence A, Mirsky R, & Jessen KR (1989) Non-myelin-forming Schwann cells proliferate rapidly during Wallerian degeneration in the rat sciatic nerve. *J Neurocytol* 18(2):185-192.
22. Thomson CE*, et al.* (1993) In vitro studies of axonally-regulated Schwann cell genes during Wallerian degeneration. *J Neurocytol* 22(8):590-602.
23. Stoll G, Griffin JW, Li CY, & Trapp BD (1989) Wallerian degeneration in the peripheral nervous system: participation of both Schwann cells and macrophages in myelin degradation. *J Neurocytol* 18(5):671-683.
24. Tofaris GK, Patterson PH, Jessen KR, & Mirsky R (2002) Denervated Schwann cells attract macrophages by secretion of leukemia inhibitory factor (LIF) and monocyte chemoattractant protein-1 in a process regulated by interleukin-6 and LIF. *J Neurosci* 22(15):6696-6703.
25. Son YJ, Trachtenberg JT, & Thompson WJ (1996) Schwann cells induce and guide sprouting and reinnervation of neuromuscular junctions. *Trends Neurosci* 19(7):280-285.
26. Horner PJ & Gage FH (2000) Regenerating the damaged central nervous system. *Nature* 407(6807):963-970.
27. He Z & Koprivica V (2004) The Nogo signaling pathway for regeneration block. *Annu Rev Neurosci* 27:341-368.
28. Bradke F, Fawcett JW, & Spira ME (2012) Assembly of a new growth cone after axotomy: the precursor to axon regeneration. *Nat Rev Neurosci* 13(3):183-193.
29. McKerracher L, Chamoux M, & Arregui CO (1996) Role of laminin and integrin interactions in growth cone guidance. *Mol Neurobiol* 12(2):95-116.
30. Fu SY & Gordon T (1997) The cellular and molecular basis of peripheral nerve regeneration. *Mol Neurobiol* 14(1-2):67-116.
31. Scheib J & Höke A (2013) Advances in peripheral nerve regeneration. *Nat Rev Neurol* 9(12):668-676.
32. Frostick SP, Yin Q, & Kemp GJ (1998) Schwann cells, neurotrophic factors, and peripheral nerve regeneration. *Microsurgery* 18(7):397-405.
33. Torigoe K, Tanaka HF, Takahashi A, Awaya A, & Hashimoto K (1996) Basic behavior of migratory Schwann cells in peripheral nerve regeneration. *Exp Neurol* 137(2):301-308.
34. Son YJ & Thompson WJ (1995) Schwann cell processes guide regeneration of peripheral axons. *Neuron* 14(1):125-132.
35. Son YJ & Thompson WJ (1995) Nerve sprouting in muscle is induced and guided by processes extended by Schwann cells. *Neuron* 14(1):133-141.
36. Vinsant S*, et al.* (2013) Characterization of early pathogenesis in the SOD1(G93A) mouse model of ALS: part II, results and discussion. *Brain Behav* 3(4):431-457.
37. Moloney EB, de Winter F, & Verhaagen J (2014) ALS as a distal axonopathy: molecular mechanisms affecting neuromuscular junction stability in the presymptomatic stages of the disease. *Front Neurosci* 8:252.
38. Plomp JJ & Willison HJ (2009) Pathophysiological actions of neuropathy-related anti-ganglioside antibodies at the neuromuscular junction. *J Physiol* 587(Pt

16):3979-3999.
39. Kaida K & Kusunoki S (2010) Antibodies to gangliosides and ganglioside complexes in Guillain-Barré syndrome and Fisher syndrome: mini-review. *J Neuroimmunol* 223(1-2):5-12.
40. Ushkaryov YA, Rohou A, & Sugita S (2008) alpha-Latrotoxin and its receptors. *Handb Exp Pharmacol* (184):171-206.
41. Gutiérrez JM & Lomonte B (2013) Phospholipases A2: unveiling the secrets of a functionally versatile group of snake venom toxins. *Toxicon* 62:27-39.
42. Duregotti E*, et al.* (2015) Mitochondrial alarmins released by degenerating motor axon terminals activate perisynaptic Schwann cells. *Proc Natl Acad Sci U S A*.
43. Tedesco E*, et al.* (2009) Calcium overload in nerve terminals of cultured neurons intoxicated by alpha-latrotoxin and snake PLA2 neurotoxins. *Toxicon* 54(2):138-144.
44. Duchen LW, Gomez S, & Queiroz LS (1981) The neuromuscular junction of the mouse after black widow spider venom. *J Physiol* 316:279-291.
45. Harris JB, Grubb BD, Maltin CA, & Dixon R (2000) The neurotoxicity of the venom phospholipases A(2), notexin and taipoxin. *Exp Neurol* 161(2):517-526.
46. Duan ZG*, et al.* (2006) Extraction and protein component analysis of venom from the dissected venom glands of Latrodectus tredecimguttatus. *Comp Biochem Physiol B Biochem Mol Biol* 145(3-4):350-357.
47. Grishin EV (1998) Black widow spider toxins: the present and the future. *Toxicon* 36(11):1693-1701.
48. Hurlbut WP & Ceccarelli B (1979) Use of black widow spider venom to study the release of neurotransmitters. *Adv Cytopharmacol* 3:87-115.
49. Ceccarelli B & Hurlbut WP (1980) Vesicle hypothesis of the release of quanta of acetylcholine. *Physiol Rev* 60(2):396-441.
50. Orlova EV*, et al.* (2000) Structure of alpha-latrotoxin oligomers reveals that divalent cation-dependent tetramers form membrane pores. *Nat Struct Biol* 7(1):48-53.
51. Cavalieri M, Corvaja N, & Grasso A (1990) Immunocytological localization by monoclonal antibodies of alpha-latrotoxin in the venom gland of the spider Latrodectus tredecimguttatus. *Toxicon* 28(3):341-346.
52. Volynski KE, Nosyreva ED, Ushkaryov YA, & Grishin EV (1999) Functional expression of alpha-latrotoxin in baculovirus system. *FEBS Lett* 442(1):25-28.
53. Finkelstein A, Rubin LL, & Tzeng MC (1976) Black widow spider venom: effect of purified toxin on lipid bilayer membranes. *Science* 193(4257):1009-1011.
54. Ashton AC*, et al.* (2001) alpha-Latrotoxin, acting via two Ca2+-dependent pathways, triggers exocytosis of two pools of synaptic vesicles. *J Biol Chem* 276(48):44695-44703.
55. Ushkaryov YA, Volynski KE, & Ashton AC (2004) The multiple actions of black widow spider toxins and their selective use in neurosecretion studies. *Toxicon* 43(5):527-542.
56. Capogna M, Gähwiler BH, & Thompson SM (1996) Calcium-independent actions of alpha-latrotoxin on spontaneous and evoked synaptic transmission in the hippocampus. *J Neurophysiol* 76(5):3149-3158.
57. Longenecker HE, Hurlbut WP, Mauro A, & Clark AW (1970) Effects of black widow spider venom on the frog neuromuscular junction. Effects on end-plate potential, miniature end-plate potential and nerve terminal spike. *Nature* 225(5234):701-

703.
58. Matteoli M*, et al.* (1988) Differential effect of alpha-latrotoxin on exocytosis from small synaptic vesicles and from large dense-core vesicles containing calcitonin gene-related peptide at the frog neuromuscular junction. *Proc Natl Acad Sci U S A* 85(19):7366-7370.
59. Duregotti E, Tedesco E, Montecucco C, & Rigoni M (2013) Calpains participate in nerve terminal degeneration induced by spider and snake presynaptic neurotoxins. *Toxicon* 64:20-28.
60. Chen IL & Lee CY (1970) Ultrastructural changes in the motor nerve terminals caused by beta-bungarotoxin. *Virchows Arch B Cell Pathol* 6(4):318-325.
61. Connolly S*, et al.* (1995) Neuromuscular effects of Papuan Taipan snake venom. *Ann Neurol* 38(6):916-920.
62. Prasarnpun S, Walsh J, Awad SS, & Harris JB (2005) Envenoming bites by kraits: the biological basis of treatment-resistant neuromuscular paralysis. *Brain* 128(Pt 12):2987-2996.
63. Schiavo G, Matteoli M, & Montecucco C (2000) Neurotoxins affecting neuroexocytosis. *Physiol Rev* 80(2):717-766.
64. Prasarnpun S, Walsh J, & Harris JB (2004) Beta-bungarotoxin-induced depletion of synaptic vesicles at the mammalian neuromuscular junction. *Neuropharmacology* 47(2):304-314.
65. Paoli M*, et al.* (2009) Mass spectrometry analysis of the phospholipase A(2) activity of snake pre-synaptic neurotoxins in cultured neurons. *J Neurochem* 111(3):737-744.
66. Kwong PD, McDonald NQ, Sigler PB, & Hendrickson WA (1995) Structure of beta 2-bungarotoxin: potassium channel binding by Kunitz modules and targeted phospholipase action. *Structure* 3(10):1109-1119.
67. Montecucco C & Rossetto O (2000) How do presynaptic PLA2 neurotoxins block nerve terminals? *Trends Biochem Sci* 25(6):266-270.
68. Montecucco C, Rossetto O, & Schiavo G (2004) Presynaptic receptor arrays for clostridial neurotoxins. *Trends Microbiol* 12(10):442-446.
69. Rigoni M*, et al.* (2005) Equivalent effects of snake PLA2 neurotoxins and lysophospholipid-fatty acid mixtures. *Science* 310(5754):1678-1680.
70. Caccin P, Rossetto O, & Montecucco C (2009) Neurotoxicity of inverted-cone shaped lipids. *Neurotoxicology* 30(2):174-181.
71. Fuller N & Rand RP (2001) The influence of lysolipids on the spontaneous curvature and bending elasticity of phospholipid membranes. *Biophys J* 81(1):243-254.
72. Chernomordik LV & Kozlov MM (2003) Protein-lipid interplay in fusion and fission of biological membranes. *Annu Rev Biochem* 72:175-207.
73. Zimmerberg J & Chernomordik LV (2005) Neuroscience. Synaptic membranes bend to the will of a neurotoxin. *Science* 310(5754):1626-1627.
74. Rossetto O, Morbiato L, Caccin P, Rigoni M, & Montecucco C (2006) Presynaptic enzymatic neurotoxins. *J Neurochem* 97(6):1534-1545.
75. Rigoni M*, et al.* (2007) Calcium influx and mitochondrial alterations at synapses exposed to snake neurotoxins or their phospholipid hydrolysis products. *J Biol Chem* 282(15):11238-11245.
76. Rigoni M*, et al.* (2004) Snake presynaptic neurotoxins with phospholipase A2 activity induce punctate swellings of neurites and exocytosis of synaptic vesicles. *J*

Cell Sci 117(Pt 16):3561-3570.
77. Cull-Candy SG, Fohlman J, Gustavsson D, Lüllmann-Rauch R, & Thesleff S (1976) The effects of taipoxin and notexin on the function and fine structure of the murine neuromuscular junction. *Neuroscience* 1(3):175-180.
78. Rigoni M*, et al.* (2008) Snake phospholipase A2 neurotoxins enter neurons, bind specifically to mitochondria, and open their transition pores. *J Biol Chem* 283(49):34013-34020.
79. Su MJ & Chang CC (1984) Presynaptic effects of snake venom toxins which have phospholipase A2 activity (beta-bungarotoxin, taipoxin, crotoxin). *Toxicon* 22(4):631-640.
80. Krysko DV*, et al.* (2011) Emerging role of damage-associated molecular patterns derived from mitochondria in inflammation. *Trends Immunol* 32(4):157-164.
81. Seong SY & Matzinger P (2004) Hydrophobicity: an ancient damage-associated molecular pattern that initiates innate immune responses. *Nat Rev Immunol* 4(6):469-478.
82. Palm NW & Medzhitov R (2009) Pattern recognition receptors and control of adaptive immunity. *Immunol Rev* 227(1):221-233.
83. Zhang Q*, et al.* (2010) Circulating mitochondrial DAMPs cause inflammatory responses to injury. *Nature* 464(7285):104-107.
84. Collins LV, Hajizadeh S, Holme E, Jonsson IM, & Tarkowski A (2004) Endogenously oxidized mitochondrial DNA induces in vivo and in vitro inflammatory responses. *J Leukoc Biol* 75(6):995-1000.
85. Carp H (1982) Mitochondrial N-formylmethionyl proteins as chemoattractants for neutrophils. *J Exp Med* 155(1):264-275.
86. Rabiet MJ, Huet E, & Boulay F (2007) The N-formyl peptide receptors and the anaphylatoxin C5a receptors: an overview. *Biochimie* 89(9):1089-1106.
87. Codina R, Vanasse A, Kelekar A, Vezys V, & Jemmerson R (2010) Cytochrome c-induced lymphocyte death from the outside in: inhibition by serum leucine-rich alpha-2-glycoprotein-1. *Apoptosis* 15(2):139-152.
88. Xiang M & Fan J (2010) Pattern recognition receptor-dependent mechanisms of acute lung injury. *Mol Med* 16(1-2):69-82.
89. Cohen MJ*, et al.* (2009) Early release of high mobility group box nuclear protein 1 after severe trauma in humans: role of injury severity and tissue hypoperfusion. *Crit Care* 13(6):R174.
90. Zhang Q, Itagaki K, & Hauser CJ (2010) Mitochondrial DNA is released by shock and activates neutrophils via p38 map kinase. *Shock* 34(1):55-59.
91. Miller TJ*, et al.* (2008) Cytochrome c: a non-invasive biomarker of drug-induced liver injury. *J Appl Toxicol* 28(7):815-828.
92. Radhakrishnan J*, et al.* (2007) Circulating levels of cytochrome c after resuscitation from cardiac arrest: a marker of mitochondrial injury and predictor of survival. *Am J Physiol Heart Circ Physiol* 292(2):H767-775.
93. Zornetta I*, et al.* (2012) Envenomations by Bothrops and Crotalus snakes induce the release of mitochondrial alarmins. *PLoS Negl Trop Dis* 6(2):e1526.
94. Finkel T & Holbrook NJ (2000) Oxidants, oxidative stress and the biology of ageing. *Nature* 408(6809):239-247.
95. Paulsen CE & Carroll KS (2010) Orchestrating redox signaling networks through regulatory cysteine switches. *ACS Chem Biol* 5(1):47-62.
96. Dickinson BC & Chang CJ (2011) Chemistry and biology of reactive oxygen species

in signaling or stress responses. *Nat Chem Biol* 7(8):504-511.
97. Murphy MP*, et al.* (2011) Unraveling the biological roles of reactive oxygen species. *Cell Metab* 13(4):361-366.
98. Gough DR & Cotter TG (2011) Hydrogen peroxide: a Jekyll and Hyde signalling molecule. *Cell Death Dis* 2:e213.
99. Miki H & Funato Y (2012) Regulation of intracellular signalling through cysteine oxidation by reactive oxygen species. *J Biochem* 151(3):255-261.
100. Shibanuma M, Kuroki T, & Nose K (1990) Stimulation by hydrogen peroxide of DNA synthesis, competence family gene expression and phosphorylation of a specific protein in quiescent Balb/3T3 cells. *Oncogene* 5(7):1025-1032.
101. Lizama-Manibusan B & McLaughlin B (2013) Redox modification of proteins as essential mediators of CNS autophagy and mitophagy. *FEBS Lett* 587(15):2291-2298.
102. Chandel NS*, et al.* (1998) Mitochondrial reactive oxygen species trigger hypoxia-induced transcription. *Proc Natl Acad Sci U S A* 95(20):11715-11720.
103. Duranteau J, Chandel NS, Kulisz A, Shao Z, & Schumacker PT (1998) Intracellular signaling by reactive oxygen species during hypoxia in cardiomyocytes. *J Biol Chem* 273(19):11619-11624.
104. West AP*, et al.* (2011) TLR signalling augments macrophage bactericidal activity through mitochondrial ROS. *Nature* 472(7344):476-480.
105. Niethammer P, Grabher C, Look AT, & Mitchison TJ (2009) A tissue-scale gradient of hydrogen peroxide mediates rapid wound detection in zebrafish. *Nature* 459(7249):996-999.
106. Li L, Yan B, Shi YQ, Zhang WQ, & Wen ZL (2012) Live imaging reveals differing roles of macrophages and neutrophils during zebrafish tail fin regeneration. *J Biol Chem* 287(30):25353-25360.
107. Van der Vliet A & Janssen-Heininger YM (2014) Hydrogen peroxide as a damage signal in tissue injury and inflammation: murderer, mediator, or messenger? *J Cell Biochem* 115(3):427-435.
108. Love NR*, et al.* (2013) Amputation-induced reactive oxygen species are required for successful Xenopus tadpole tail regeneration. *Nat Cell Biol* 15(2):222-228.
109. Xu S & Chisholm AD (2014) C. elegans epidermal wounding induces a mitochondrial ROS burst that promotes wound repair. *Dev Cell* 31(1):48-60.
110. Mallon BS, Shick HE, Kidd GJ, & Macklin WB (2002) Proteolipid promoter activity distinguishes two populations of NG2-positive cells throughout neonatal cortical development. *J Neurosci* 22(3):876-885.
111. Brill MS, Lichtman JW, Thompson W, Zuo Y, & Misgeld T (2011) Spatial constraints dictate glial territories at murine neuromuscular junctions. *J Cell Biol* 195(2):293-305.
112. Levi G, Aloisi F, Ciotti MT, & Gallo V (1984) Autoradiographic localization and depolarization-induced release of acidic amino acids in differentiating cerebellar granule cell cultures. *Brain Res* 290(1):77-86.
113. Arce V*, et al.* (1999) Cardiotrophin-1 requires LIFRbeta to promote survival of mouse motoneurons purified by a novel technique. *J Neurosci Res* 55(1):119-126.
114. Dickinson BC & Chang CJ (2008) A targetable fluorescent probe for imaging hydrogen peroxide in the mitochondria of living cells. *J Am Chem Soc* 130(30):9638-9639.
115. Dickinson BC, Peltier J, Stone D, Schaffer DV, & Chang CJ (2011) Nox2 redox

signaling maintains essential cell populations in the brain. *Nat Chem Biol* 7(2):106-112.
116. Napoli I*, et al.* (2012) A central role for the ERK-signaling pathway in controlling Schwann cell plasticity and peripheral nerve regeneration in vivo. *Neuron* 73(4):729-742.
117. Song JW*, et al.* (2008) Lysosomal activity associated with developmental axon pruning. *J Neurosci* 28(36):8993-9001.
118. Gao HM, Zhou H, & Hong JS (2012) NADPH oxidases: novel therapeutic targets for neurodegenerative diseases. *Trends Pharmacol Sci* 33(6):295-303.
119. Abe MK*, et al.* (1998) Hydrogen peroxide activates extracellular signal-regulated kinase via protein kinase C, Raf-1, and MEK1. *Am J Respir Cell Mol Biol* 18(4):562-569.
120. Kemmerling U*, et al.* (2007) Calcium release by ryanodine receptors mediates hydrogen peroxide-induced activation of ERK and CREB phosphorylation in N2a cells and hippocampal neurons. *Cell Calcium* 41(5):491-502.
121. Crossthwaite AJ, Hasan S, & Williams RJ (2002) Hydrogen peroxide-mediated phosphorylation of ERK1/2, Akt/PKB and JNK in cortical neurones: dependence on Ca(2+) and PI3-kinase. *J Neurochem* 80(1):24-35.
122. Harrisingh MC*, et al.* (2004) The Ras/Raf/ERK signalling pathway drives Schwann cell dedifferentiation. *EMBO J* 23(15):3061-3071.
123. Caunt CJ & McArdle CA (2012) ERK phosphorylation and nuclear accumulation: insights from single-cell imaging. *Biochem Soc Trans* 40(1):224-229.
124. Angaut-Petit D, Molgo J, Connold AL, & Faille L (1987) The levator auris longus muscle of the mouse: a convenient preparation for studies of short- and long-term presynaptic effects of drugs or toxins. *Neurosci Lett* 82(1):83-88.
125. Murray LM, Gillingwater TH, & Parson SH (2010) Using mouse cranial muscles to investigate neuromuscular pathology in vivo. *Neuromuscul Disord* 20(11):740-743.
126. Dudley DT, Pang L, Decker SJ, Bridges AJ, & Saltiel AR (1995) A synthetic inhibitor of the mitogen-activated protein kinase cascade. *Proc Natl Acad Sci U S A* 92(17):7686-7689.
127. Holness CL, da Silva RP, Fawcett J, Gordon S, & Simmons DL (1993) Macrosialin, a mouse macrophage-restricted glycoprotein, is a member of the lamp/lgp family. *J Biol Chem* 268(13):9661-9666.
128. Fontana X*, et al.* (2012) c-Jun in Schwann cells promotes axonal regeneration and motoneuron survival via paracrine signaling. *J Cell Biol* 198(1):127-141.

7. APPENDICES

Note: supplementary information of: [Duregotti E, et al. (2015) Mitochondrial alarmins released by degenerating motor axon terminals activate perisynaptic Schwann cells. Proc Natl Acad Sci U S A] are available at:
http://www.sciencedirect.com/science/article/pii/S0041010112008367#

Toxicon 64 (2013) 20–28

Contents lists available at SciVerse ScienceDirect

Toxicon

journal homepage: www.elsevier.com/locate/toxicon

Calpains participate in nerve terminal degeneration induced by spider and snake presynaptic neurotoxins

Elisa Duregotti [a,1], Erik Tedesco [b,1], Cesare Montecucco [a,*], Michela Rigoni [a,*]

[a] Department of Biomedical Sciences, CNR Institute of Neuroscience, University of Padova, Italy
[b] Département de Physiologie, Université de Montréal, Montreal, Canada

ARTICLE INFO

Article history:
Received 9 July 2012
Received in revised form 13 November 2012
Accepted 13 December 2012
Available online 22 December 2012

Keywords:
Presynaptic neurotoxins
Calpain
Ca^{2+} toxicity
Neurodegeneration

ABSTRACT

α-latrotoxin and snake presynaptic phospholipases A2 neurotoxins target the presynaptic membrane of axon terminals of the neuromuscular junction causing paralysis. These neurotoxins display different biochemical activities, but similarly alter the presynaptic membrane permeability causing Ca^{2+} overload within the nerve terminals, which in turn induces nerve degeneration. Using different methods, here we show that the calcium-activated proteases calpains are involved in the cytoskeletal rearrangements that we have previously documented in neurons exposed to α-latrotoxin or to snake presynaptic phospholipases A2 neurotoxins. These results indicate that calpains, activated by the massive calcium influx from the extracellular medium, target fundamental components of neuronal cytoskeleton such as spectrin and neurofilaments, whose cleavage is functional to the ensuing nerve terminal fragmentation.

1. Introduction

Many animal toxins target the neuromuscular junction (NMJ), interfering with its key function, the neurotransmission: among them the presynaptic toxins block acetylcholine (Ach) release by different, but often related, mechanisms of action, eventually leading to paralysis.

The black widow spiders (genus *Latrodectus*) are largely diffused in many parts of the world. The venom of *Latrodectus* spp. contains at least 86 unique proteins, some of which play a role in its toxicity towards insects and crustaceans, with only one component, alpha-latrotoxin (α-Ltx), that specifically targets vertebrates. A large body of evidence shows that Ca^{2+} influx through membrane channels induced by α-Ltx in the presynaptic membrane accounts for a major part of its effects (Ushkaryov et al., 2004, 2008; Vassilevski et al., 2009).

Presynaptic snake neurotoxins endowed with PLA2 activity (SPANs) are major components of the venom of four families of venomous snakes (Crotalidae, Elapidae, Hydrophiidae and Viperidae). These neurotoxins play a major role in the envenomation of the prey by causing a persistent blockade of neurotransmitter release from nerve terminal (Harris, 1985; Kini, 1997; Pungercar and Krizaj, 2007). Once bound to the presynaptic membrane they hydrolyse phospholipids, leading to a progressive accumulation of lysophospholipids (LysoPLs) and fatty acids (FA) and the consequent degeneration of the NMJ (Montecucco and Rossetto, 2000; Rigoni et al., 2005; Rossetto and Montecucco, 2008).

A recent side by side comparative study of SPANs and α-Ltx action in primary cultures of central neurons and in

Abbreviations: Ach, acetylcholine; [Ca^{2+}], calcium concentration; FA, fatty acid; α-Ltx, alpha-latrotoxin; LysoPC, lysophosphatidylcholine; NF, neurofilament; NMJ, neuromuscular junction; Ntx, notexin; OA, oleic acid; PLA2, phospholipase A2; SPANs, snake presynaptic PLA2 neurotoxins.

* Corresponding authors. Laboratory of Host-Pathogen Interactions, Department of Biomedical Sciences, University of Padova, Viale G. Colombo 3, 35121 Padova, Italy. Tel.: +39 0498276058; fax: +39 0498276049.

E-mail addresses: cesare.montecucco@unipd.it (C. Montecucco), rigonimic@gmail.com (M. Rigoni).

[1] These authors contributed equally to the present study.

0041-0101/$ – see front matter © 2013 Elsevier Ltd. All rights reserved.
http://dx.doi.org/10.1016/j.toxicon.2012.12.007

mice showed that, despite the different molecular mechanisms of intoxication, both kind of toxins exert their degenerative activity via inducing a large calcium influx inside nerve terminals (Tedesco et al., 2009). Both SPANs and α-Ltx cause phenotypical alterations in neurites of cultured primary neurons called *bulges*, hallmarks of their neurotoxicity. *Bulges* are sites of unbalanced endo–exocytosis and of intracellular calcium overload, where the neuronal cytoskeleton appears dramatically affected, with accumulation of neurofilaments (NF) and actin staining (Rigoni et al., 2004, 2007; Tedesco et al., 2009).

In light of these observations we have considered the possible involvement of calcium-activated proteases in the cytoskeletal rearrangements observed in cultured neurons exposed to both classes of neurotoxins and have focused our attention on calpains, a class of cysteine-proteases involved in cell damage following Ca^{2+} accumulation in the cytosol (Vosler et al., 2008). The two ubiquitously expressed isoforms of the calpain superfamily, m-calpain and μ-calpain, are the best-characterized ones and are conventionally termed calpains. These proteases are localized in the cytosol in their inactive form; in response to $[Ca^{2+}]$ increase they translocate to membranes where they are activated by autolytic processing. The calpain isoforms differ in $[Ca^{2+}]$ sensitivity: μ-calpain requires micromolar while m-calpain requires millimolar $[Ca^{2+}]$ for activation. Calpain physiological substrates include enzymes such as protein kinase C (PKC), as well as structural cytoskeletal proteins including spectrin, tubulin, microtubule-associated protein 2 (MAP2) and neurofilament proteins. At resting physiological conditions, when $[Ca^{2+}]$ oscillates around 100 nM, slight proteolytic modification of some calpain substrates is associated with normal cell functioning and protein turnover. Calpain inhibitors elicit accumulation of NF at the nerve terminal, suggesting that these proteases are indeed important in the normal regulation of synaptic structure (O'Hanlon et al., 2003). At pathological higher $[Ca^{2+}]$ calpains were shown to act particularly in models of hypoxic and traumatic brain injury as well as in many neurodegenerative diseases (Schumacher et al., 1999; Vosler et al., 2008; Kilinc et al., 2009).

Neurofilaments are composed of three proteins with apparent molecular weights of 200, 160, and 68 kDa referred to as heavy (NF-H), medium (NF-M) and light neurofilaments (NF-L), respectively. The neurofilament proteins are phosphorylated *in vivo*, particularly at multiple repeats of the Lys-Ser-Pro (KSP) motif. Neurofilaments are good substrates for calpains and their susceptibility is enhanced by dephosphorylation (Geddes et al., 1995; Pant, 1988). Calpain targets also include spectrin, a major membrane-skeletal protein, whose cleavage leads to the generation of two unique and highly stable breakdown products, which is an early event in neural cell pathology (Czogalla and Sikorski, 2005).

We have tested calpain contribution to neuronal cytoskeletal fragmentation in primary neuronal cultures from cerebellum and cortex exposed to α-Ltx and notexin (Ntx), a prototype snake PLA2 presynaptic neurotoxin, in the absence or presence of calpain inhibitors, using different experimental approaches: i) analysis of spectrin and NF Western blotting profiles; ii) time-course of *bulge* formation; iii) *live-imaging* of calpain activity with a fluorigenic calpain substrate. Our results indicate that these proteases participate in the degeneration process initiated by these two classes of animal toxins.

2. Methods

2.1. Chemicals

BME (*Basal Eagle Medium*), Neurobasal A, B27, Glutamax and the fluorigenic calpain substrate *t*-BOC-L-leucyl-L-methionine amide have been purchased from Invitrogen; AraC (cytosine β-D-arabinofuranoside), trypsin, trypsin inhibitor, DNAse I, poly-L-lysine, gentamycin, bovine serum albumin and oleic acid (OA) are Sigma–Aldrich; 1-myristoil-2-lysophosphatidylcholine (mLysoPC) is Avanti Polar Lipids; FBS is Euroclone. For Western Blot detection we employed the ECL LUMINATA from Millipore.

2.1.1. Toxins

Notexin was obtained from Latoxan (France), α-latrotoxin from Alomone (Israel). The purity of these toxins was checked by SDS-PAGE and their neurotoxicity by *ex-vivo* mouse nerve-hemidiaphragm preparation as previously described (Rigoni et al., 2005). The lipid mixture (mLysoPC + OA) was prepared following the procedure reported in Rigoni et al. (2005).

2.1.2. Calpain inhibitors

The following calpain inhibitors have been used at 20 μM final concentration: MDL28170 (Sigma–Aldrich), ALLN and PD150606 (Calbiochem). In experiments involving calpain inhibitors samples were preincubated 30 min to 1 h with the compounds and the inhibitors were kept in the medium throughout the experiment.

2.1.3. Antibodies

The following antibodies were used: mouse monoclonal anti-spectrin (Chemicon, working dilution in WB 1:1000); mouse monoclonal anti-neurofilaments (SMI31 and SMI32, Sternberg Monoclonals, 1:1000); mouse monoclonal anti-Hsc70 (Synaptic Systems, 1:5000); goat anti-mouse HRP-conjugated (Calbiochem, 1:2000).

2.2. Primary neuronal cultures

All experiments were performed in accordance with Italian animal care guidelines, law no. 116/1992. Rat cerebellar granule neurons (CGNs) and cortical neurons were prepared from 6 or 2-days-old Wistar rats respectively as previously described (Levi et al., 1984; Rigoni et al., 2004) and used 6–8 days after plating.

2.3. Sample preparation for Western blotting

CGNs (250,000/w, 24w plates) or cortical neurons (160,000/w, 24w plates) were exposed to α-Ltx, Ntx or mLysoPC + OA (0.1 nM for 30 min, 25 nM for 45 min and 25 μM for 30 min, respectively) in Krebs Ringer Buffer (KRH: 125 mM NaCl, 5 mM KCl, 1.2 mM $MgSO_4$, 2 mM $CaCl_2$,

1.2 mM KH_2PO_4, 6 mM glucose and 25 mM HEPES, pH 7.4), then washed twice with PBS 5 mM EDTA and lysed in Lysis Buffer (Hepes 10 mM, NaCl 150 mM, SDS 1%, EDTA 4 mM, protease inhibitors cocktail (Roche)). Protein concentration was quantified using the BCA assay (Protein Assay Kit, Pierce). 7–10 μg were loaded onto 10-well gels (Protogel, stacking gel 4%, resolving gel 6.5%, Minigel II Biorad) and then transblotted onto a nitrocellulose membrane. Following saturation (PBST 5% milk in the case of spectrin detection and PBS 5% BSA for phosphoneurofilaments), membranes were incubated o/n at 4 °C with the primary antibodies and, after washings, for 1 h at RT with the corresponding secondary antibodies HRP-conjugated. For densitometric quantification the bands of interest were normalized with the housekeeping protein Hsc70.

2.4. Time course of bulging

CGNs or cortical neurons at 6 to 8 DIV plated onto poly-L-lysine-coated 24 mm coverslips were washed and incubated in KRH at 37 °C in the absence or presence of the toxins (α-Ltx 0.1 nM for 40 min, Ntx 25 nM for 45 min) or the lipid mixture (25 μM for 30 min) and w/o calpain inhibitors (inhibitors were added to the medium at 20 μM final concentration 45 min before toxin addition and maintained throughout the experiment). Brightfield images with Nomarsky optics were acquired at 5–10 min intervals for a maximum of 45 min (Leica DMI6000 epifluorescence microscope).

2.5. Live-imaging of calpain activity and quantification

To detect calpain activity in living neurons, cells were loaded with the fluorogenic calpain substrate 7-amino-4-chloromethylcoumarin, *t*-BOC-L-leucyl-L-methionine amide (t-BOC). Non-fluorescent t-BOC freely diffuses into the cell and becomes membrane-impermeant after being conjugated to a thiol. Cleavage of t-BOC-thiol by calpain results in the release of fluorescent 7-amino-4-methylcoumarin-thiol (MAC-thiol). The formation of MAC-thiol is not reversible. Calpain activity at steady state results in an increase in fluorescence due to the accumulation of MAC-thiols. Changes in calpain activity can thus be detected by considering the rate of change in the MAC-thiol fluorescent signal (Rosser et al., 1993). CGNs or cortical neurons were incubated in Krebs buffer containing 50 μM t-BOC for 15 min at 37 °C, than the loading medium was washed out and fluorescence levels monitored in control conditions or following exposure to α-Ltx (0.1 nM for 30 min), Ntx (25 nM for 45 min) or to an equimolar mixture of mLysoPC + OA that has been previously found to mimic the neurotoxic effects of SPANs (25 μM for 30 min). A selected area on the coverslip was imaged at 10 min intervals. An excitation/emission filter set suitable for DAPI was used to record t-BOC fluorescence (Ex = 351 nm; Em = 430 nm; Leica DMI6000, LAS AF software). Since t-BOC is susceptible of photo-activation and this may turn out in cell photo-toxicity, exposure to ultraviolet light was kept at a minimum. The same experimental conditions were employed in the presence of calpain inhibitors; in this case cells were pre-treated with the inhibitors 45 min before intoxication and kept in the medium throughout the experiment. The changes in fluorescence with time within specific regions of interest at the level of cell bodies, neurites or *bulges* were measured (ImageJ software) and expressed as fold increase with respect to the fluorescence value at $t = 0$ for each sample.

3. Results

3.1. Analysis of calpain proteolytic activity by Western blotting

As a first assay of the contribution of calpains to the phenotypical alterations observed in primary cultures of neurons treated with α-Ltx or SPANs, we performed a Western blotting analysis of cell lysates from intoxicated cerebellar and cortical neurons. Two major targets of these proteases, spectrin and neurofilaments, were detected with specific antibodies. In fact, α-spectrin cleavage is a reliable method to detect calpain activation and has extensively been used as a quantitative measure of calpain activity (Vanderklish and Bahr, 2000). The primary antibody used here recognizes the intact spectrin 280 kDa band as well as the 150–145 kDa doublet that corresponds to calpain-specific cleavage products. Treatment of neurons with staurosporine, a compound known to activate both calpains and caspases (Nath et al., 1996), gave rise to the expected pattern, whilst pretreatment with calpain inhibitors (MDL28170, ALLN and PD150606) protected against staurosporine-mediated spectrin proteolysis (Fig. 1, panel A). Both α-Ltx and Ntx led to a reduction of the 280 kDa band and an increase of the bands corresponding to the cleavage products, and this effect was reduced in the presence of calpain inhibitors (Fig. 1, panels B and C). Closely similar results were obtained with cortical neurons (not shown). Also a lipid mixture composed of myristoyl-lysophosphatidylcholine (LysoPC) and oleic acid (OA) in equimolar concentrations, the products of the PLA2 activity of SPANs that were previously shown to mimic their overall neurotoxic action in both neuronal cultures and isolated NMJs (Rigoni et al., 2005, 2007), caused α-spectrin cleavage (Supplementary Fig. S1, panel A). A small reduction in calpain basal activity was observed in control samples incubated with the inhibitors alone (not shown).

We next extended such analysis to another important calpain substrate, the neurofilament proteins. No signal was detected in toxins-treated lysates w/o calpain inhibitors when a primary antibody directed against the phosphorylated H subunit was employed (SMI31), suggesting the possibility that the activation of cellular phosphatases by toxins-induced calcium entry with consequent dephosphorylation of such epitope might have occurred during treatments (Fig. 2, panel A). Indeed, incubation of neurons with the toxins in the presence of phosphatase inhibitors restored the phospho-NF signal (not shown). Following α-Ltx or Ntx exposure a decrease of the 200 kDa band was observed when an anti-NF antibody raised against a non-phosphorylated epitope in neurofilament H was employed (SMI32). In both treatments a partial protection by pretreatment with calpain inhibitors was observed (Fig. 2, panels B and C). A decrease in NF staining

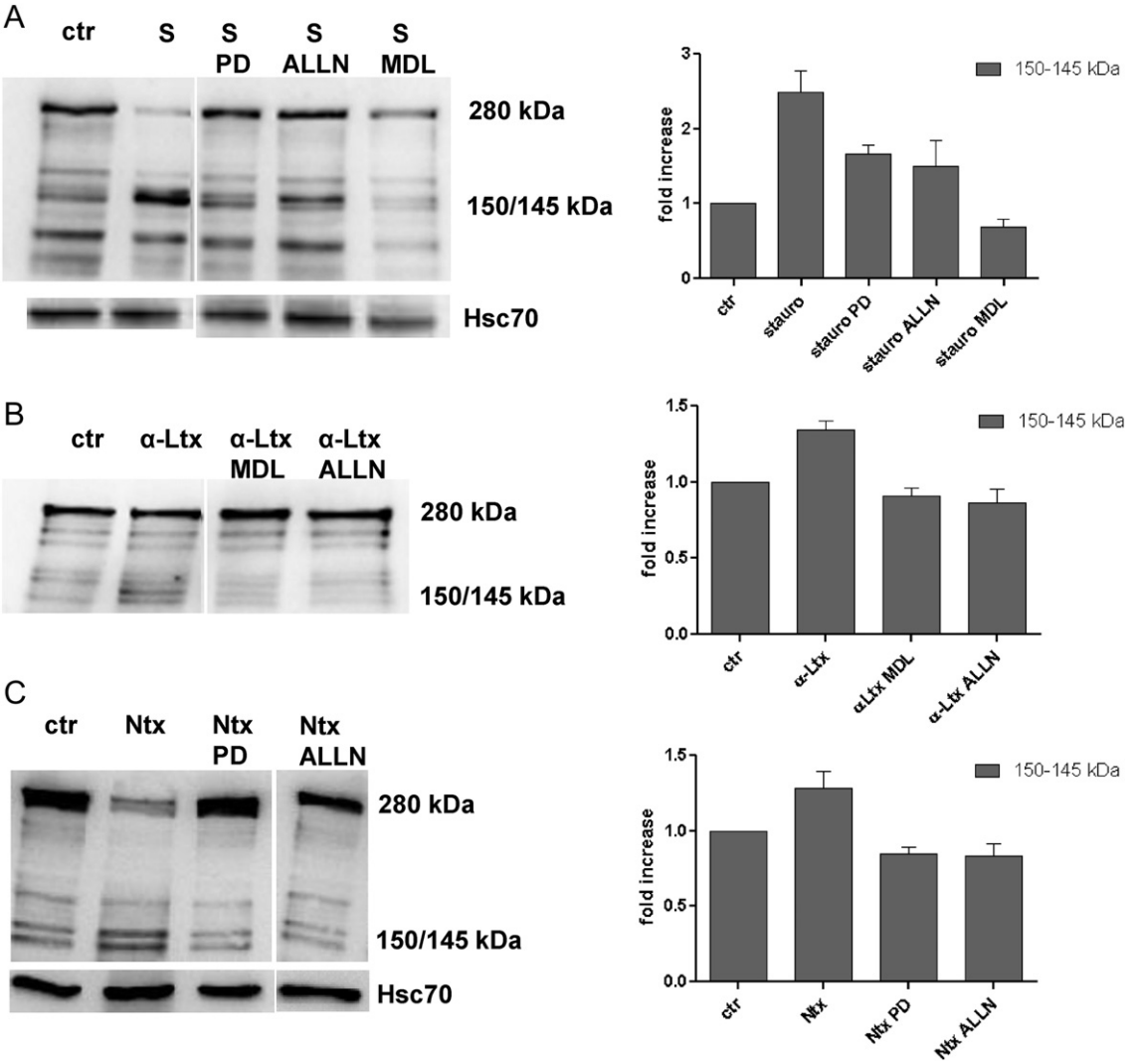

Fig. 1. Calpain-mediated proteolysis of spectrin in cerebellar neurons treated with staurosporine, α-Ltx or Ntx. Representative Western blots of neurons exposed to 0.5 μM staurosporine (S) for 16 h (panel A), 0.1 nM α-Ltx for 30 min (panel B) or 25 nM Ntx for 45 min (panel C) in complete medium in absence or presence of the calpain inhibitors PD150606, ALLN and MDL28170. Calpain-specific proteolysis of spectrin leads to a reduction of the 280 kDa band and the concomitant increase of the 150–145 kDa doublet. The 150–145 kDa doublet was quantified by densitometric analysis and normalized to the housekeeping protein Hsc70; the rate of cleavage is expressed as fold increase of the 150–145 kDa bands intensity with respect to the control as shown in the histograms (mean ± SD, $n = 4$).

was induced also by lipid mixture treatment (Fig.S1, panel B). Similar results were obtained in cortical neurons (not shown).

3.2. Calpain is not involved in the generation of neuronal bulges

The exposure of cerebellar and cortical neurons to α-Ltx or Ntx leads to the formation of characteristic swellings along neurites that we referred to as *bulges* (Rigoni et al., 2004, 2005). In the case of α-Ltx, *bulges* result mainly from the stimulation of exocytosis elicited by the toxin triggered by calcium influx, with consequent addition of vesicular membrane to the cell surface and neurotransmitter emptying of the terminal (Ceccarelli et al., 1972; Duchen et al., 1981; Ushkaryov et al., 2004). In the case of SPANs, the PLA2 activity exerted on the plasma membrane initiates the formation of *bulges*, with the ensuing unbalance between exocytosis and endocytosis, as shown by FRET and FM 1–43 experiments and by the surface exposure of the intraluminal domain of the vesicular protein synaptotagmin I (Rigoni et al., 2004, 2005; Bonanomi et al., 2005). Indeed, LysoPLs and FAs alone are capable of inducing neuronal *bulging* and this is reversed upon their removal (Caccin et al., 2006). However, with both classes of neurotoxins, vesicle exocytosis is not the only process involved in nerve terminal swelling, which nevertheless remains a good indicator of these presynaptic neurotoxins activity *in vitro*. We tested here the possibility that calpains are involved in nerve terminal *bulging* and found that preincubation of neurons with calpain inhibitors followed by toxins or lipid mixture addition did not decrease the rate

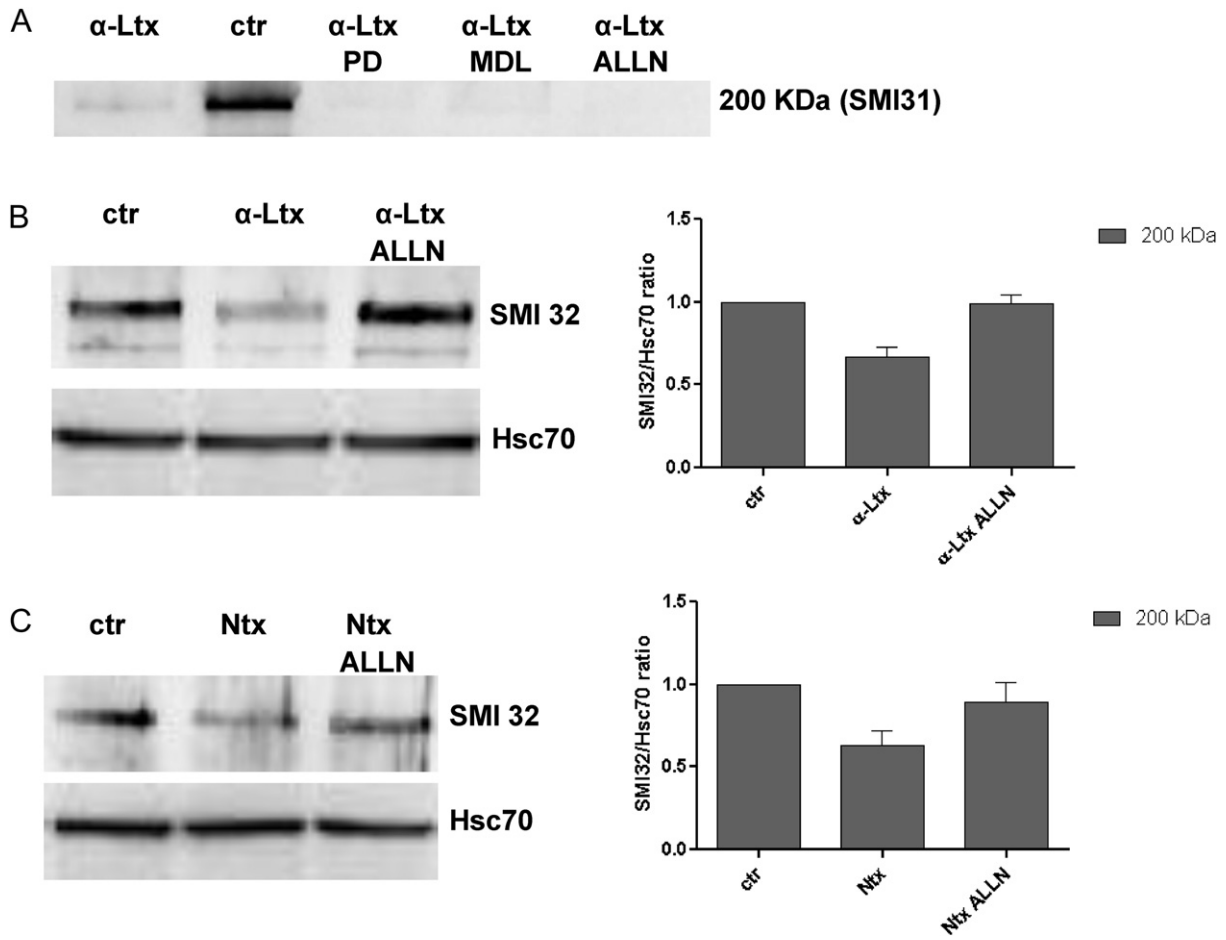

Fig. 2. Calpain-mediated proteolysis of neurofilaments in cerebellar neurons treated with α-Ltx and Ntx. Treatment of cerebellar neurons with α-Ltx 0.1 nM for 30 min led to disappearance of the 200 kDa band of the phosphorylated heavy NF subunit (SMI31 primary antibody, panel A); no recovery was observed with the inhibitors. B, C NF heavy subunit staining following incubation with a primary antibody raised against a non-phosphorylated epitope (SMI32 antibody). Both toxins cause a decrease of the 200 kDa band. In both cases a protection by ALLN was observed. The histograms show the densitometric analysis of the 200 kDa heavy chain normalized to the housekeeping protein Hsc70 (mean ± SD, $n = 4$).

of *bulge* formation nor affected their overall morphology (Fig. 3 and Supplementary Fig. S2). No toxicity was elicited by the inhibitors alone (not shown).

3.3. Live imaging of calpain activity in cultured neurons

To assay calpain involvement in later stages of toxins-induced neurodegeneration, neurons were loaded with a fluorogenic calpain substrate (7-amino-4-chlor-omethylcoumarin, *t*-BOC-L-leucyl-L-methionine amide, t-BOC) which becomes fluorescent once specifically cleaved by these proteases. Using this approach, we expected not only to confirm the results obtained in Western blot, but also to obtain a picture of the spatial distribution of calpain activity. Once added to culture medium t-BOC freely diffuses across the membranes into the cell cytosol, where it is retained because it is modified and becomes membrane-impermeable. Control neurons loaded with t-BOC showed an increase in fluorescence with time due to the basal activity of these enzymes in the cells and the photo-activation of the fluorogenic substrate (Fig. 4, panel A). Using the same acquisition parameters, the samples treated with α-Ltx, Ntx or the mLysoPC + OA lipid mixture (that was previously shown to induce Ca^{2+} influx, Rigoni et al., 2007) showed a more pronounced increase in fluorescence with respect to controls; in addition, the fluorescent signal was localized within swellings, indicating that *bulges* are indeed major sites not only of Ca^{2+} entry (Rigoni et al., 2007) but also of calpain activation (Fig. 4, panels B and C and Supplementary Fig. S3). Quantification of selected regions of interest (ROI) shows that the increase in fluorescence at the level of cell bodies was comparable between controls and treated samples, and that the mean fluorescence measured at the level of the neurites of toxin-treated neurons was lower than that measured in the *bulges*. The mean fluorescence within *bulges* increased with time and, judging from the fluorescence signal, the potency of the two toxins was comparable among them and with the lipid mixture (Fig. S4). Pretreatment with calpain inhibitors reduced both the resting calpain activity in

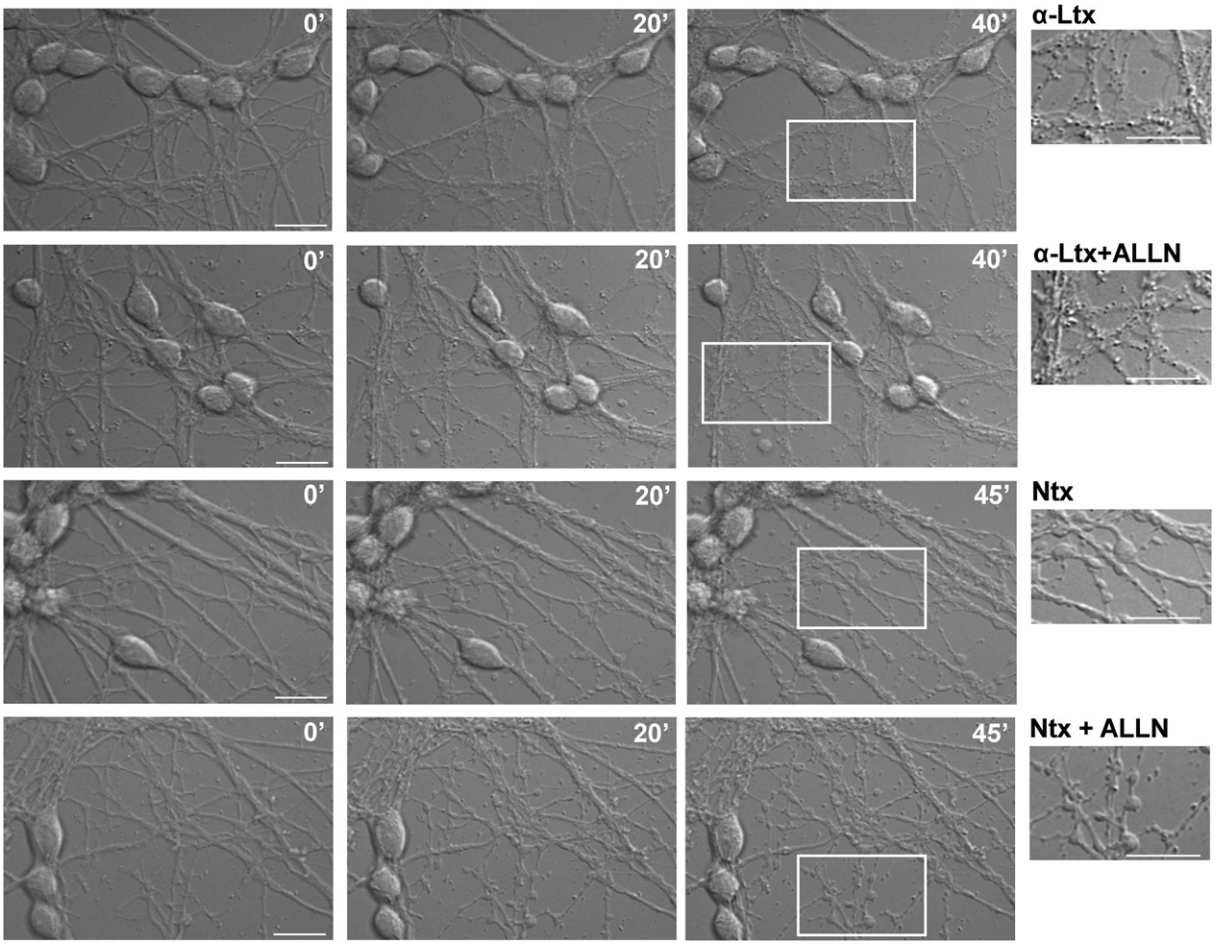

Fig. 3. Time course of *bulge* formation in cerebellar granule neurons treated with α-Ltx (0.1 nM for 40 min) or Ntx (25 nM for 45 min) in the absence or presence of the calpain inhibitor ALLN (20 μM). The same experiments were performed in cortical neurons and with the other inhibitors with similar results (not shown). White squares indicate areas shown at higher magnification on the right. Scale bar: 25 μm.

control neurons and that measured in treated samples, supporting the specificity of the phenomenon and confirming the results obtained by Western blotting (Fig. 5). Similar results were obtained using cortical neurons (not shown).

4. Discussion

Neuronal Ca^{2+} homeostasis and Ca^{2+} signalling regulate multiple neuronal functions, including synaptic transmission, plasticity and cell survival. Disturbances in calcium homeostasis due to energy depletion have been described in acute neurodegenerative disorders, as well as in tissues from aged humans both with and without associated age-related pathologies such as Alzheimer's disease. Alterations in Ca^{2+} homeostasis can affect the physiology of neurons in different ways and to various extents. A common observation from the pathologies mentioned above is the activation of the cysteine protease calpain, a calcium-dependent, non-lysosomal enzyme known to be widely expressed in animal tissues. The calcium sensitivity of calpains suggests that they are important effectors of changes in neurons brought about by calcium influx, a rather common pathological alteration in various forms of damage and/or degeneration of neurons (Nicotera et al., 1992; Bertipaglia and Carafoli, 2007). Alterations in calcium homeostasis during ischaemia, TBI and epilepsy result in the overwhelming activation of calpain *in vitro*, *in vivo* and in *post-mortem* brain. Chronic neurodegenerative diseases also show calcium disregulation with ensuing calpain activation (Vosler et al., 2008). Thus calcium-dependent processes represent points of convergence among a heterogeneous set of degenerative mechanisms. Pathologic activation of calpain results in the cleavage of a number of neuronal substrates that negatively affect neuronal structure and function, leading to inhibition of essential neuronal survival mechanisms. Experimental findings suggest that caspase and/or calpain inhibitors can attenuate neuronal degeneration in models of these neurodegenerative disorders (Vanderklish and Bahr, 2000; Chan and Mattson, 1999).

SPANs and α-Ltx cause similar degeneration of nerve terminals (Chen and Lee, 1970; Ceccarelli et al., 1972; Cull-Candy et al., 1976; Ceccarelli and Hurlbut, 1980; Duchen

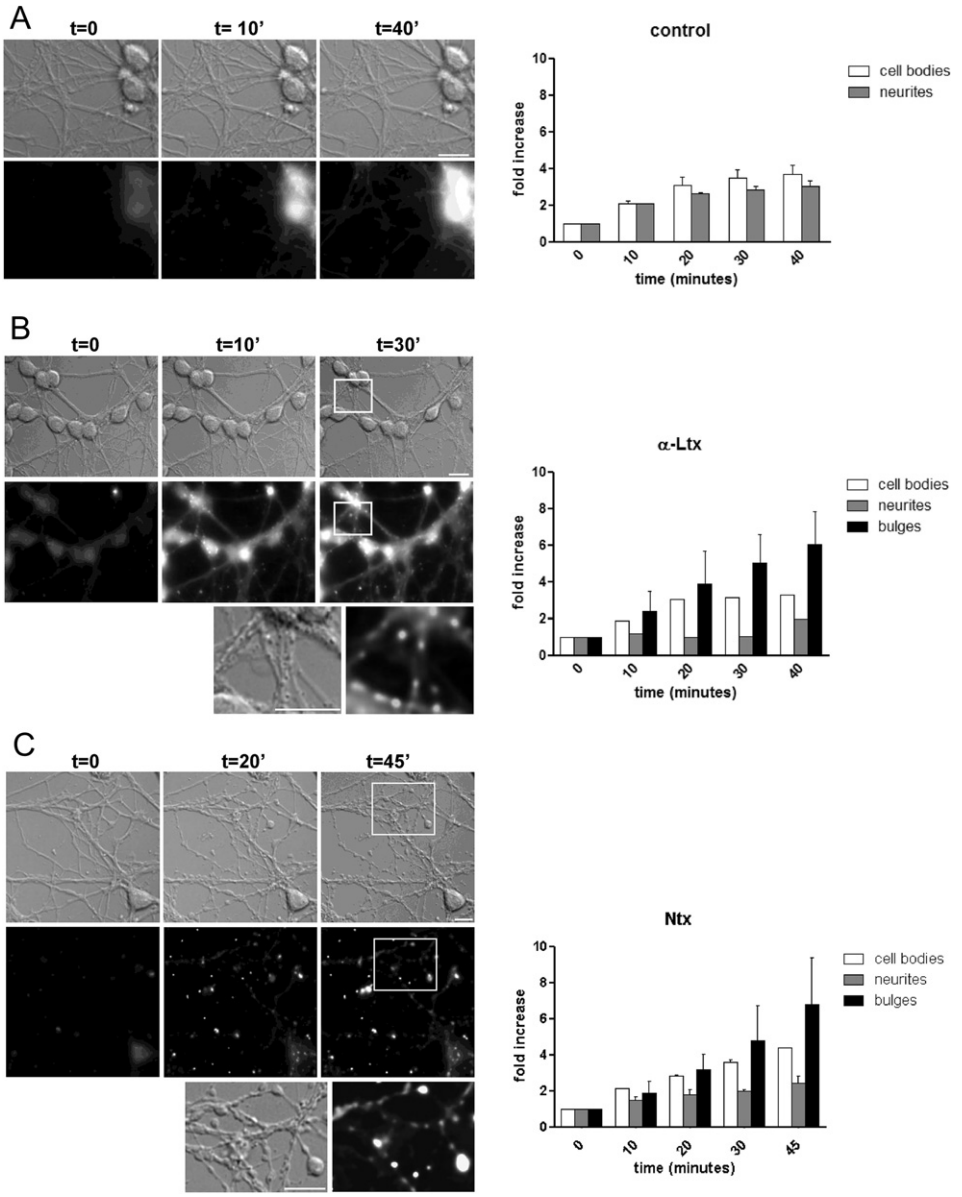

Fig. 4. *Live-imaging* of calpain activity in cultured neurons. CGNs were loaded with the fluorogenic compound t-BOC 50 μM for 15 min at 37 °C, washed, exposed to α-Ltx 0.1 nM for 30 min (B), Ntx 25 nM for 45 min (C) or left untreated (A) and their brightfield and fluorescence were monitored. Scale bar, 10 μm. Calpain activity with time was measured in defined regions of interest (ROI) at the level of cell bodies, neurites or *bulges* and expressed as ratio between the fluorescence level at each time point of the kinetic and that at $t = 0$ for the same ROI (see histograms).

et al., 1981; Lee et al., 1984; Gopalakrishnakone and Hawgood, 1984) with disappearance of neurofilaments and synaptic proteins (Dixon and Harris, 1999; Harris et al., 2000). We found previously that calcium overloading is the common eventual result of the different biochemical activities of these two classes of animal presynaptic neurotoxins (the PLA2 activity of SPANs and the ion channel activity of α-Ltx) (Rigoni et al., 2007, 2008; Tedesco et al., 2009).

Here, using different techniques, we have shown that calpains are indeed activated following intoxication with both classes of neurotoxins: their cleavage of spectrin and neurofilaments, two typical calpain substrates, detected by Western blot, is largely inhibited by preincubation with calpain inhibitors. Following toxins treatment, the NF heavy subunit is dephosphorylated and degraded; these results fit with previous observations that dephosphorylation enhances neurofilaments susceptibility to calpains (Pant, 1988).

Calpain involvement was further confirmed by *live-imaging* experiments of calpain activity in cultured neurons, showing a localized action within *bulges*, that are phenotypical hallmarks of intoxication by both α-Ltx and SPANs. *Bulging* derives mainly from membrane accumulation that

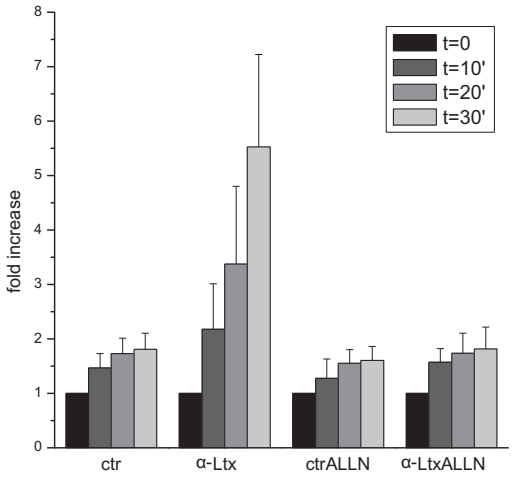

Fig. 5. The generation of MAC-thiol by α-Ltx is calpain-specific. CGNs were loaded with the calpain fluorogenic substrate t-BOC as described in the legend of Fig. 4 and in the methods section and then treated w/o α-Ltx in the presence or absence of the calpain inhibitor ALLN. In α-Ltx-treated samples the increase in fluorescence within *bulges*, due to the formation of a MAC-thiol by calpain cleavage, is almost abolished by the calpain inhibitor pretreatment. Similar results were obtained with Ntx and the lipid mixture (not shown).

follows unbalanced exo–endocytosis. In the case of α-Ltx, calcium entry is the major event responsible for nerve swelling from the beginning, as this toxin is a Ca^{2+} channel itself, whereas in the case of snake PLA2 the initial process in *bulge* formation is the production of LysoPLs, which favour synaptic vesicle exocytosis not followed by endocytosis. This is then followed by the entry of calcium mediated by transient LysoPLs pores (Rigoni et al., 2004, 2005; Bonanomi et al., 2005). Indeed, *bulge* appearance preceeds intracellular calcium rise (Rigoni M., unpublished observations). Accordingly, calpain inhibitors did not prevent *bulging*, in line with the observations that *bulges* are not the mere result of cytoskeletal rearrangements and with electrophysiological experiments demonstrating that calpain inhibition does not prevent the induction of neuroexocytosis by α-Ltx (O'Hanlon et al., 2003).

Calpain activation appears to be a later event in the intoxication process by these two classes of presynaptic neurotoxins, which manifests itself as cytosolic protein cleavage, and particularly as the cleavage of cytoskeletal proteins. The fragmentation of the cytoskeleton components by calpains found here appears to be an important prerequisite for the following step which is the degeneration of the nerve terminal into fragments, necessary for the subsequent removal of the degraded terminals by phagocytosis. In turn, this is essential for the final regeneration of the neuromuscular junction which takes place *in vivo* (Grubb et al., 1991; Prasarnpun et al., 2005).

Axon degeneration with fragmentation of axonal cytoskeleton is a characteristic event in many chronic neurodegenerative conditions as well after acute nerve injuries. As early as 5–10 min after nerve transection, for example, the axonal segments immediately proximal and distal to the injury site rapidly degenerate by several hundred micrometres in either directions, and this process is thought to be driven by influx of extracellular calcium, with subsequent activation of calpains. Increased calpain cleavage of spectrin occurs as early as 30 min after injury *in vivo*, indicating that calpain activity is the primary effector of the acute axonal degeneration (AAD) (Wang et al., 2012).

The present study provides further insights into the molecular mechanisms of action of these two types of animal toxins, α-Ltx and Ntx, that have very different biological activities but block the NMJ functionality in a similar way, via the induction of the entry of calcium ions inside axon terminals. Our results demonstrate the involvement of the calcium-activated proteases calpains in the degeneration of the nerve terminals induced by both type of neurotoxins, and suggest that their study can provide useful information to the understanding of other neurodegenerative conditions.

Ethical statement

All experimental procedures involving animals were carried out in accordance with the Italian Animal Welfare Act and with the European Community Council Directive of November 24, 1986 (86/609/EEC). All experiments were approved by the local veterinary service, the University of Padua Ethic Committee for Animal Research (Comitato Etico di Ateneo per la Sperimentazione Animale, CEASA) and by the Italian Ministry of Health.

Funding

This work was supported by the Università di Padova, Progetto Strategico "An *in vivo* approach to the physiopathology of signal transduction" to C. M.

Appendix A. Supplementary data

Supplementary data related to this article can be found at http://dx.doi.org/10.1016/j.toxicon.2012.12.007.

Conflict of interest statement

The authors declare that there are no conflicts of interest.

References

Bertipaglia, I., Carafoli, E., 2007. Calpains and human diseases. Subcell. Biochem. 45, 29–53.
Bonanomi, D., Pennuto, M., Rigoni, M., Rossetto, O., Montecucco, C., Valtorta, F., 2005. Taipoxin induces synaptic vesicle exocytosis and disrupts the interaction of synaptophysin I with VAMP2. Mol. Pharmacol. 67, 1901–1908.
Caccin, P., Rigoni, M., Bisceglie, A., Rossetto, O., Montecucco, C., 2006. Reversible skeletal neuromuscular paralysis induced by different lysophospholipids. FEBS Lett. 580, 6317–6321.
Ceccarelli, B., Hurlbut, W.P., 1980. Vesicle hypothesis of the release of quanta of acetylcholine. Physiol. Rev. 60, 396–441.
Ceccarelli, B., Hurlbut, W.P., Mauro, A., 1972. Depletion of vesicle from frog neuromuscular junction by prolonged tetanic stimulation. J. Cell. Biol. 50, 30–38.
Chan, S.L., Mattson, M.P., 1999. Caspase and calpain substrates: roles in synaptic plasticity and cell death. J. Neurosci. Res. 58, 167–190.
Chen, I.L., Lee, C.Y., 1970. Ultrastructural changes in the motor nerve terminals caused by beta-bungarotoxin. Virchows Arch. B Cell. Pathol. 6, 318–325.

Cull-Candy, S.G., Fohlman, J., Gustavsson, D., Lullmann-Rauch, R., Thesleff, S., 1976. The effects of taipoxin and notexin on the function and fine structure of the murine neuromuscular junction. Neuroscience 1, 175–180.

Czogalla, A., Sikorski, A.F., 2005. Spectrin and calpain: a 'target' and a 'sniper' in the pathology of neuronal cells. Mol. Life Sci. 62, 1913–1924.

Dixon, R.W., Harris, J.B., 1999. Nerve terminal damage by beta-bungarotoxin: its clinical significance. Am. J. Pathol. 154, 447–455.

Duchen, L.W., Gomez, S., Queiroz, L.S., 1981. The neuromuscular junction of the mouse after black widow spider venom. J. Physiol. 316, 279–291.

Geddes, J.W., Bondada, V., Tekirian, T.L., Pang, Z., Siman, R.G., 1995. Perikaryal accumulation and proteolysis of neurofilament proteins in the post-mortem rat brain. Neurobiol. Aging 16, 651–660.

Gopalakrishnakone, P., Hawgood, B.J., 1984. Morphological changes induced by crotoxin in murine nerve and neuromuscular junction. Toxicon 22, 791–804.

Grubb, B.D., Harris, J.B., Schofield, I.S., 1991. Neuromuscular transmission at newly formed neuromuscular junctions in the regenerating soleus muscle of the rat. J. Phisiol. 441, 405–421.

Harris, J.B., Grubb, B.D., Maltin, C.A., Dixon, R., 2000. The neurotoxicity of the venom phospholipases A2, notexin and taipoxin. Exp. Neurol. 161, 517–526.

Harris, J.B., 1985. Phospholipases in snake venoms and their effects on nerve and muscle. Pharmacol. Ther. 31, 79–102.

Kilinc, D., Gallo, G., Barbee, K.A., 2009. Mechanical membrane injury induces axonal beading through localized activation of calpain. Exp. Neurol. 219, 553–561.

Kini, R.M., 1997. Venom Phospholipase A2 Enzymes. John Wiley & Sons.

Lee, C.Y., Tsai, M.C., Chen, J.M., Ritonja, A., Gubensek, F., 1984. Mode of neuromuscular blocking action of toxic phospholipases A2 from *Vipera ammodytes* venom. Arch. Int. Pharmacodyn. Ther. 268, 313–324.

Levi, G., Aloisi, F., Ciotti, M.T., Gallo, V., 1984. Autoradiographic localization and depolarization-induced release of acidic amino acids in differentiating cerebellar granule cell cultures. Brain Res. 290, 77–86.

Montecucco, C., Rossetto, O., 2000. How do presynaptic PLA2 neurotoxins block nerve terminals? Trends Biochem. Sci. 25, 266–270.

Nath, R., Raser, K.J., Stafford, D., Iradj Hajimohammadreza, I., Posner, A., Allen, H., Talanian, R.V., Yuen, P., Gilbertse, R.B., Wang, K.K.W., 1996. Non-erythroid alpha-spectrin breakdown by calpain and interleukin 1 beta-converting-enzyme-like protease(s) in apoptotic cells: contributory roles of both protease families in neuronal apoptosis. Biochem. J. 319, 683–690.

Nicotera, P., Bellomo, G., Orrenius, S., 1992. Calcium-mediated mechanisms in chemically induced cell death. Annu. Rev. Pharmacol. Toxicol. 32, 449–470.

O'Hanlon, G.M., Humphreys, P.D., Goldman, R.S., Halstead, S.K., Bullens, R.W.M., Plomp, J.J., Ushkaryov, Y., Willison, H.J., 2003. Calpain inhibitors protect against axonal degeneration in a model of anti-ganglioside antibody-mediated motor nerve terminal injury. Brain 126, 2497–2509.

Pant, H.C., 1988. Dephosphorylation of neurofilament proteins enhances their susceptibility to degradation by calpain. Biochem. J. 256, 665–668.

Prasarnpun, S., Walsh, J., Awad, S.S., Harris, J.B., 2005. Envenoming bites by kraits: the biological basis of treatment-resistant neuromuscular paralysis. Brain 128, 2987–2996.

Pungercar, J., Krizaj, I., 2007. Understanding the molecular mechanism underlying the presynaptic toxicity of secreted phospholipases A2. Toxicon 50, 871–892.

Rigoni, M., Schiavo, G., Weston, A.E., Caccin, P., Allegrini, F., Pennuto, M., Valtorta, F., Montecucco, C., Rossetto, O., 2004. Snake presynaptic neurotoxins with phospholipase A2 activity induce punctate swellings of neurites and exocytosis of synaptic vesicles. J. Cell. Sci. 117, 3561–3570.

Rigoni, M., Caccin, P., Gschmeissner, S., Koster, G., Postle, D.A., Rossetto, O., Schiavo, G., Montecucco, C., 2005. Equivalent effects of snake PLA2 neurotoxins and lysophospholipid-fatty acid mixtures. Science 210, 1678–1680.

Rigoni, M., Pizzo, P., Schiavo, G., Weston, A.E., Zatti, G., Caccin, P., Rossetto, O., Pozzan, T., Montecucco, C., 2007. Calcium influx and mitochondrial alterations at synapses exposed to snake neurotoxins or their phospholipid hydrolysis products. J. Biol. Chem. 282, 11238–11245.

Rigoni, M., Paoli, M., Milanesi, E., Caccin, P., Rasola, A., Bernardi, P., Montecucco, C., 2008. Snake phospholipase A2 neurotoxins enter neurons, bind specifically to mitochondria, and open their transition pores. J. Biol. Chem. 283, 34013–34020.

Rosser, B.G., Powers, S.P., Gores, G.J., 1993. Calpain activity increases in hepatocytes following addition of ATP. Demonstration by a novel fluorescent approach. J. Biol. Chem. 268, 23593–23600.

Rossetto, O., Montecucco, C., 2008. Presynaptic neurotoxins with enzymatic activities. Handb. Exp. Pharmacol. 184, 129–170.

Schumacher, P.A., Eubanks, J.H., Fehlings, M.G., 1999. Increased calpain I-mediated proteolysis, and preferential loss of dephosphorylated NF200, following traumatic spinal cord injury. Neuroscience 91, 733–744.

Tedesco, E., Rigoni, M., Caccin, P., Grishin, E., Rossetto, O., Montecucco, C., 2009. Calcium overload in nerve terminals of cultured neurons intoxicated by alpha-latrotoxin and snake PLA2 neurotoxins. Toxicon 54, 138–144.

Ushkaryov, Y.A., Volynski, K.E., Ashton, A.C., 2004. The multiple actions of black widow spider toxins and their selective use in neurosecretion studies. Toxicon 43, 527–542.

Ushkaryov, Y.A., Rohou, A., Sugita, S., 2008. alpha-Latrotoxin and its receptors. Handb. Exp. Pharmacol. 184, 171–206.

Vanderklish, P.W., Bahr, B.A., 2000. The pathogenic activation of calpain: a marker and mediator of cellular toxicity and disease states. Int. J. Exp. Pathol. 81, 323–339.

Vassilevski, A.A., Kozlov, S.A., Grishin, E.V., 2009. Molecular diversity of spider venom. Biochemistry (Mosc.) 74, 1505–1534.

Vosler, P.S., Brennan, C.S., Chen, J., 2008. Calpain-mediated signaling mechanisms in neuronal injury and neurodegeneration. Mol. Neurobiol. 38, 78–100.

Wang, J.T., Medress, Z.A., Barres, B.A., 2012. Axon degeneration: molecular mechanisms of a self-destruction pathway. J. Cell. Biol. 196, 7–18.

Mitochondrial alarmins released by degenerating motor axon terminals activate perisynaptic Schwann cells

Elisa Duregotti[a], Samuele Negro[a], Michele Scorzeto[a], Irene Zornetta[a], Bryan C. Dickinson[b,c,1], Christopher J. Chang[b,c], Cesare Montecucco[a,d,2], and Michela Rigoni[a,2]

[a]Department of Biomedical Sciences, University of Padua, Padua 35131, Italy; [b]Department of Chemistry and Molecular and Cell Biology and [c]Howard Hughes Medical Institute, University of California, Berkeley, CA 94720; and [d]Italian National Research Council Institute of Neuroscience, Padua 35131, Italy

Edited by Thomas C. Südhof, Stanford University School of Medicine, Stanford, CA, and approved December 22, 2014 (received for review September 5, 2014)

An acute and highly reproducible motor axon terminal degeneration followed by complete regeneration is induced by some animal presynaptic neurotoxins, representing an appropriate and controlled system to dissect the molecular mechanisms underlying degeneration and regeneration of peripheral nerve terminals. We have previously shown that nerve terminals exposed to spider or snake presynaptic neurotoxins degenerate as a result of calcium overload and mitochondrial failure. Here we show that toxin-treated primary neurons release signaling molecules derived from mitochondria: hydrogen peroxide, mitochondrial DNA, and cytochrome c. These molecules activate isolated primary Schwann cells, Schwann cells cocultured with neurons and at neuromuscular junction in vivo through the MAPK pathway. We propose that this inter- and intracellular signaling is involved in triggering the regeneration of peripheral nerve terminals affected by other forms of neurodegenerative diseases.

motor axon degeneration | presynaptic neurotoxins | mitochondrial alarmins | Schwann cells

The venoms of the black widow spider *Latrodectus mactans*, the Australian taipan snake *Oxyuranus scutellatus scutellatus*, and the Taiwan krait *Bungarus multinctus* cause the paralysis of peripheral skeletal and autonomic nerve terminals in envenomated subjects. Such paralysis is completely reversible, and within a month or so, patients, supported by mechanical ventilation, recover completely (1–3). Paralysis in mice/rodents has a shorter duration, and again recovery is complete (4, 5). Major presynaptic toxins of these venoms are α-latrotoxin (α-Ltx), taipoxin (Tpx), and β-bungarotoxin (β-Btx), respectively (6, 7). α-Ltx induces a very rapid nerve terminal paralysis by forming transmembrane ion channels that cause a massive Ca^{2+} entry, with exocytosis of synaptic vesicles and mitochondrial damage (7–11). This is followed by Ca^{2+}-induced degeneration of motor axon terminals, which is remarkably limited to the unmyelinated endplate. Complete regeneration is achieved in mice within 8–10 d (4). Tpx and β-Btx are representative of a large family of presynaptic snake neurotoxins endowed with phospholipase A2 activity (SPANs), which are important, although neglected, human pathogens (12–15). We have contributed to the definition of their mechanism of action, which involves generation of lysophospholipids and fatty acids on the external layer of the plasma membrane (16, 17). The mixture of these lipid products favors exocytosis of ready-to-release synaptic vesicles and mediates the rise of cytosolic Ca^{2+}, presumably via transient lipid ion channels (16, 18). In turn, this Ca^{2+} influx causes a massive release of synaptic vesicles and mitochondrial damage, with ensuing complete degeneration of axon terminals (5, 18–20). Similar to α-Ltx, SPANs-induced peripheral paralysis is followed by a complete recovery: regeneration and functional reinnervation are almost fully restored in rats by 5 d (20). The similar outcome and time-course of the paralysis induced by the two types of presynaptic neurotoxins suggest that the common property of inducing Ca^{2+} entry into the nerve terminals is the main cause of nerve terminal degeneration (21). Indeed, these neurotoxins cause activation of the calcium-activated calpains that contribute to cytoskeleton fragmentation (22).

Although clearly documented (4, 5, 20), the regeneration of the motor axon terminals after presynaptic neurotoxins injection is poorly known in its cellular and molecular aspects. Available evidence indicates that, in general, regeneration of mechanically damaged motor neuron terminals relies on all three cellular components of the neuromuscular junction (NMJ): the neuron, the perisynaptic Schwann cells (PSCs), and the muscle cells (23, 24). The regeneration steps that take place on animal neurotoxin poisoning are likely to be similar to those after the cut or crush of nerves, as a closely similar cascade of toxic events occurs in both conditions (i.e., calcium overload, mitochondrial impairment, and cytoskeleton degradation). Similar neurodegenerative events are also shared by traumatized patients. However, the model system used here provides the advantage of being much more controlled and more reproducible. In addition, it does not involve the death of many cell types, as it follows a well-characterized biochemical lesion of the end plate only (7, 8, 10–12, 16, 18). Therefore, the mouse NMJ treated with α-Ltx, Tpx, or β-Btx represents a relevant model of acute motor axon terminal

Significance

The neuromuscular junction is the site of transmission of the nerve impulse to the muscle. This finely tuned synapse relies on at least three components: the motor neuron, the muscle fiber, and the Schwann cells, which assist nerve recovery after injury. Using animal neurotoxins to induce an acute and reversible nerve degeneration, we have identified several mitochondrial molecules through which the damaged nerve terminal communicates with nearby cells, activating signaling pathways in Schwann cells involved in nerve regeneration. Among these messengers, hydrogen peroxide appears to be crucial at the initial stages of regeneration, because its inactivation delays the functional recovery of the damaged neuromuscular junction in vivo. These findings provide important indications about the pharmacological treatment of traumatized patients.

Author contributions: C.M. and M.R. designed research; E.D., S.N., M.S., and I.Z. performed research; B.C.D. and C.J.C. contributed new reagents/analytic tools; E.D., S.N., M.S., I.Z., C.M., and M.R. analyzed data; and E.D., S.N., M.S., I.Z., B.C.D., C.J.C., C.M., and M.R. wrote the paper.

The authors declare no conflict of interest.

This article is a PNAS Direct Submission.

Freely available online through the PNAS open access option.

[1]Present address: Gordon Center for Integrative Sciences, University of Chicago, Chicago, IL 60637.

[2]To whom correspondence may be addressed. Email: michela.rigoni@unipd.it or cesare.montecucco@unipd.it.

This article contains supporting information online at www.pnas.org/lookup/suppl/doi:10.1073/pnas.1417108112/-/DCSupplemental.

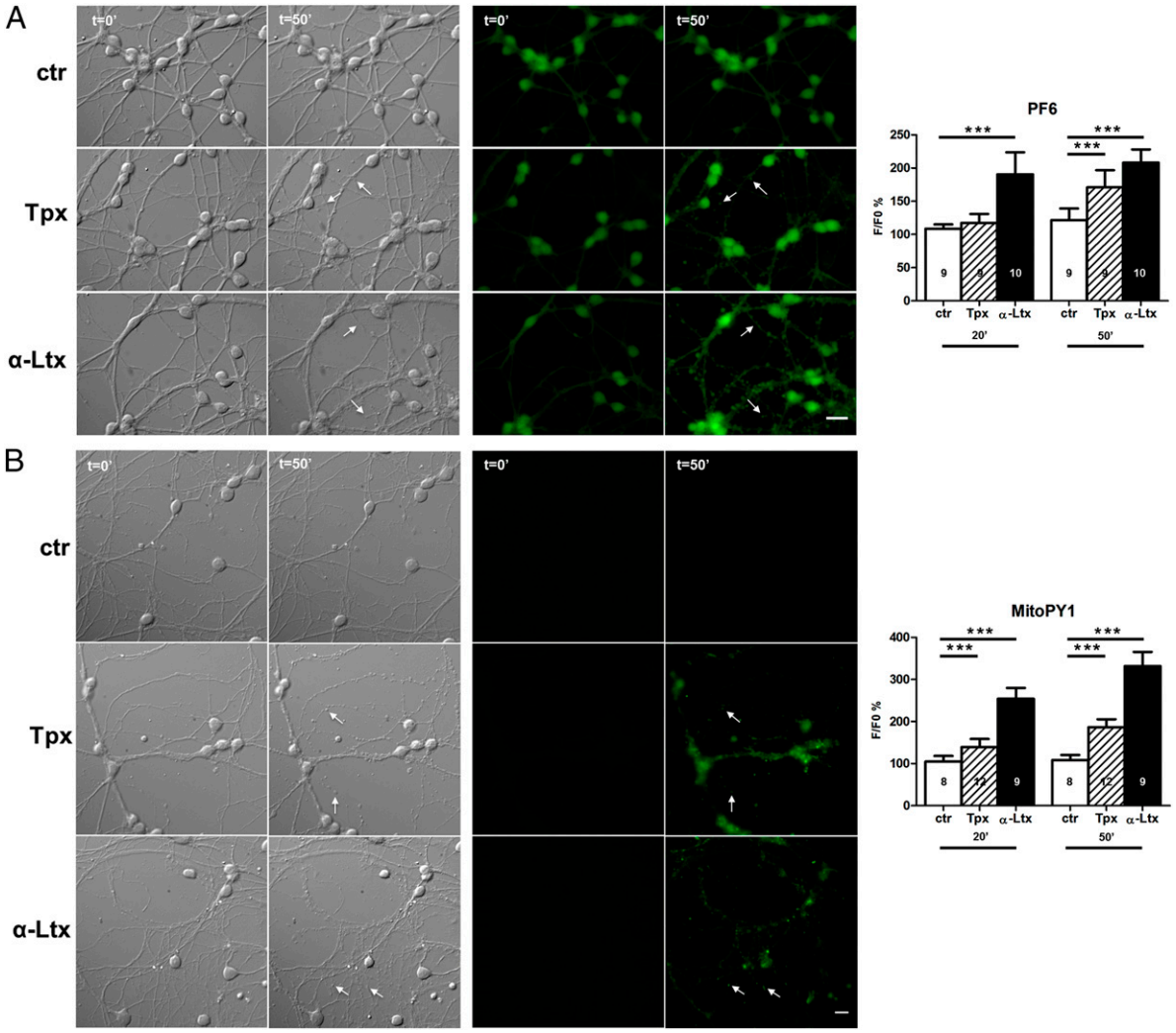

Fig. 1. Live-imaging of neuronal hydrogen peroxide production. Rat CGNs were loaded with the H_2O_2-specific probes PF6-AM (*A*) or MitoPY1 (*B*), washed, and then exposed to Tpx 6 nM or α-Ltx 0.1 nM for 50 min. Changes in fluorescence resulting from H_2O_2 production were monitored with time and expressed as a percentage of the fluorescence value at $t = 0$ (*Right*). ***$P < 0.001$. Arrows in bright-field images and in the green channel point to neuronal bulges. (Scale bars: 10 μm.)

degeneration and regeneration, which is likely to provide information useful to the understanding of the pathogenesis not only of envenomation but also, more in general, of other human pathological syndromes.

Cell death and injury often lead to the release or exposure of intracellular molecules called damage-associated molecular patterns (DAMPs) or alarmins. Recently, mitochondria have emerged as major sources of DAMPs (25). Mitochondria are abundant subcellular components of the NMJ that have been recently shown to release mitochondrial DNA (mtDNA) and cytochrome c (Cyt c) after trauma or snake myotoxin-induced muscle damage, thus contributing to the systemic or local inflammatory responses associated with such conditions (26, 27). In this study, we tested whether α-Ltx and SPANs induce the release of mitochondrial signaling molecules from primary neuronal cultures and found that, in addition to mtDNA and Cyt c, hydrogen peroxide (H_2O_2) is released. First candidate targets of these mitochondrial mediators released by damaged neurons are nonmyelinating PSCs, which are intimately associated with the end plate. They play an active role in the formation, function, maintenance, and repair of the NMJ (28–33). PSC activation parallels nerve degeneration and contributes to neuronal regeneration by phagocytosis of cellular debris and by extension of processes that guide reinnervation (34, 35). We therefore investigated whether mitochondrial DAMPs released by injured neurons were able to activate SCs, and through which downstream pathway. Using isolated primary cells, neuron-Schwann cell cocultures, and the NMJ in vivo, we found that PSCs are activated by mitochondrial alarmins and that the MAPK signaling pathway is involved in this process.

Results

Hydrogen Peroxide Is Produced by Neurons Exposed to Spider or Snake Presynaptic Neurotoxins. Given that mitochondria of stressed cells produce superoxide anion, which is rapidly converted into H_2O_2, and that in neurons exposed to the neurotoxins, mitochondria functionality is impaired, we asked whether intoxication of neurons by α-Ltx or SPANs leads to H_2O_2 production, an ideal candidate as intercellular signaling molecule (36–38). We therefore loaded rat cerebellar granular neurons (CGNs) with specific H_2O_2 probes with different cellular localization and monitored the samples for up to an hour. MitoPY1 is a bifunctional molecule that combines a chemoselective boronate-based switch and a mitochondrial-targeting phosphonium moiety for the detection

of H_2O_2 localized to mitochondria (39). PF6-AM takes advantage of multiple masked carboxylates to increase cellular retention, and hence sensitivity to low levels of peroxide. In its ester-protected form, PF6-AM can readily enter cells. Once inside cells, the protecting groups are rapidly cleaved by intracellular esterases to produce their anionic carboxylate forms, which are effectively trapped within cells (40).

After exposure to α-Ltx or Tpx, H_2O_2 levels increased with time, markedly at the level of neurite enlargements (so-called bulges), which are a hallmark of intoxication (16, 41), as shown in Fig. 1. Bulges are sites of calcium overload and accumulation of depolarized mitochondria (18), and the MitoPY1 signal indicates that these mitochondria produce H_2O_2. Quantification of the signals indicates a more pronounced effect of α-Ltx with respect to Tpx, in agreement with the fact that the pore formed by the former neurotoxin mediates a larger Ca^{2+} entry than Tpx (21). Similar results were obtained following intoxication of rat spinal cord motor neurons (MNs; Fig. S1). That mitochondria are the major source of H_2O_2 is reinforced by the finding that toxins failed to induce membrane translocation of cytoplasmic p47phox, a regulatory component of the NADPH oxidase complex, which excludes a role of the NADPH oxidase system (Fig. S2).

Hydrogen Peroxide Released by Degenerating Nerve Terminals Activates Schwann Cells and Stimulates Regeneration. Growing evidence indicates that H_2O_2 is a largely used intercellular signaling molecule regulating kinase-driven pathways (37, 38, 42): it triggers ERK phosphorylation in different cell types (43), with consequent activation of downstream gene transcription, and ERK signaling was recently shown to play a central role in the orchestration of axon repair by SCs (44, 45).

In preliminary experiments, we checked whether primary SCs isolated from rat sciatic nerves were responsive to H_2O_2 by analyzing ERK phosphorylation by Western blotting and immunofluorescence. Exposure of primary SCs to H_2O_2 led to ERK phosphorylation and translocation of p-ERK into the nucleus (Fig. S3 *A* and *B*). Cocultures of primary spinal cord motor neurons and sciatic nerve-derived SCs were then exposed to α-Ltx or Tpx: bulges appeared within few minutes along neuronal processes, and p-ERK was detected in the cytoplasm and nucleus of SCs (Fig. 2*A*). Phospho-ERK-positive cells were also positive for S-100, a specific SC marker (Fig. S3*C*). In cocultures, the score of S-100-positive cells that become p-ERK-positive is 59% on intoxication with β-Btx ($n = 81$) and 78% in the case of α-Ltx ($n = 69$). These percentages were obtained by counting many S-100-positive cells randomly distributed in different fields, but the value is actually much higher if one considers only clustered SCs in close proximity of intoxicated neurites; this observation further supports the conclusion that molecules released by injured neurons reach nearby SCs, thus activating them.

ERK phosphorylation was reduced in cocultures preincubated with catalase, which converts H_2O_2 into water and O_2, indicating that H_2O_2 produced inside neurons diffuses to reach nearby SCs, contributing to their ERK activation (Fig. 2*B*). Residual p-ERK signal might be a result of mediators other than H_2O_2 released on neuronal injury. Toxins failed to induce a direct ERK phosphorylation either in isolated SCs (Fig. S3*D*) or in isolated primary neurons (Fig. 2*B*).

Next we tested whether the ERK pathway is activated also within PSCs at the NMJs of intoxicated mice. Sublethal doses of the neurotoxins were s.c. injected in transgenic mice expressing a cytoplasmic GFP specifically in SCs under the *plp* promoter (46, 47), in proximity to the levator auris longus (LAL) (48), a thin muscle ideal for imaging. Twenty-four hours later, muscles were collected and processed for indirect immunohistochemistry. A clear p-ERK signal was detected at the level of PSCs in treated NMJs, thus extending in vivo the results obtained in cocultures

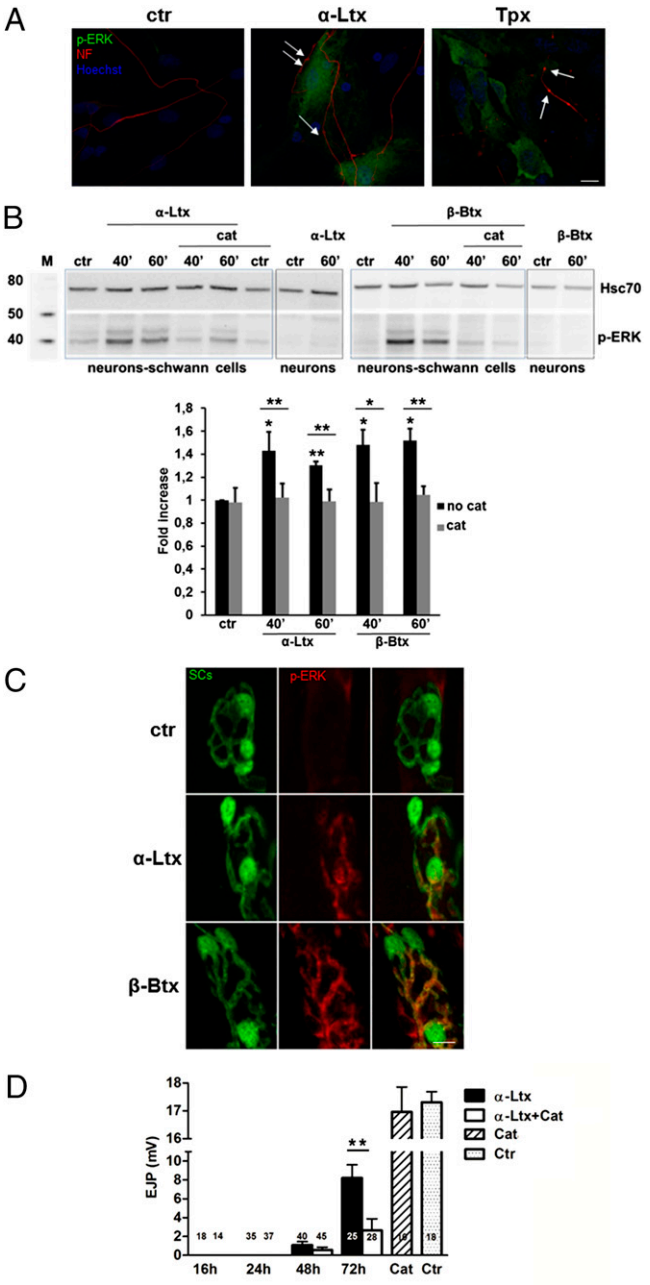

Fig. 2. Hydrogen peroxide released after nerve terminal degeneration activates ERK in Schwann cells and stimulates regeneration. Phospho-ERK (green) was detected in primary SCs cocultured with spinal cord MNs on exposure to α-Ltx (0.1 nM) or SPANs (6 nM) for 50 min by immunofluorescence (*A*), as well as by Western blots of total lysates (*B*). Arrows in *A* point to neuronal bulges stained with an antibody against neurofilaments (NF; red). Nuclei are stained with Hoechst (blue). (Scale bars: 10 μm.) (*B*) Catalase pretreatment of cocultures (1,000 U) significantly reduced ERK phosphorylation induced by the toxins (Western blot and quantification). No ERK phosphorylation is induced in neurons by the toxins. $*P < 0.05$; $**P < 0.01$; $n = 4$. (*C*) α-Ltx or β-Btx s.c. injections in LAL muscle of transgenic mice trigger ERK phosphorylation (p-ERK; red) in PSCs (green). Muscles were collected 24 h after injection. (Scale bars: 10 μm.) *(D)* Electrophysiological recordings of EJPs at soleus NMJs treated with α-Ltx alone (5 μg/kg; black bars) or with α-Ltx plus catalase (750 U; white bars). At 72 h EJP amplitudes of fibers exposed to toxin plus catalase are significantly smaller than those exposed to the sole toxin ($**P < 0.01$).

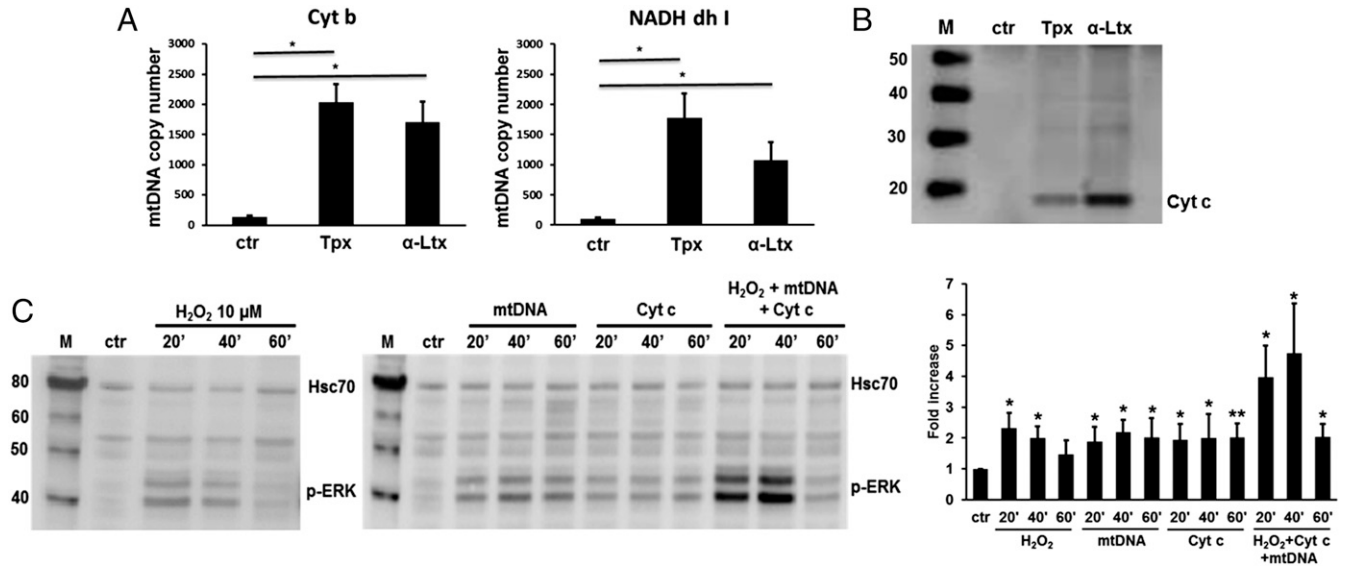

Fig. 3. Mitochondrial DNA and cytochrome *c* are released by degenerating neurons and activate the ERK pathway, together with hydrogen peroxide. (*A*) Real-time qPCR performed on CGNs supernatants from control and toxin-treated samples (Tpx 6 nM or α-Ltx 0.1 nM for 50 min), using primers specific for rat mitochondrial genes Cyt b and NADH dhI. DNA copy numbers of control and treated samples have been quantified. $*P < 0{,}05$; $n = 11$. (*B*) Supernatants from control and neurons treated as described earlier were precipitated with TCA and probed for Cyt c immunoreactivity in Western blot. (*C*) Time-course of ERK-phosphorylation induced in primary SCs by H_2O_2 (10 μM), mtDNA (10 μg/mL), and Cyt c (1 μg/mL) added alone or in a mixture and the relative quantification. Phospho-ERK signal was normalized to the Hsc70 band. $*P < 0.05$; $**P < 0.01$; $n = 3$.

(Fig. 2*C*). The importance of ERK pathway for SCs activation and regeneration was addressed by a pharmacologic approach: SCs-MNs cocultures exposed to the neurotoxins show a decreased ERK phosphorylation in the presence of the MEK 1 inhibitor PD98059 (Fig. S4 *A* and *B*); moreover, soleus muscles of mice pretreated with PD98059 and then locally injected with α-Ltx show a delayed recovery from paralysis with respect to mice injected with toxin only (Fig. S4*C*).

PSCs respond to neurotoxin-induced nerve degeneration by forming long sproutings and bridges between junctions of different fibers by the first day of injection (Fig. S5). This response has been long known to follow nerve terminal damage (35), and therefore, the present toxin-based model of acute nerve degeneration reproduces the known crucial aspects of regeneration.

To test whether H_2O_2 production by injured nerve terminals is important for functional regeneration, we performed electrophysiological recordings at soleus NMJs 16, 24, 48, and 72 h after i.m. injections of α-Ltx alone or α-Ltx plus catalase. Three days after treatment, fibers injected with α-Ltx plus catalase showed evoked junction potentials (EJPs) with significantly smaller amplitudes than those injected only with the toxin, indicating a slowdown of the regeneration process; muscles treated with catalase alone showed EJPs indistinguishable from the control (Fig. 2*D*). Immunohistochemistry on LAL muscles treated as described earlier confirmed the electrophysiological results, showing a delay in the recovery of synaptosomal-associated protein 25 (SNAP-25) staining, a presynaptic marker, in samples exposed to α-Ltx plus catalase compared with muscles injected with α-Ltx only (Fig. S6). At 24 h, SNAP-25 staining is recovered in 80% of the NMJs treated with α-Ltx (90% at 48 h) compared with 17% of the NMJs treated with α-Ltx plus catalase (33% at 48 h; $n = 40$). The disappearance of SNAP-25 during the degeneration steps takes place with a closely similar kinetic under the two conditions (Fig. S6). Four hours after intoxication, SNAP-25 displays a spotty distribution in nearly all NMJs analyzed (indicative of nerve terminal degeneration), both in the presence and absence of catalase; at 16 h, 68% of α-Ltx-treated NMJs have no more SNAP-25 versus 60% of catalase and α-Ltx-treated NMJs ($n = 30$).

mtDNA and Cyt C Are Released by Degenerating Neurons and Activate the ERK Pathway in Schwann Cells. We next tested whether mtDNA and Cyt c could act together with H_2O_2 as neuronal mediators of PSCs activation. For mtDNA detection, primary neurons were intoxicated, the supernatants collected, and DNA purified. The eluates were subjected to real-time PCR, using primers specific for the rat mitochondrial genes Cyt b and NADH dhI. Fig. 3*A* shows that mtDNA is indeed released in the neuronal supernatant after treatment with Tpx or α-Ltx. In another set of experiments, TCA-precipitated cell supernatants (sham or toxin-treated) were loaded in SDS/PAGE, followed by Western blotting. Samples were probed with an antibody against Cyt c: only toxin-treated samples showed a clear band corresponding to the intact, monomeric form of the protein (Fig. 3*B*). Control experiments showed no amplification when primers for the nuclear gene GAPDH were used (Fig. S7*A*), and the LDH assay on neuronal supernatant excluded a loss of membrane integrity (Fig. S7*B*). Thioredoxin 2, a mitochondrial protein with a molecular weight similar to Cyt c, was undetectable by Western blot of toxin-treated supernatants precipitated with TCA, thus supporting the conclusion that neuronal alarmins are released from intact membranes (Fig. S7*C*). Moreover, CGNs loaded with calcein-AM did not lose dye during 50 min incubation with both the toxins, indicating conservation of plasma membrane integrity (Fig. S7*D*).

Exposure of isolated SCs to mtDNA or Cyt c led to a sustained ERK phosphorylation, whereas a peak of p-ERK followed by progressive decline was observed upon H_2O_2 stimulation. When the three mitochondrial alarmins were added together, an additive effect on ERK phosphorylation was observed (Fig. 3*C*).

Mitochondrial Alarmins Exit from Neurons. H_2O_2 is permeable to biological membranes (49), whereas mtDNA and Cyt c must be released from mitochondrial and plasma membranes to reach the extracellular medium. Pretreatment of neurons with cyclosporin A, a drug that desensitizes the mitochondrial permeability transition pore (PTP) via its binding to cyclophilin D (50), reduces both mtDNA and Cyt c release triggered by the toxins (Fig. 4 *A* and *B*), suggesting these molecules can exit mitochondria and

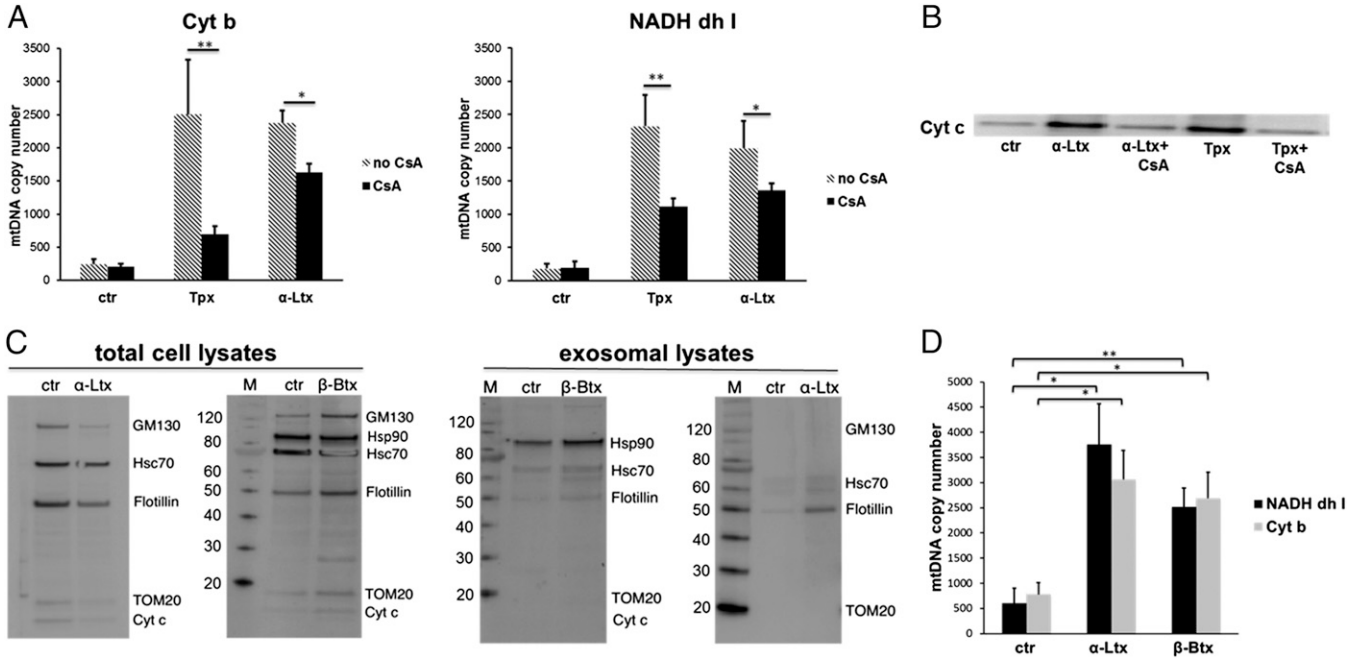

Fig. 4. Mitochondrial alarmins exit from neurons. Preincubation with cyclosporine A (5 μM for 30 min) significantly reduced both mtDNA (*A*) and Cyt c release (*B*) induced by exposure of CGNs to Tpx or α-Ltx (6 nM and 0.1 nM for 50 min, respectively). $*P < 0.05$; $**P < 0.01$; $n = 3$. (*C*) Exosomes were purified from CGNs supernatants and probed for the exosome-enriched proteins flotillin, Hsc70, and Hsp90. The absence of the Golgi marker GM130 and of the mitochondrial one Tom20 is indicative of uncontaminated preparations (*Right*). Cellular lysates are positive for all markers tested (*Left*). (*D*) DNA was extracted from exosomes purified from the supernatants of α-Ltx- and β-Btx-treated CGNs (0.1 and 6 nM for 50 min, respectively) and subjected to real-time qPCR for the detection of mtDNA. $*P < 0.05$; $**P < 0.01$; $n = 5$.

reach the cytoplasm through the PTP, whose opening is indeed induced by snake neurotoxins (51).

Because neuronal plasma membrane integrity is preserved, how do these alarmins reach the extracellular medium? We posited that exosomes might be involved and have purified them from control and treated neuronal supernatants. Purified exosomes were found enriched in Hsp90, Hsc70, flotillin, and CD63; no contamination with Golgi, mitochondrial, or plasma membranes was detected (Fig. 4*C* and Fig. S8 *A* and *B*). Electron microscopy and immunogold labeling of purified exosomes confirmed their correct morphology, size, and positivity for Hsp90 (Fig. S8*C*). Next, we purified total DNA from exosomes and performed real-time PCR to check for their mtDNA content. Fig. 4*D* shows that exosomes released by α-Ltx- and β-Btx-intoxicated neurons do contain mtDNA. Similar mtDNA copy numbers were found before and after DNase treatment of exosomal fractions, indicating that mtDNA is indeed inside exosomes (Fig. S8*D*). In contrast, no Cyt c was detected in exosomes by Western blotting; this is likely to be a result of the much lower sensitivity of Western blotting with respect to RT-PCR, but the possibility that Cyt c is released from damaged nerve terminals via other mechanisms cannot be discarded.

Phagocytosis Is Induced in PSCs During Nerve Terminal Injury. During toxin-induced neurodegeneration, PSCs at poisoned NMJs undergo evident morphological changes, showing a number of intracellular structures appearing dense by light microscopy (Fig. 5*A*, *Lower*). These structures are particularly evident at 4 h after α-Ltx injection, with a reduction in number and size with time (Fig. 5*A*).

The appearance and life span of these structures parallel nerve terminal degeneration, suggesting they might be phagosomes involved in the clearance of nerve debris. Accordingly, immunostaining of sham or poisoned LAL muscles for the scavenger macrophage receptor CD68 was performed. After α-Ltx injection, perineural SCs of LAL NMJs do express CD68 on these intracellular structures, supporting their phagocytic role (Fig. 5*B*). CD68-positive structures also appear after β-Btx treatment, but at a later time (16 h), as expected on the basis of the different time course of pathogenesis of the two neurotoxins (Fig. 5*B*). Lysotracker-positive staining confirmed the acidic nature of such compartments (Fig. 5*C*). CD68-positive macrophages were also recruited in the proximity of neurotoxin-treated NMJs, with a typical migrating phenotype (Fig. S9); this is consistent with the chemoattractant role of H_2O_2 (52–54). In contrast, polymorphonuclear leukocytes, which are recruited by axonal degradation (54), were rarely seen in the many samples we have inspected.

Four hours after α-Ltx injection, the distribution of the presynaptic markers neurofilaments (NF) and SNAP-25 is altered, with clear fragmentation in many junctions, as a result of the specific and localized nerve terminal degeneration induced by the neurotoxins (Fig. 6 *A* and *B*). SNAP-25-positive spots localize within PSCs phagosomes (the same holds true for NF), as shown by orthogonal projections (Fig. 6*C*), confirming that phagocytosis by PSCs and macrophages is taking place during nerve terminal degeneration.

Discussion

The present article describes an original approach to study motor axon terminals degeneration and regeneration. This model system is based on the use of animal presynaptic neurotoxins highly specific for nerve terminals with a well-defined biochemical mechanism of action (10, 12, 16, 18). Here, these neurotoxins are used as tools to induce localized and reversible nerve degeneration, followed by complete regeneration. This system is more controllable than the classical cut and crush approaches, which are invasive and inevitably damage several cell types, triggering a pronounced inflammatory response (55). Moreover, this model avoids some adverse effects of techniques such as laser ablation (high temperatures, photooxidation, etc). The model proposed here is therefore better suited to

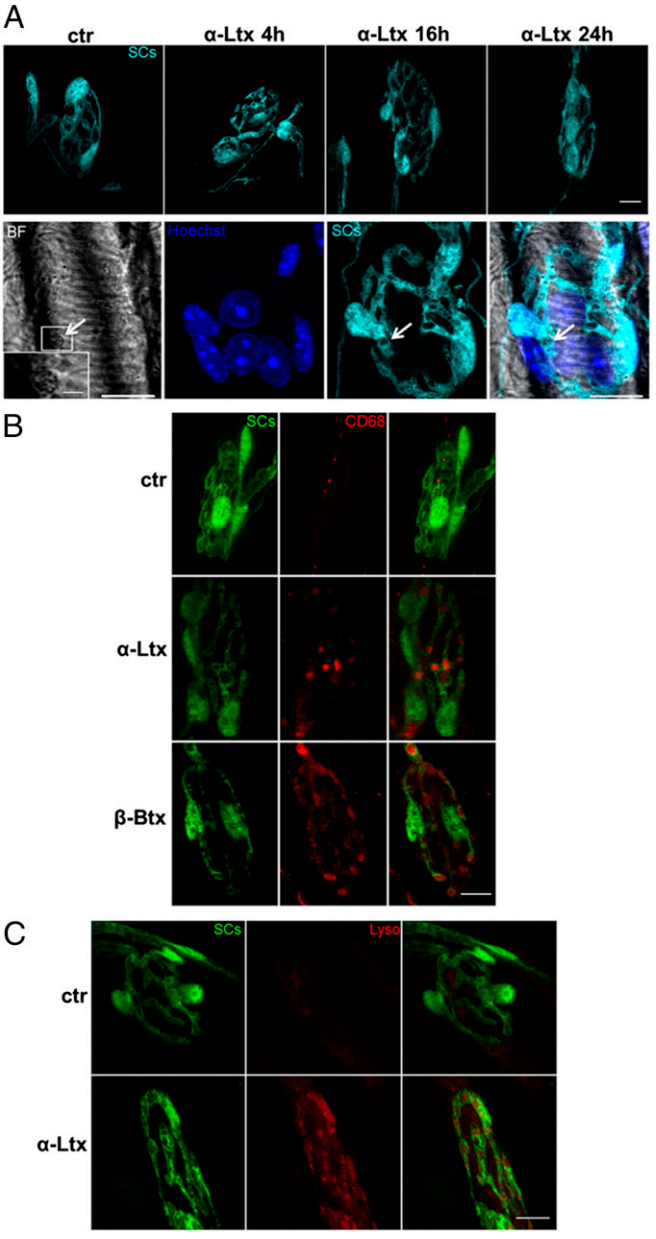

Fig. 5. Nerve terminal degeneration triggers phagocytosis in terminal SCs at the NMJ. (*A*) LAL muscles from transgenic mice were injected with α-Ltx (5 μg/kg), collected at different time points (4, 16, 24 h), and processed for indirect immunohistochemistry. PSCs (cyan) show intracellular structures of different size that are particularly evident after 4 h of intoxication. These structures appear dense by light microscopy (brightfield, *Lower*, arrows). Nuclei are stained with Hoechst (blue). (Scale bars: 10 μm.) (*B*) PSCs (green) at α-Ltx- and β-Btx-treated NMJs (4 and 16 h of intoxication, respectively) are positive for the phagocytic marker CD68 (red), which stains intracellular vesicular structures. A very low CD68 signal is detected in control NMJs. (Scale bars: 10 μm.) (*C*) Ex vivo Lysotracker staining (red) of α-Ltx-treated LAL (4 h) confirms the acidic nature of intracellular vacuoles. (Scale bar: 10 μm.)

study the inter- and intracellular signaling and transcriptomic events involved in the regeneration process.

Spider and snake presynaptic neurotoxins induce, by different biochemical mechanisms, a large entry of calcium in axon terminals, which in turn leads to mitochondrial failure and nerve terminal degeneration. At the same time, PSCs perceive the damage occurring to the motor axons and respond by dedifferentiating to a progenitor-like state, proliferating and assisting nerve regeneration. They acquire macrophagic-like activities that contribute to the removal of nerve cell debris and facilitate reinnervation, similar to what was found previously after nerve crush (23). Moreover, upon extensive cytoskeletal reorganization, PSCs send out long projections, along which the regenerating nerve terminals extend sprouts, which originate from the nonmyelinated axon terminal to innervate adjacent denervated junctions (34, 35).

It was recently shown that the MAPK signaling pathway has a central role in controlling SC plasticity and peripheral nerve regeneration via the activation of ERK1/2 and JNK, which activate the transcription complex activator protein 1, of which c-Jun is a key component (44, 45, 56). The major result obtained here, using p-ERK as a read-out, is that alarmins released by mitochondria of degenerating axon terminals activate SCs. Mitochondria are abundant components of the motor axons terminals, and here we define them as a source of mediators that are released under cytosolic calcium overload. The rapid accumulation of Ca^{2+} inside mitochondria causes the opening of the PTP and the exit of alarmins (50). Mitochondrial alterations are hallmarks of nerve terminal damage (19, 20), and therefore the present findings can be extrapolated to several other nerve terminal pathological conditions.

Mitochondria of stressed cells produce reactive oxygen species (ROS), among which H_2O_2 is the most stable species (37, 38, 57). It is a very reactive molecule that can permeate biological membranes. As PSCs and axon terminals are in close contact within the NMJ, significant amounts of H_2O_2 released by axon terminals can reach PSCs before it becomes inactivated by cellular antioxidant defense systems. Once within the target cell, H_2O_2 can act as a second messenger via chemoselective oxidation of cysteine residues in signaling proteins and via ERK phosphorylation. Collectively, these properties make H_2O_2 an ideal mediator of signal transduction processes (36–38, 42, 58). Recent experimental

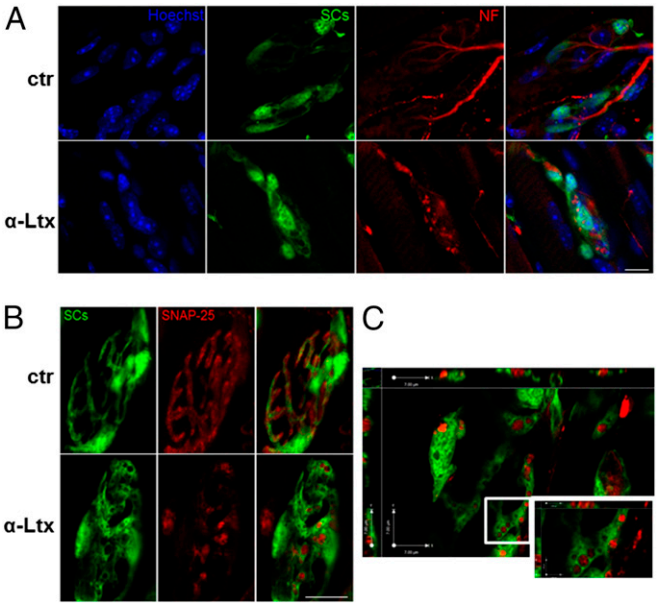

Fig. 6. Degenerating terminals are engulfed by perisynaptic SCs. (*A*) PSCs engulf presynaptic components, as shown by NF-positive staining of PSCs phagosomes at NMJs treated for 4 h with α-Ltx (red, *Lower*). (*Upper*) control NMJs. Nuclei are stained with Hoechst (blue). (Scale bars: 10 μm.) (*B*) Control NMJs with typical SNAP-25 presynaptic localization (red). In α-Ltx-treated NMJs (4 h), SNAP-25 aggregates localize within PSC phagosomes. (Scale bars: 10 μm.) (*C*) Orthogonal projections of α-Ltx-treated NMJs show that SNAP-25 positive aggregates are inside PSCs phagosomes. (Scale bars: 10 μm.)

evidence in different animal models demonstrated that a rapid concentration gradient of H_2O_2 is generated during injury and that H_2O_2 is a powerful chemoattractant of leukocytes (53, 54). Moreover, lowering ROS levels by pharmacologic or genetic approaches reduces cell proliferation and impairs regeneration (59). We therefore have imaged H_2O_2 in living neurons exposed to neurotoxins with novel specific fluorescent probes (39, 40) and found that the degenerating nerve terminals release H_2O_2 of mitochondrial origin. This H_2O_2 activates PSCs in vitro and in vivo. We also found that macrophages are recruited around the neurotoxin-treated NMJs. It is therefore likely that these macrophages are attracted by H_2O_2, as well as by molecules released by activated PSCs, as previously found (60, 61). The prominent role of H_2O_2 in neurotoxin-induced nerve degeneration and repair is proved by the impaired regeneration we observed in the presence of catalase.

In addition to H_2O_2, we found that mtDNA and Cyt c can act as mediators of neuronal damage and activate SCs via ERK pathway. When added in a mixture with H_2O_2, an additive effect on ERK phosphorylation is observed. As neuronal membrane integrity is preserved, the question arises of how mtDNA and Cyt c, coming from the mitochondrial matrix or the intermembrane space, respectively, can exit the cell. Several pieces of evidence indicate that mitochondria are central sensors for axonal degenerative stimuli (62), and the release of mtDNA fragments from PTP in isolated mitochondria has been documented (63). Here, the mitochondrial PTP was found to be involved in the exit of both mtDNA and Cyt c from mitochondria, with a significant reduction in the presence of the PTP desensitizing molecule cyclosporin A. Once in the cytosol, mtDNA and Cyt c could be released via the nonclassical or unconventional secretory route, including secretory lysosomes, membrane blebbing, multivesicular body-derived exosomes, or autophagy (64). Here, we found that exosomes purified from intoxicated neuronal supernatants contain mtDNA, whereas Cyt c was not detected, possibly because of the insufficient sensitivity of Western blot. It is also possible that Cyt c is released directly via contact sites between mitochondria and the presynaptic membrane, similar to those observed by electron microscopy in a closely similar pathological condition caused by autoimmune anti-ganglioside antibodies (65).

The present work has identified three mitochondrial alarmins involved in PSCs activation after an acute nerve injury and proposes H_2O_2 as the strongest inducer of PSCs response. Inactivation of H_2O_2 by catalase reduces ERK phosphorylation in SCs in culture and delays NMJ recovery in vivo after toxin-induced neuroparalysis and degeneration, supporting a crucial role of this molecule in the regeneration process.

Nerve damage triggers important morphologic and functional changes in PSCs aimed at promoting NMJ regeneration, confirming their endowed high plasticity and their crucial role in the clearance of nerve debris. Indeed, during nerve terminal degeneration, PSCs become CD68-positive, indicating an acquired phagocytic activity. Together with macrophages, but not neutrophils, activated PSCs were found here to remove nerve debris, thus permitting a functional nerve regeneration. This is at variance from what was found during axonal degeneration, where a pronounced neutrophil infiltration was detected (54).

The phagocytic features of PSCs described here represent an additional early read-out of PSCs activation at the injured NMJ. PSCs respond to axonal damage caused by neurotoxin poisoning by engulfing degenerating terminals, by extending long processes, and by activating intracellular signaling pathways crucial for regeneration. On the basis of these perspectives, we plan to study more in detail the intracellular signaling and transcriptomic events taking place inside activated PSCs. More in general, it appears that the present experimental approach can be extended to the investigation of other motor neuron diseases, including the non-cell-autonomous and dying-back axonopathy of ALS and autoimmune neuropathies including Guillain-Barré and Miller-Fisher syndromes (66, 67). Such studies are likely to provide relevant insights for future therapeutic endeavors.

Materials and Methods

Animal Strains. C57BL/6 mice expressing cytosolic GFP under the *plp* promoter (46, 47) were kindly provided by W. B. Macklin (Aurora, CO) via the collaboration of T. Misgeld (Munchen, Germany). All experiments were performed in accordance with the European Communities Council Directive n° 2010/63/UE and approved by the Italian Ministry of Health.

Hydrogen Peroxide Detection. Hydrogen peroxide generation in primary neurons was measured using Mitochondria Peroxy Yellow 1 (MitoPY1) (39) or Peroxyfluor 6 acetoxymethyl ester (PF6-AM) (40), synthesized in the C.J.C. laboratory (Berkeley, CA), specific probes of H_2O_2 production in mitochondria and cytoplasm, respectively. Both probes were loaded at 5 μM for 30 min at 37 °C in Krebs ringer buffer (KRH: Hepes 25 mM at pH 7.4, NaCl 124 mM, KCl 5 mM, $MgSO_4$ 1.25 mM, CaCl2 1.25 mM, KH_2PO_4 1.25 mM, glucose 8 mM). Images were acquired at different points after toxin exposure with a DMI6000 inverted epifluorescence microscope (Leica) equipped with a 63× HCX PL APO oil immersion objective NA 1.4. Filter cubes (Chroma Technology) have an excitation range of 470/40 nm, a dichroic mirror 495LPXR, and an emission of 525/50 nm. Images were acquired with an Orca-Flash4 digital camera (Hamamatsu). Illumination was kept at a minimum to avoid ROS generation because of phototoxicity. To detect neuronal bulges, we took advantage of differential interference contrast microscopy. Fluorescence intensity quantification was carried out with ImageJ, and the statistical analysis with Prism (GraphPad).

Cell Treatments. CGNs (6 d in culture) plated onto 35-mm dishes (1.2 million cells per well) were exposed for 50–60 min to SPANs (6 nM) or to α-Ltx (0.1 nM) at 37 °C. In some experiments, neurons were preincubated for 30 min with cyclosporin A 5 μM before toxin addition. Supernatants or cell lysates were collected and then processed for real-time quantitative PCR (qPCR) or Western blot.

Primary SCs were exposed to different mitochondrial alarmins [H_2O_2 10–100 μM, Cyt c (R&D) 1 μg/mL, mtDNA 10 μg/mL] or to the toxins for different times and lysed in Lysis Buffer [Hepes 10 mM, NaCl 150 mM, SDS 1%, EDTA 4 mM, protease inhibitors mixture (Roche), and phosphatase inhibitor mixture].

Cocultures were treated with the toxins and then lysed after different points; in a set of experiments, 1,000 U per well catalase was added 5 min before intoxication and kept throughout the experiment; in another set, cocultures were incubated with the MEK1 inhibitor PD98059 (Cell Signaling; 80 μM) 1 h before toxins addition. Samples were then probed for p-ERK.

Immunofluorescence. After treatments, isolated SCs or cocultures were fixed for 15 min in 4% (wt/vol) paraformaldehyde (PFA) in PBS, quenched (0.38% glycine, 0.24% NH_4Cl in PBS), and permeabilized with 0.3% Triton X-100 in PBS for 5 min at room temperature (RT). After saturation with 3% (vol/vol) goat serum in PBS for 1 h, samples were incubated with primary antibodies [anti-Phospho-p44/42 MAPK (Cell Signaling), 1:1,000; anti- anti-NF200 (Sigma), 1:200; anti-S100 (Sigma), 1:1,000] diluted in 3% (vol/vol) goat serum in PBS overnight at 4 °C, washed, and then incubated with the correspondent secondary antibodies (Alexa-conjugated, 1:200; Life Technologies) for 1 h at RT. Coverslips were mounted in Mowiol and examined by confocal (Leica SP5) or epifluorescence (Leica CTR6000) microscopy.

In a set of experiments, CGNs were exposed to α-Ltx (0.1 nM, 50 min) or PMA (phorbol 12-myristate 13-acetate, 1 μg/mL, 20 min) and processed for immunofluorescence as described earlier. p47phox was detected by a monoclonal antibody (Santa Cruz; 1:200).

NMJ Immunohistochemistry. α-Ltx (5 μg/kg) or β-Btx (10 μg/kg) were diluted in 25 μL physiological saline (0.9% wt/vol NaCl in distilled water) and injected s.c. in proximity of the LAL muscle of anesthetized transgenic C57BL/6 male mice (expressing a cytosolic GFP under the *plp* promoter) (46, 47) of around 20–25 g. Control animals were injected with saline. LAL muscles were dissected at different points after injections and fixed in 4% (wt/vol) PFA in PBS for 30 min at RT. Samples were quenched, permeabilized, and saturated for 2 h in 15% (vol/vol) goat serum, 2% (wt/vol) BSA, 0.25% gelatin, 0.20% glycine, and 0.5% Triton X-100 in PBS. Incubation with the following primary antibodies was carried out for at least 48 h in blocking solution: anti-neurofilaments (mouse monoclonal, anti-NF200, 1:200; Sigma), anti-SNAP-25 (SMI81 mouse monoclonal, 1:200; Covance), and anti-CD68 (mouse monoclonal, 1:200; Santa Cruz). Muscles were then washed and incubated with secondary antibodies (Alexa-conjugated, 1:200 in PBS; Life Technologies). Nuclei were stained with Hoechst. For p-ERK detection incubation with the

primary antibody (anti-Phospho-p44/42 MAPK, 1:1,000; Cell Signaling) was carried out for 72 h and the tyramide signal amplification kit (Perkin-Elmer) was used (45).

To stain acidic compartments, LAL muscles collected after 4 h of intoxication were loaded ex vivo with LysoTracker Red DND-99 (1:5,000; Life Technologies) for 2–3 min (68) while being continuously perfused with oxygenated Neurobasal A medium (Life Technologies). Samples were then fixed and processed for indirect immunohistochemistry, as described earlier. Images were collected with a Leica SP5 confocal microscope equipped with a 63× HCX PL APO NA 1.4. Laser excitation line, power intensity, and emission range were chosen according to each fluorophore in different samples to minimize bleed-through.

Electrophysiological Recordings. Electrophysiological recordings were performed in oxygenated Krebs-Ringer solution on sham or α-Ltx-injected soleus muscles (α-Ltx 5 μg/kg, with or without 750 U catalase), using intracellular glass microelectrodes (WPI) filled with one part 3 M KCl and two parts 3 M CH_3COOK. In another set of experiments, muscles were locally injected with PD98059 (50 μg in DMSO) 1 h before α-Ltx injection.

Evoked neurotransmitter release was recorded in current-clamp mode, and resting membrane potential was adjusted with current injection to −70 mV. EJPs were elicited by supramaximal nerve stimulation at 0.5 Hz, using a suction microelectrode connected to a S88 stimulator (Grass). To prevent muscle contraction after dissection, samples were incubated for 10 min with 1 μM μ-Conotoxin GIIIB (Alomone).

Signals were amplified with intracellular bridge mode amplifier (BA-01X, NPI), sampled using a digital interface (NI PCI-6221, National Instruments) and recorded by means of electrophysiological software (WinEDR; Strathclyde University). EJPs measurements were carried out with Clampfit software (Molecular Devices).

Statistical Analysis. The sample size (N) of each experimental group is described in each corresponding figure legend, and at least three biological replicates were performed. Prism (GraphPad Software) was used for all statistical analyses. Quantitative data displayed as histograms are expressed as means ± SEM (represented as error bars). Results from each group were averaged and used to calculate descriptive statistics. Significance was calculated by Student's *t* test (unpaired, two-side). *P* values less than 0.05 were considered significant.

ACKNOWLEDGMENTS. We gratefully thank Dr. W. B. Macklin and Dr. T. Misgeld for providing the C57BL/6 transgenic mice strain and Dr. P. Caccin for the kind help with EM experiments. This work was supported by the Cariparo Foundation and the Provincia autonoma di Trento, Bando Grandi Progetti 2012 (to C.M.). M.R. is the recipient of Young Investigators Grant GR-2010-2320779 from the Italian Ministry of Health. C.J.C. is an Investigator with the Howard Hughes Medical Institute, and his contributions are supported by NIH Grant GM79465.

1. Pearn JH (1971) Survival after snake-bite with prolonged neurotoxic envenomation. *Med J Aust* 2(5):259–261.
2. Connolly S, et al. (1995) Neuromuscular effects of Papuan Taipan snake venom. *Ann Neurol* 38(6):916–920.
3. Kularatne SA, Senanayake N (2014) Venomous snake bites, scorpions, and spiders. *Handb Clin Neurol* 120:987–1001.
4. Duchen LW, Gomez S, Queiroz LS (1981) The neuromuscular junction of the mouse after black widow spider venom. *J Physiol* 316:279–291.
5. Dixon RW, Harris JB (1999) Nerve terminal damage by beta-bungarotoxin: Its clinical significance. *Am J Pathol* 154(2):447–455.
6. Chang CC, Chen TF, Lee CY (1973) Studies of the presynaptic effect of -bungarotoxin on neuromuscular transmission. *J Pharmacol Exp Ther* 184(2):339–345.
7. Rosenthal L, Zacchetti D, Madeddu L, Meldolesi J (1990) Mode of action of alpha-latrotoxin: Role of divalent cations in Ca2(+)-dependent and Ca2(+)-independent effects mediated by the toxin. *Mol Pharmacol* 38(6):917–923.
8. Hurlbut WP, Ceccarelli B (1979) Use of black widow spider venom to study the release of neurotransmitters. *Adv Cytopharmacol* 3:87–115.
9. Ceccarelli B, Hurlbut WP (1980) Vesicle hypothesis of the release of quanta of acetylcholine. *Physiol Rev* 60(2):396–441.
10. Südhof TC (2001) alpha-Latrotoxin and its receptors: Neurexins and CIRL/latrophilins. *Annu Rev Neurosci* 24:933–962.
11. Ushkaryov YA, Rohou A, Sugita S (2008) alpha-Latrotoxin and its receptors. *Handbook Exp Pharmacol* (184):171–206.
12. Rossetto O, Montecucco C (2008) Presynaptic neurotoxins with enzymatic activities. *Handbook Exp Pharmacol* (184):129–170.
13. Gutiérrez JM, Theakston RD, Warrell DA (2006) Confronting the neglected problem of snake bite envenoming: The need for a global partnership. *PLoS Med* 3(6):e150.
14. Pungercar J, Krizaj I (2007) Understanding the molecular mechanism underlying the presynaptic toxicity of secreted phospholipases A2. *Toxicon* 50(7):871–892.
15. Kasturiratne A, et al. (2008) The global burden of snakebite: A literature analysis and modelling based on regional estimates of envenoming and deaths. *PLoS Med* 5(11): e218.
16. Rigoni M, et al. (2005) Equivalent effects of snake PLA2 neurotoxins and lysophospholipid-fatty acid mixtures. *Science* 310(5754):1678–1680.
17. Paoli M, et al. (2009) Mass spectrometry analysis of the phospholipase A(2) activity of snake pre-synaptic neurotoxins in cultured neurons. *J Neurochem* 111(3):737–744.
18. Rigoni M, et al. (2007) Calcium influx and mitochondrial alterations at synapses exposed to snake neurotoxins or their phospholipid hydrolysis products. *J Biol Chem* 282(15):11238–11245.
19. Cull-Candy SG, Fohlman J, Gustavsson D, Lüllmann-Rauch R, Thesleff S (1976) The effects of taipoxin and notexin on the function and fine structure of the murine neuromuscular junction. *Neuroscience* 1(3):175–180.
20. Harris JB, Grubb BD, Maltin CA, Dixon R (2000) The neurotoxicity of the venom phospholipases A(2), notexin and taipoxin. *Exp Neurol* 161(2):517–526.
21. Tedesco E, et al. (2009) Calcium overload in nerve terminals of cultured neurons intoxicated by alpha-latrotoxin and snake PLA2 neurotoxins. *Toxicon* 54(2):138–144.
22. Duregotti E, Tedesco E, Montecucco C, Rigoni M (2013) Calpains participate in nerve terminal degeneration induced by spider and snake presynaptic neurotoxins. *Toxicon* 64:20–28.
23. Son YJ, Trachtenberg JT, Thompson WJ (1996) Schwann cells induce and guide sprouting and reinnervation of neuromuscular junctions. *Trends Neurosci* 19(7): 280–285.
24. Feng Z, Ko CP (2008) The role of glial cells in the formation and maintenance of the neuromuscular junction. *Ann N Y Acad Sci* 1132:19–28.
25. Krysko DV, et al. (2011) Emerging role of damage-associated molecular patterns derived from mitochondria in inflammation. *Trends Immunol* 32(4):157–164.
26. Zhang Q, et al. (2010) Circulating mitochondrial DAMPs cause inflammatory responses to injury. *Nature* 464(7285):104–107.
27. Zornetta I, et al. (2012) Envenomations by Bothrops and Crotalus snakes induce the release of mitochondrial alarmins. *PLoS Negl Trop Dis* 6(2):e1526.
28. Robitaille R (1998) Modulation of synaptic efficacy and synaptic depression by glial cells at the frog neuromuscular junction. *Neuron* 21(4):847–855.
29. Rochon D, Rousse I, Robitaille R (2001) Synapse-glia interactions at the mammalian neuromuscular junction. *J Neurosci* 21(11):3819–3829.
30. Auld DS, Robitaille R (2003) Perisynaptic Schwann cells at the neuromuscular junction: Nerve- and activity-dependent contributions to synaptic efficacy, plasticity, and reinnervation. *Neuroscientist* 9(2):144–157.
31. Todd KJ, Auld DS, Robitaille R (2007) Neurotrophins modulate neuron-glia interactions at a vertebrate synapse. *Eur J Neurosci* 25(5):1287–1296.
32. Todd KJ, Darabid H, Robitaille R (2010) Perisynaptic glia discriminate patterns of motor nerve activity and influence plasticity at the neuromuscular junction. *J Neurosci* 30(35):11870–11882.
33. Griffin JW, Thompson WJ (2008) Biology and pathology of nonmyelinating Schwann cells. *Glia* 56(14):1518–1531.
34. Son YJ, Thompson WJ (1995) Schwann cell processes guide regeneration of peripheral axons. *Neuron* 14(1):125–132.
35. Son YJ, Thompson WJ (1995) Nerve sprouting in muscle is induced and guided by processes extended by Schwann cells. *Neuron* 14(1):133–141.
36. Paulsen CE, Carroll KS (2010) Orchestrating redox signaling networks through regulatory cysteine switches. *ACS Chem Biol* 5(1):47–62.
37. Dickinson BC, Chang CJ (2011) Chemistry and biology of reactive oxygen species in signaling or stress responses. *Nat Chem Biol* 7(8):504–511.
38. Murphy MP, et al. (2011) Unraveling the biological roles of reactive oxygen species. *Cell Metab* 13(4):361–366.
39. Dickinson BC, Chang CJ (2008) A targetable fluorescent probe for imaging hydrogen peroxide in the mitochondria of living cells. *J Am Chem Soc* 130(30):9638–9639.
40. Dickinson BC, Peltier J, Stone D, Schaffer DV, Chang CJ (2011) Nox2 redox signaling maintains essential cell populations in the brain. *Nat Chem Biol* 7(2):106–112.
41. Rigoni M, et al. (2004) Snake presynaptic neurotoxins with phospholipase A2 activity induce punctate swellings of neurites and exocytosis of synaptic vesicles. *J Cell Sci* 117(Pt 16):3561–3570.
42. Gough DR, Cotter TG (2011) Hydrogen peroxide: A Jekyll and Hyde signalling molecule. *Cell Death Dis* 2:e213.
43. Kemmerling U, et al. (2007) Calcium release by ryanodine receptors mediates hydrogen peroxide-induced activation of ERK and CREB phosphorylation in N2a cells and hippocampal neurons. *Cell Calcium* 41(5):491–502.
44. Harrisingh MC, et al. (2004) The Ras/Raf/ERK signalling pathway drives Schwann cell dedifferentiation. *EMBO J* 23(15):3061–3071.
45. Napoli I, et al. (2012) A central role for the ERK-signaling pathway in controlling Schwann cell plasticity and peripheral nerve regeneration in vivo. *Neuron* 73(4): 729–742.
46. Mallon BS, Shick HE, Kidd GJ, Macklin WB (2002) Proteolipid promoter activity distinguishes two populations of NG2-positive cells throughout neonatal cortical development. *J Neurosci* 22(3):876–885.
47. Brill MS, Lichtman JW, Thompson W, Zuo Y, Misgeld T (2011) Spatial constraints dictate glial territories at murine neuromuscular junctions. *J Cell Biol* 195(2):293–305.
48. Angaut-Petit D, Molgo J, Connold AL, Faille L (1987) The levator auris longus muscle of the mouse: A convenient preparation for studies of short- and long-term presynaptic effects of drugs or toxins. *Neurosci Lett* 82(1):83–88.
49. Miller EW, Dickinson BC, Chang CJ (2010) Aquaporin-3 mediates hydrogen peroxide uptake to regulate downstream intracellular signaling. *Proc Natl Acad Sci USA* 107(36):15681–15686.

50. Rasola A, Sciacovelli M, Pantic B, Bernardi P (2010) Signal transduction to the permeability transition pore. *FEBS Lett* 584(10):1989–1996.
51. Rigoni M, et al. (2008) Snake phospholipase A2 neurotoxins enter neurons, bind specifically to mitochondria, and open their transition pores. *J Biol Chem* 283(49): 34013–34020.
52. Klyubin IV, Kirpichnikova KM, Gamaley IA (1996) Hydrogen peroxide-induced chemotaxis of mouse peritoneal neutrophils. *Eur J Cell Biol* 70(4):347–351.
53. Niethammer P, Grabher C, Look AT, Mitchison TJ (2009) A tissue-scale gradient of hydrogen peroxide mediates rapid wound detection in zebrafish. *Nature* 459(7249): 996–999.
54. Li L, Yan B, Shi YQ, Zhang WQ, Wen ZL (2012) Live imaging reveals differing roles of macrophages and neutrophils during zebrafish tail fin regeneration. *J Biol Chem* 287(30):25353–25360.
55. Conforti L, Gilley J, Coleman MP (2014) Wallerian degeneration: An emerging axon death pathway linking injury and disease. *Nat Rev Neurosci* 15(6):394–409.
56. Arthur-Farraj PJ, et al. (2012) c-Jun reprograms Schwann cells of injured nerves to generate a repair cell essential for regeneration. *Neuron* 75(4):633–647.
57. Lambert AJ, Brand MD (2009) Reactive oxygen species production by mitochondria. *Methods Mol Biol* 554:165–181.
58. Holmström KM, Finkel T (2014) Cellular mechanisms and physiological consequences of redox-dependent signalling. *Nat Rev Mol Cell Biol* 15(6):411–421.
59. Love NR, et al. (2013) Amputation-induced reactive oxygen species are required for successful *Xenopus* tadpole tail regeneration. *Nat Cell Biol* 15(2):222–228.
60. Tofaris GK, Patterson PH, Jessen KR, Mirsky R (2002) Denervated Schwann cells attract macrophages by secretion of leukemia inhibitory factor (LIF) and monocyte chemoattractant protein-1 in a process regulated by interleukin-6 and LIF. *J Neurosci* 22(15): 6696–6703.
61. Martini R, Fischer S, López-Vales R, David S (2008) Interactions between Schwann cells and macrophages in injury and inherited demyelinating disease. *Glia* 56(14): 1566–1577.
62. Court FA, Coleman MP (2012) Mitochondria as a central sensor for axonal degenerative stimuli. *Trends Neurosci* 35(6):364–372.
63. Patrushev M, et al. (2004) Mitochondrial permeability transition triggers the release of mtDNA fragments. *Cell Mol Life Sci* 61(24):3100–3103.
64. Frühbeis C, Fröhlich D, Krämer-Albers EM (2012) Emerging roles of exosomes in neuron-glia communication. *Front Physiol* 3:119.
65. Halstead SK, et al. (2005) Anti-disialosyl antibodies mediate selective neuronal or Schwann cell injury at mouse neuromuscular junctions. *Glia* 52(3):177–189.
66. Vinsant S, et al. (2013) Characterization of early pathogenesis in the SOD1(G93A) mouse model of ALS: Part II, results and discussion. *Brain Behav* 3(4):431–457.
67. Plomp JJ, Willison HJ (2009) Pathophysiological actions of neuropathy-related anti-ganglioside antibodies at the neuromuscular junction. *J Physiol* 587(Pt 16): 3979–3999.
68. Song JW, et al. (2008) Lysosomal activity associated with developmental axon pruning. *J Neurosci* 28(36):8993–9001.

Supporting Information

Duregotti et al. 10.1073/pnas.1417108112

SI Materials and Methods

Toxins. α-Ltx and Tpx were purchased from Alomone, and β-Btx from Sigma. The purity of the toxins was checked by SDS/PAGE, and their neurotoxicity by ex vivo mouse nerve-hemidiaphragm preparation, as previously described (1).

Chemicals. Unless otherwise stated, all reagents were purchased from Sigma.

Primary Cell Cultures. Rat cerebellar granular neurons and rat spinal motoneurons were purified as described in ref. 2. Primary SCs were purified from sciatic nerves of six P3 Wistar rats. Briefly, sciatic nerves were dissected and tissues digested in 0.1% wt/vol collagenase and 0.25% wt/vol trypsin in L15 medium (Life Technologies), plus 0.3% BSA for 1 h. Dissociated cells were seeded onto uncoated Petri dishes in DMEM 10% (vol/vol) FBS; 24 h after seeding, 10 μM arabinoside C was added to the medium and kept for 2 d to prevent fibroblasts mitosis. Five days after seeding, an immunopanning with an anti-Thy1.1 antibody followed by rabbit complement addition was performed to eliminate contaminating fibroblasts. Purified SCs were subsequently plated on poly-L-lysine-coated dishes and allowed to grow in expansion medium consisting of DMEM, supplemented with 10% (vol/vol) FBS, 2 μM forskolin, and 10 nM heregulin β-1.

Primary Neurons-SCs Cocultures. CGNs and spinal MNs were used to set up cocultures with primary SCs. Briefly, 4 d after primary neurons seeding, primary SCs were added to neuronal cultures at an average density of 1×10^4 cells/cm^2. Cocultures were kept for 2–3 d in CGNs or MNs medium, respectively, and then processed for immunofluorescence or Western blotting.

Sample Preparation for Western Blotting.

Cyt c detection. CGNs were intoxicated as previously described, the supernatant was collected, and total proteins were precipitated with TCA [10% (vol/vol) final concentration]. The resulting pellet was suspended in loading sample buffer and denatured at 95 °C for 5 min. Samples were loaded on Precast 4–12% SDS-polyacrylamide gels (Life Technologies) and transferred to a nitrocellulose in a refrigerated chamber. After saturation, membranes were incubated overnight with a mouse monoclonal anti-Cyt c antibody (BD Biosciences; 1:1,000) followed by a secondary anti-mouse antibody HRP-conjugated (Life Technologies; 1:2,000). Chemiluminescence was developed with the Luminata TM Crescendo (Millipore) or ECL Advance Western blotting detection system (GE Healthcare) and was emission measured with ChemiDoc XRS (Bio-Rad). Band intensities were quantified on the original files with the software Quantity One (Bio-Rad). None of the bands reached signal saturation. In another set of experiments, TCA-precipitated supernatants were probed with a monoclonal antibody specific for thioredoxin 2 (Abcam; 1:1,000).

Phospho-ERK detection. Seven to 10 μg of total lysates from SCs or cocultures were loaded on SDS/PAGE. Protein concentration was quantified using the BCA assay (Protein Assay Kit; Pierce). Phospho-ERK was detected with a rabbit polyclonal antibody (anti-Phospho-p44/42 MAPK, 1:1,000; Cell Signaling). For densitometric quantification, the bands of interest were normalized to the housekeeping protein Hsc70 (monoclonal anti-Hsc70, 1:10,000; Synaptic Systems).

Real-Time qPCR. Supernatants of intoxicated neurons were collected and total DNA was extracted using the DNeasy Blood & Tissue kit (Qiagen) following manufacturer's instructions and subjected to real-time PCR. Primers for rat cytochrome B (forward 5′- TCCACTTCATCCTCCCATTC-3′ and reverse 5′-CTGCGTCGGAGTTTAATCCT-3′), rat NADH dehydrogenase I (forward 5′- CAATACCCCACCCCCTTATCAA-3′ and reverse 5′- GAGGCTCATCCCGATCATAGAA-3′), and rat GAPDH (forward 5′-ATTTCCTTTAATAAAGCCGGT-3′ and reverse 5′- TAAGAGACTTAAAATGACTTTG-3′) were synthesized by Life Technologies. Primer sequences have no significant homology with DNA found in any bacterial species published on BLAST.

Standards for quantification were obtained by PCR on total DNA isolated from cultured CGNs. Samples that produced no PCR products after 33 cycles were considered undetectable. Real-time qPCR was performed using iCyclerH thermal cycler (Bio-Rad). Amplification conditions were the following: 10 min at 95 °C, 40 cycles: 10 s at 95 °C, 30 s at 47.6 °C. A melting curve analysis, consisting of an initial step of 10 s at 65 °C and a slow elevation of temperature (0.5 °C/s) to 95 °C, was performed at the end of the amplification cycles to check for the absence of primer dimers and nonspecific products, using iQ SYBR Green supermix (BioRad). Results were expressed as copy numbers of target genes.

Mitochondrial DNA Purification. Mitochondrial DNA was extracted from 25 μg mice tibialis muscle, using the DNeasy Blood & Tissue kit (Qiagen), following manufacturer's instructions. DNA concentration was determined by spectrophotometer. No protein contamination was found. We checked the purity of mtDNA by real-time PCR, using primers for nuclear GAPDH.

Lactate Dehydrogenase Assay. Lactate dehydrogenase (LDH) activity was measured on the supernatants of CGNs plated on 96-well plates (150,000 cells/well) and exposed to the toxins as previously described, following manufacturer's instructions (Sigma). LDH activity measured in the total cell lysate was taken as 100% ($n = 3$).

Calcein Imaging. CGNs were loaded with calcein-AM (Life Technologies), 1 μM for 15 min at 37 °C in KRH, washed, and then exposed to α-Ltx 0.1 nM or Tpx 6 nM for 50 min. Fluorescence was monitored with time. Loss of calcein dye because of membrane permeabilization was achieved by the addition of 0.1% saponin. Images were acquired by epifluorescence (Leica CTR6000) microscopy.

Exosomes Purification. Exosomes were obtained from CGNs isolated from four rat cerebella (P6) following standard protocols (3). The mean total cell yield was 50–60 million cells (Mc). Cells plated on poly-L-lysine-coated 100-mm Petri dishes (10 Mc/dish) were grown till 6 d in culture; on the day of the experiment, plates were washed three to four times with warm KRH to remove the culture medium. α-Ltx 0.1 nM or β-Btx 6 nM were incubated in KRH for 45–60 min, and control samples were incubated with saline. Supernatants were then collected and subjected to cycles of centrifugations ($300 \times g$ for 10 min at 4 °C and $16,500 \times g$ for 20 min at 4 °C). The supernatant was then filtered through a 0.2-μm filter and centrifuged again at $120,000 \times g$ for 70 min at 4 °C to pellet exosomes, which were resuspended in loading buffer for SDS/PAGE analysis or in lysis buffer for DNA extraction. Each lane of SDS/PAGE corresponds to exosomes obtained from the medium of 10^7 neurons. Proteins enriched in exosomes such as flotillin, Hsc70, Hsp90, and CD63 were detected in both the exosomal and the total lysate fractions [anti-flotillin, 1:500 (BD

Biosciences); anti-Hsc70, 1:10,000 (Synaptic Systems); anti-Hsp90, 1:1,000 (BD Biosciences); and anti-CD63, 1:200 (Santa Cruz)]. To exclude contamination with other cell compartments, the exosomal fraction was assayed for Golgi (anti-GM130, 1:1,000; BD Transduction laboratories), mitochondrial (anti-TOM20, 1:1,000; Santa Cruz), and plasma membrane markers (anti-syntaxin 1A, 1:2,000; Synaptic Systems). DNA extraction from exosomes and real-time qPCR were performed as described earlier. In a set of experiments, exosomes were pretreated with purified DNase (1 U/μL, 1 h at 37 °C); DNase was inactivated at 65 °C for 10 min before DNA extraction and real-time qPCR.

Exosomes Identification by Electron Microscopy

The exosome-enriched pellet (purified from 60 Mc) was resuspended in PBS and ultracentrifuged at 120,000g for 70 min at 4 °C to repellet the exosomes. The pellets were immediately fixed by 2% (wt/vol) paraformaldehyde and applied to formvar-carbon-coated EM grids. For immunogold labeling, grids were incubated with anti-Hsp90 primary antibodies, which were then revealed using 5-nm gold-conjugated secondary antibodies (Sigma, 1:100). The exosomes were then stained with 1% uranyl acetate for 30 min. Observations were made using a transmission electron microscope (TECNAI G12, FEI) at 100 kV, equipped with a digital camera (Veleta, OSIS).

1. Rigoni M, et al. (2005) Equivalent effects of snake PLA2 neurotoxins and lysophospholipid-fatty acid mixtures. *Science* 310(5754):1678–1680.
2. Rigoni M, et al. (2007) Calcium influx and mitochondrial alterations at synapses exposed to snake neurotoxins or their phospholipid hydrolysis products. *J Biol Chem* 282(15):11238–11245.
3. Lachenal G, et al. (2011) Release of exosomes from differentiated neurons and its regulation by synaptic glutamatergic activity. *Mol Cell Neurosci* 46(2):409–418.

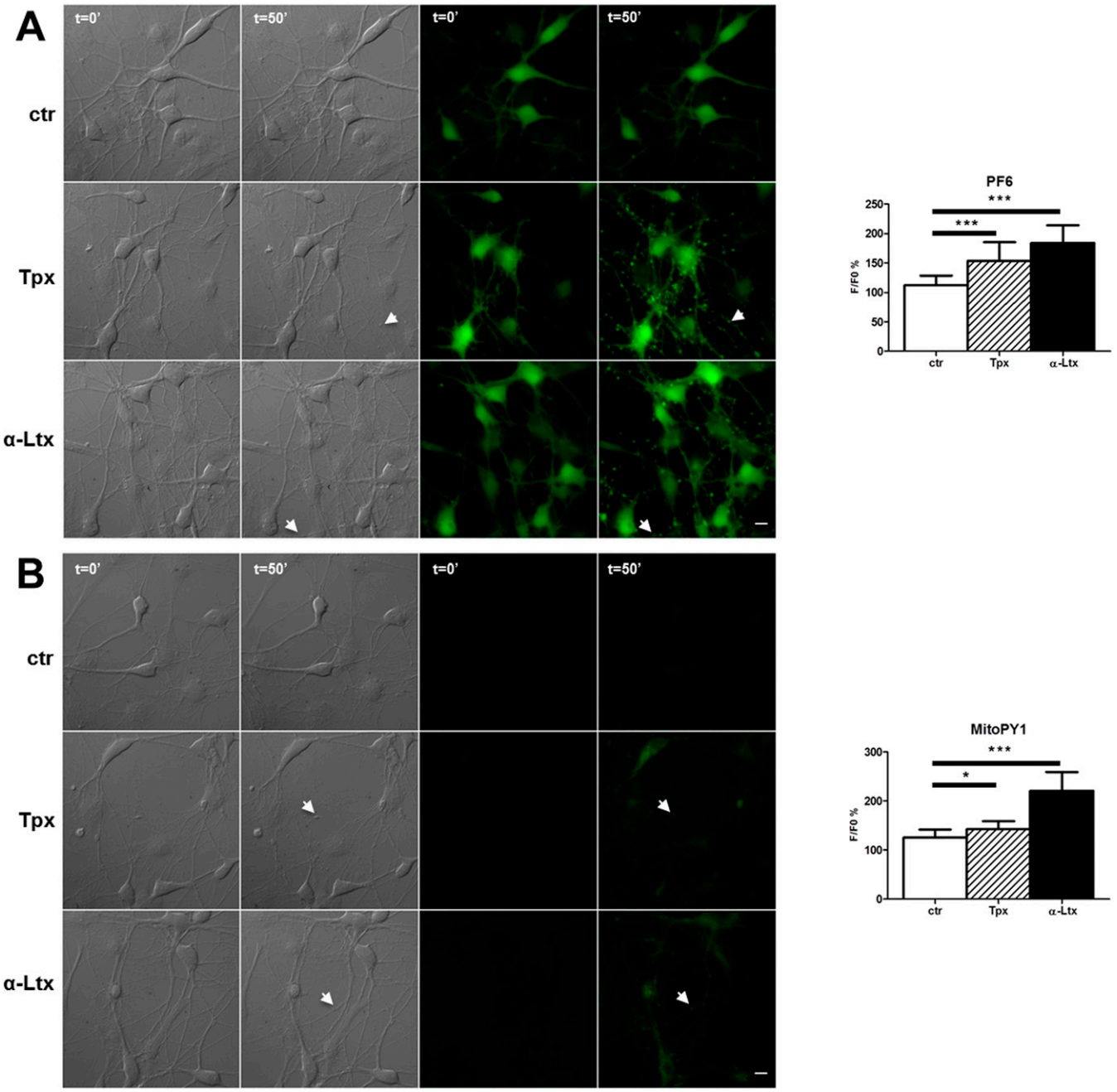

Fig. S1. *Live-imaging* of hydrogen peroxide production in spinal cord MNs. Rat MNs were loaded with the H_2O_2-specific probes PF6-AM (*A*) or MitoPY1 (*B*), washed, and then exposed to Tpx 6 nM or α-Ltx 0.1 nM for 50 min. Changes in fluorescence resulting from H_2O_2 production were measured at $t = 50$ min and expressed as a percentage of the fluorescence value at $t = 0$ (*Right*). $^*P < 0.05$; $^{***}P < 0.001$; $n = 15$. Arrows in bright-field images and in the green channel point to neuronal bulges. (Scale bars: 10 μm.)

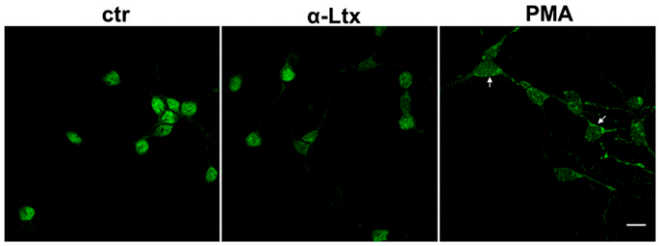

Fig. S2. NADPH oxidase is not involved in hydrogen peroxide production. p47phox staining was performed in CGNs exposed to α-Ltx (0.1 nM for 50 min) or to PMA (1 μg/mL for 20 min) as positive control for p47phox translocation. Arrows point to membrane accumulation of p47phox signal in PMA-treated cells. (Scale bar: 10 μm.)

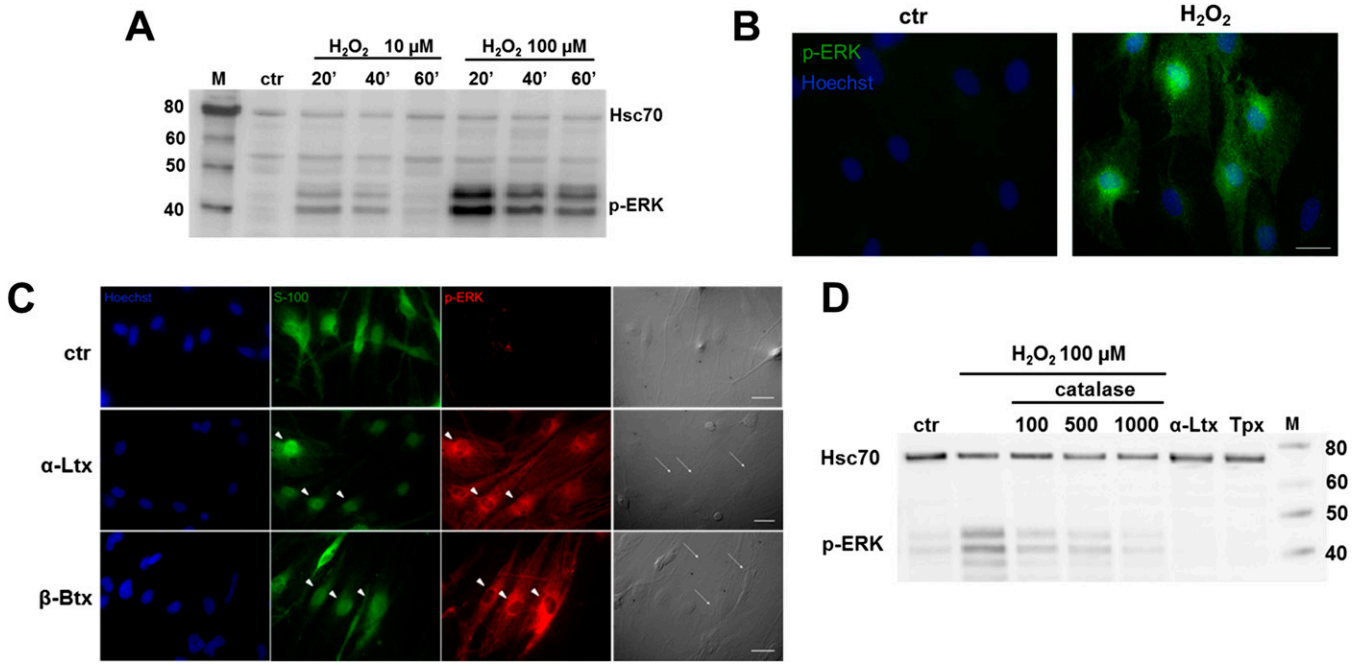

Fig. S3. Primary SCs respond to hydrogen peroxide by phosphorylating ERK. (*A*) Kinetic and dose-dependence of ERK phosphorylation induced in primary SCs by H_2O_2. (*B*) Immunofluorescence of p-ERK (green) in SCs after exposure to H_2O_2 (100 μM for 60 min). Nuclei are stained in blue. (Scale bar: 10 μm.) (*C*) Phospho-ERK positive cells (red) in SCs-MNs cocultures exposed to the neurotoxins are positive for the SCs marker S-100 (green, arrowheads). Arrows in bright-field panels point to bulges. (Scale bar: 20 μm.) (*D*) Preincubation of SCs with increasing amounts of catalase prevents ERK-phosphorylation by H_2O_2 to a different extent. Both α-Ltx and SPANs are ineffective in phosphorylating ERK in SCs.

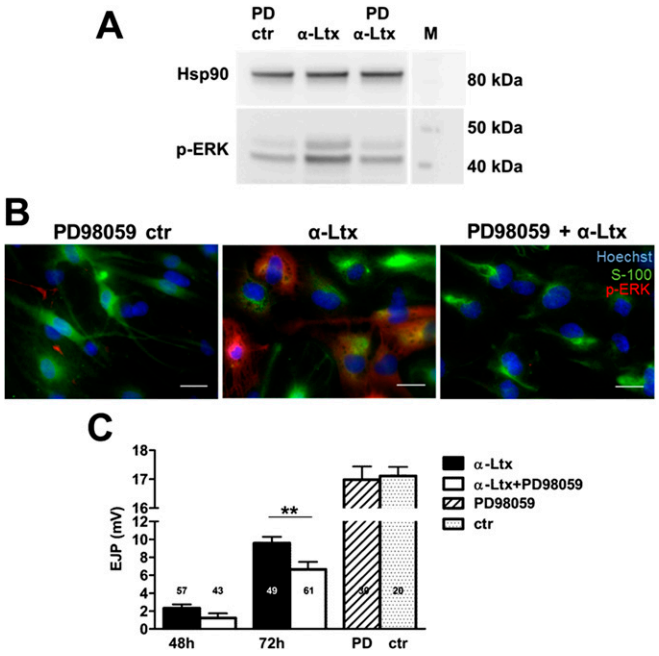

Fig. S4. ERK pathway is involved in SCs activation and subsequent nerve regeneration. SCs-MNs cocultures were pretreated with the MEK1 inhibitor PD98059 before α-Ltx exposure and then probed for p-ERK both in Western blot (*A*) and in immunofluorescence (*B*). The red channel represents p-ERK, and the green one the S-100 marker. Nuclei are stained with Hoechst. (Scale bar in *B*: 20 μm.) (*C*) Electrophysiological recordings of EJPs at soleus NMJs treated with α-Ltx alone (5 μg/kg, black bars) or pretreated with PD98059 (50 μg) before α-Ltx injection (white bars). At 72 h, EJP amplitudes of fibers pretreated with the inhibitor are significantly smaller than those exposed to toxin only (**$P < 0.01$).

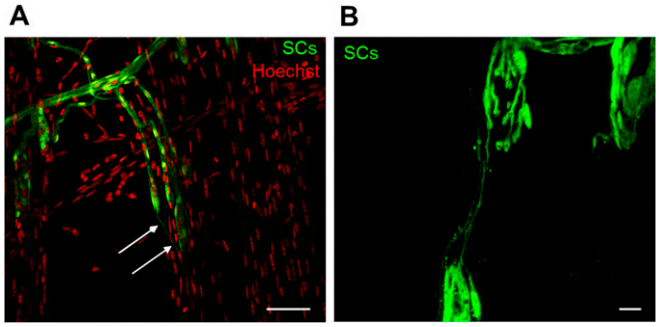

Fig. S5. PSCs activation after toxin-induced nerve terminal degeneration. (*A*) PSCs sproutings (green), typical hallmarks of regeneration, are observed at poisoned LAL NMJs by 24 h from α-Ltx injection. Nuclei are stained with Hoechst (red). In some instances, PSCs sproutings form bridges between adjacent junctions (*B*). (Scale bar: 50 μm in *A*, 10 μm in *B*.)

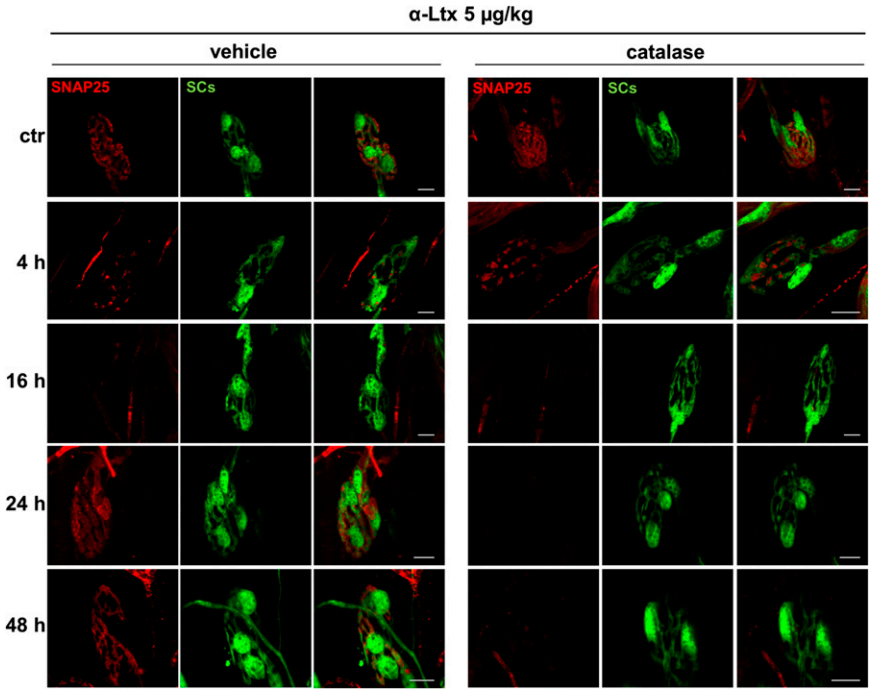

Fig. S6. Regeneration of poisoned presynaptic nerve terminals is delayed by catalase. SNAP-25 labeling (red) was used as read-out to monitor degeneration and regeneration of nerve terminals at the NMJs of LAL muscles s.c. injected with α-Ltx or α-Ltx plus catalase (750 U). Muscles were collected after 4, 16, 24, and 48 h, and representative images are shown. (Scale bars: 10 μm.)

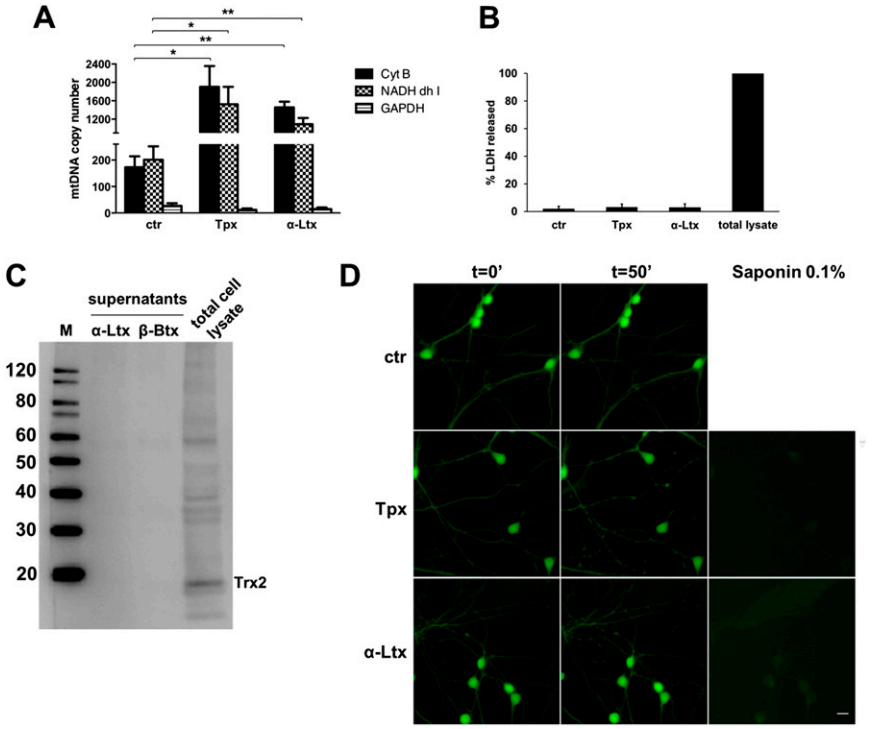

Fig. S7. Neuronal DAMPs are released from intact membranes. (*A*) No GAPDH amplification (nuclear housekeeping gene) was detected by real-time qPCR in neuronal supernatants after 50 min intoxication with α-Ltx or SPANs. $*P < 0.05$; $**P < 0.01$; $n = 3$. (*B*) LDH enzymatic activity was determined in the supernatants of neurons exposed for 50 min to Tpx or to α-Ltx. LDH release is an index of loss of membrane integrity. Data represent the mean of three independent experiments. (*C*) Thioredoxin 2, a mitochondrial protein of similar size to Cyt c, is detectable by Western blot only in CGNs lysates, but not in supernatants of neurons treated with α-Ltx or β-Btx (0.1 or 6 nM for 50 min, respectively) after TCA precipitation. (*D*) Membrane integrity was also assessed by calcein-AM retention in CGNs treated with Tpx or α-Ltx for 50 min. Calcein staining is lost after saponin-induced membrane permeabilization. (Scale bar: 10 μm.)

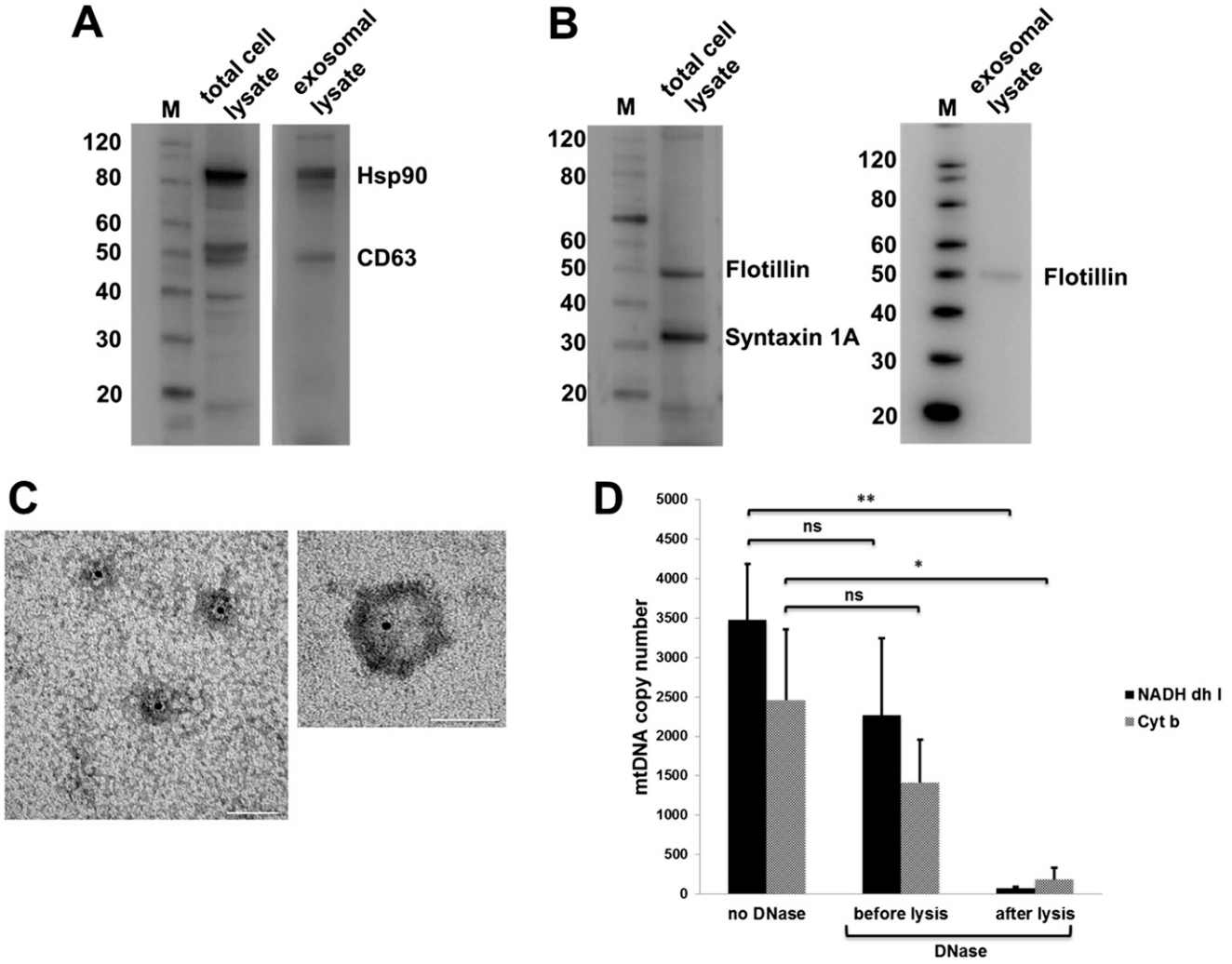

Fig. S8. Mitochondrial DNA is carried inside exosomes. Purified exosomes are positive for the exosomal marker CD63 (*A*) and negative for the plasma membrane marker syntaxin 1A (*B*). (*C*) Immunogold labeling of purified exosomes shows positivity for the exosomal marker Hsp90 and confirms their correct size and morphology. (Scale bars: 50 nm.) (*D*) Real-time PCR for the detection of mtDNA in exosomes treated with DNase (1 U/μL for 60 min). Exosomes were incubated with DNase before or after lysis and DNA purification. $*P < 0.05$; $**P < 0.01$; $n = 3$.

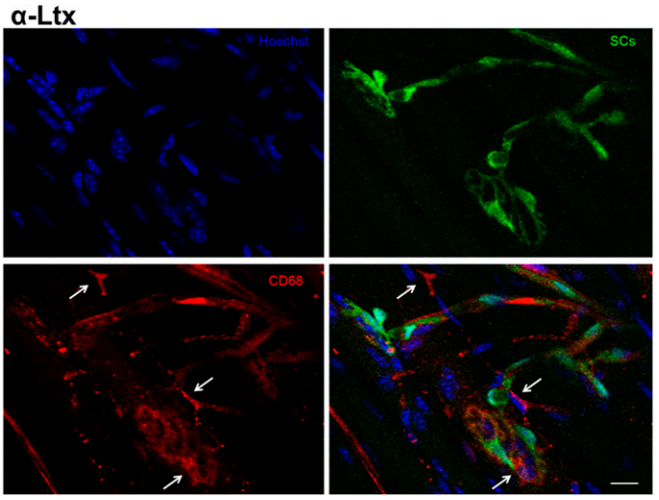

Fig. S9. Macrophages are recruited at the poisoned NMJ. CD68-positive macrophages (red, white arrows) are observed at the NMJs of LAL muscles injected with α-Ltx during nerve terminal degeneration (16 h intoxication). (Scale bar: 10 μm.)